

ABSTRACT

Title of Document: Genetic Suppressors of *mrp-5* Lethality in *C. elegans*

Simon Beardsley, Master of Science, 2016

Directed By: Professor Iqbal Hamza, Department of Animal
and Avian sciences

Heme is an essential cofactor in numerous proteins, but is also cytotoxic. Thus, directed pathways must exist for regulating heme homeostasis. *C. elegans* is a powerful genetic animal model for elucidating these pathways because it is a heme auxotroph. Worms acquire dietary heme through HRG-1-related importers, and intestinal export was demonstrated to be mediated by the ABC transporter MRP-5. Loss of *mrp-5* results in embryonic lethality. Although heme transporters have been identified, there are significant gaps in our understanding for the heme trafficking beyond HRG-1 and MRP-5. To identify additional components, we conducted a forward genetic screen utilizing the null allele *mrp-5(ok2067)*. Screening of 160,000 haploid genomes yielded thirty-two *mrp-5(ok2067)* suppressor mutants. Deep-sequencing variant analysis revealed three of the suppressors are subunits of adaptor protein complex 3 (AP-3). We now seek to identify mechanisms for how adaptor protein deficiencies bypass a defect in MRP-5-mediated heme export.

GENETIC SUPPRESSORS OF *MRP-5* LETHALITY IN *C. ELEGANS*

By

Simon Beardsley

Thesis submitted to the Faculty of the Graduate School of the
University of Maryland, College Park, in partial fulfillment
of the requirements for the degree of
Master in Science
2016

Advisory Committee:

Professor Iqbal Hamza, Ph.D; Chair

Michael W. Krause, Ph.D.

Assistant Professor Antony Jose, Ph.D

Assistant Professor Li Ma, Ph.D

© Copyright by
Simon Beardsley
[2016]

Dedication

I dedicate this work first to my parents for their omnipresent, complete support of whatever decisions I make for my own future, and for teaching me to always seek happiness from its source: within.

Second, I dedicate this work to nematodes who died during the course of the four years that I conducted these experiments. Thank you for your sacrifice.

Acknowledgements

There are many who made this work possible. First, I'd like to acknowledge and thank my advisor Iqbal for his total support, teaching me the value an assertive demeanor, and above all else for always challenging me. I'd also like to thank my thesis committee for their prolonged assistance in guiding my progress through this work, and for the dedication of their attention, time, and intellect.

This work would not have been possible without the daily help and input of my labmates. Xiaojing: you took me under your wing when I first joined and taught me so much, and you were a superb role model. Thank you. Jianbing and Kate: our friendships endured for my entire time in graduate school; I hope it continues long after as well. Cheers. Tammy, Jason, Tamika, and Carine: as senior lab members, you all taught me so much more than you realize and provided excellent friendship and support. I'd also like to thank the members of the Kim Lab. Thank you Byeung-Eun for your mentorship, and thank you to Haarin, Sai, and Anuj for your friendship as well as for prolonged discussions on our mutual interest and research in micronutrient trafficking in *C. elegans*. I'd also like to thank the many fellow graduate students in the department and ASGSA who were great friends and colleagues throughout the many trials graduate school imposed.

Mike Krause and Harold Smith were responsible for sequencing my suppressor strains. Thank you; this was an instrumental aspect of my project. I'd also like to thank all the faculty of the Animal Science department. They were always extremely supportive and responsive to any difficulties or requests I voiced. Additionally, I'd like to thank the staff members of Facilities Management and Housekeeping and acknowledge their dedication which made the Animal Science Wing 1 and 4 an excellent place to work, ensuring all spaces were clean and in working order, and for waking me up at 4:30am when I'd fallen asleep at my desk.

I'd also like to acknowledge the Baltimore Worm Club for serving as an excellent source for learning of ongoing research in nematodes, as well as providing invaluable feedback regarding my own work. Also, telling my friends "I have to go to UMBC this Friday for Worm Club" always served as an entertaining talking point.

Finally, I'd like to thank the CGC for supplying *C. elegans* strains.

Table of Contents

Dedication.....	ii
Acknowledgements.....	iii
Table of Contents.....	iv
Chapter 1: Literature Review.....	1
Introduction.....	1
Arguments for Intracellular Heme Trafficking.....	1
Arguments for Intercellular Heme Trafficking.....	2
Components of Prokaryotic Heme Trafficking.....	3
Components of Unicellular Eukaryotic Heme Trafficking.....	4
Components Mammalian Heme Trafficking.....	4
The Need for an Animal Model: Enter <i>C. elegans</i>	6
HRG-1 and its Paralogs.....	7
HRG-3.....	9
MRP-5.....	10
Trafficking of Heme Homeostatic Components.....	12
Gaps in Knowledge of <i>C. elegans</i> Heme Trafficking.....	15
Figure 1: Summary of <i>C. elegans</i> Heme Trafficking.....	16
Chapter 2: Materials and Methods.....	18
Growth Conditions.....	18
NGM Plate Heme Supplementation.....	18
Hemin Chloride Prep.....	18
Bleaching.....	18
RNAi feeding.....	19
Worm Strains.....	20
Ethyl Methanesulfonate (EMS) Mutagenesis.....	20
ZnMP treatment.....	21
Mapping.....	21
Mapping cross experiment.....	21
Genomic DNA Extraction.....	22
Library Prep.....	23
Sequencing.....	23
Sequencing Analysis.....	23
Genotyping.....	24
<i>mrp-5(ok2067)</i>	24
<i>apb-3(ok429)</i>	25
N2, Hawaiian genotyping for mapping cross.....	26
Assay for RNAi suppression of <i>mrp-5(ok2067/ok2067)</i> lethality.....	27
Combinatorial RNAi.....	28
Worm Growth Assay.....	28
Transcriptional reporter under RNAi.....	28
ReFLx Analysis by COPAS BioSort (Union Biometrica).....	29
Confocal.....	29

Chapter 3:	
Results.....	31
A system of <i>mrp-5</i> deficiency.....	31
A Forward Mutagenesis Screen for Suppression of <i>mrp-5(ok2067)</i> Lethality.....	32
Hawaiian Variant Mapping of <i>mrp-5</i> Suppressor Mutants.....	36
AP-3 suppression of general <i>mrp-5</i> deficiency.....	40
Testing of other Adaptor Protein Complexes.....	41
Effect of AP-3 Subunit loss on Systemic Heme Status.....	42
Gut Granules.....	45
Role of Other Heme Homeostatic Components in AP-3 Deficiency.....	47
Figure 1: <i>mrp-5</i> RNAi embryonic lethality is increased later in brood.....	51
Figure 2: <i>mrp-5(ok2067)</i> genomic structure and putative protein topology.....	53
Figure 3: <i>mrp-5(ok2067/ok2067)</i> heme growth curve.....	55
Figure 4: EMS Screen Schematic.....	57
Figure 5: Mating deficiency in <i>mrp-5(ok2067/o)</i> males.....	59
Figure 6: Suppression strength assay.....	61
Figure 7: GaPPIX lethality in <i>mrp-5</i> suppressor mutants.....	63
Figure 8: ZnMP uptake in <i>mrp-5</i> suppressor mutants	65
Figure 9: Hawaiian Variant Mapping Strategy.....	67
Figure 10: Hawaiian Variant Mapping – F ₁ , F ₃ screening.....	69
Figure 11: Hawaiian variant Mapping results – IQ1003, IQ1004, IQ1005.....	71
Figure 12: Candidate testing by RNAi in <i>mrp-5(ok2067/ok2067)</i>	76
Figure 13: AP-3 subunit suppressor alleles.....	78
Figure 14: Candidate Testing by combinatorial RNAi.....	81
Figure 15: RNAi against AP-1 or AP-2 in <i>mrp-5(ok2067/ok2067)</i>	83
Figure 16: Combinatorial RNAi against AP-1 or AP-2 and vector or <i>mrp-5</i>	85
Figure 17: AP-3 subunit RNAi in <i>P_{hrg-1}::GFP::unc-54 UTR</i>	87
Figure 18: AP-3 subunit RNAi in <i>P_{hrg-2}::HRG-2-YFP::unc-54 UTR</i>	89
Figure 19: HRP activity Assay in RNAi model of <i>mrp-5</i> suppression.....	91
Figure 20: <i>cua-1(ok904)</i> suppression assay.....	93
Figure 21: ZnMP Treatment in suppressor mutants.....	95
Figure 22: <i>mrp-5</i> RNAi Suppression Assay.....	97
Figure 23: AP-2 and AP-3 RNAi in <i>P_{vha-6}::HRG-1-mCherry::unc-54 UTR</i>	99
Figure 24: <i>mrp-5</i> Suppressor Reversion Assay.....	101
Chapter 4:	
Discussion.....	103
Figure 1: Potential suppression mechanism: global secretion of gut granules...	109
Figure 2: Model for AP-3 mediated suppression of <i>mrp-5</i> deficiency.....	111
Appendix A: <i>C. elegans</i>	
Strains.....	113
References.....	118

Chapter 1: Literature Review

Introduction

Heme is a protein prosthetic group of fundamental biological importance. It serves as a critical component in the activity of a diverse set of proteins, whose functions include oxidative metabolism (cytochrome c oxidase), gas transport (globins), xenobiotic detoxification (GSTs), gas sensing (NOSynthase, guanylate cyclases) and microRNA processing (DGCR8).¹⁻³ Heme consists of an organic tetrapyrrole ring with iron coordinated at the center, where each pyrrole is joined at the alpha position by methine bridges¹. The iron coordinated by heme can undergo reduction or oxidation between the ferric and ferrous states. Proteins possessing heme as a cofactor are then able to harness this property to mediate redox reactions for various substrates. The use of heme in this capacity evolved early in biology, evidenced by the highly conserved cytochromes used in oxidative phosphorylation, critical for efficient synthesis of ATP.⁴

Many of the properties which make heme biologically essential concurrently manifest in cytotoxicity.⁵ By itself, iron can generate reactive oxygen species (ROS) which has been shown to cause oxidative damage to proteins, lipids, and nucleic acids. Heme-iron maintains these properties, and heme's hydrophobic tetrapyrrole ring increases relative cytotoxicity by its tendency to insert into and intercalate between lipid bilayers and bind to many proteins non-specifically^{1,3,6-8}.

Arguments for Intracellular Heme Trafficking

In most metazoans, heme is synthesized by the well characterized eight-step Shemin Pathway. It begins in the mitochondria with the condensation of succinyl CoA and glycine by ALAS to form δ -aminolevulinic acid (ALA). ALA is then converted through five enzymatic reactions to Coproporphyrinogen III (CPgenIII) in the cytosol. In

the mitochondrial IMS, CPgenIII undergoes two more enzymatic reactions which results in Protoporphyrin IX (PPIX). The final insertion of iron into PPIX results in the release of heme *b*, the most abundant heme, into the mitochondrial matrix.^{1,2}

Heme is synthesized de novo in the mitochondrial matrix, while proteins which require heme as a prosthetic group reside in most subcellular compartments. This necessitates the intracellular transport of heme from the mitochondrial matrix to other compartments for incorporation into hemoproteins. Due to inherent cytotoxicity, organisms have likely evolved mechanisms to tightly regulate heme trafficking in order to avoid spurious cell damage. Although heme synthesis is well characterized, the pathways underlying heme trafficking are relatively poorly understood.¹

Arguments for Intercellular Heme Trafficking

While intracellular heme trafficking is implied by the necessity for traversing intracellular membranes, several lines of experimental evidence suggest that pathways for the intercellular transport of heme are utilized in higher vertebrates. First, acute intermittent porphyria (AIP) is a human disease which is due to deficiency in hydroxymethylbilane synthase (the third enzyme in the Shemin Pathway) which results in an overproduction of the upstream heme synthesis intermediates aminolevulinic acid (ALA) and porphobilinogen (PBG).⁹ The most common treatment for an acute attack and prevention of recurrent attacks is intravenous infusion of heme¹⁰; either as heme-albumin¹¹, heme arginate, or lyophilized hematin.⁹ Infusion of heme acts to repress ALAS, attenuating accumulation of ALA and PBG⁹. It has also been shown to replete regulatory heme pools and restore activity of liver hemoproteins¹¹. These observations indicate that centrally infused heme can be utilized in peripheral tissues.²

Another set of striking observations emerge in the phenotypes of mutant animals where the heme synthesis pathway is genetically disrupted. In mice, deletion in ferrochelatase (the final enzyme in the heme synthesis) is unsurprisingly embryonic lethal; however, homozygous mutants survive until at least E3.5¹², indicating that developing embryos can access maternal heme.² Similarly, mutation in zebrafish protoporphyrinogen oxidase (*ppox*) results in embryonic lethality, but some mutants survive until approximately 27 days post-fertilization¹³, implying maternal deposition of heme is sufficient for early embryonic development.²

Finally, polarized Caco-2 cells (epithelial colorectal adenocarcinoma cells) are capable of transporting heme from the apical to basolateral side¹⁴, raising the possibility that this process may also occur *in vivo* for delivery of heme to circulation, where it is available to peripheral tissues.²

Components of Prokaryotic Heme Trafficking

Despite the challenges associated with the identification of factors mediating the trafficking of heme, significant advancements have been made in several traditional model systems. Bacteria represent a simplistic system for trafficking studies without the confounding factors of inter-organelle transport. Bacterial heme uptake systems have been relatively well characterized. They tend to be robust due to the fact that bacteria generally live in iron restricted environments¹⁵, thus heme represents a significant source of iron.¹⁶ Variations of two common heme uptake systems exist in many gram-negative bacteria, and are usually clustered into iron-regulated operons.¹⁷ The first involves binding of heme or hemoproteins by an outer membrane (OM) receptor (HemR) and transport by an ABC transporter into the periplasmic space¹⁸ where a periplasmic

transport protein (HemT) delivers heme to cytoplasmic membrane ABC transporters (HemU, HemV) for translocation into the cytosol. The second uptake pathway involves secretion of a hemophore (HasA) into extracellular space where it binds heme and delivers it to an OM receptor (HasR); once in the periplasm, heme follows the pathway previously described to traverse the plasma membrane. Once in the cytosol, heme is degraded by heme-oxygenase like enzymes (HemS) which may also function as a chaperone.^{16,17}

Components of Unicellular Eukaryotic Heme Trafficking

Heme uptake systems in simple unicellular eukaryotic systems such as yeast are poorly defined relative to prokaryotes. Although the budding yeast *S. cerevisiae* lacks a robust heme uptake system, the pathogenic yeast *C. albicans* efficiently utilizes exogenous heme.¹⁹ Genome wide screening in *C. albicans* identified two genes involved in heme uptake: RBT5 and RBT51²⁰. Both are GPI-anchored proteins which localize to the plasma membrane and are necessary for receptor mediated endocytosis of free heme and hemoglobin, respectively. Once endocytosed, heme is delivered to the vacuole and catabolized.^{16,21}

Components Mammalian Heme Trafficking

Although the evidence for intercellular heme trafficking in mammals is not widely recognized, it is well established that exogenous heme is imported from dietary sources present in the intestinal lumen.²² Iron absorption is poor in the small intestine due to the fact that under conditions present therein it is readily oxidized and forms insoluble complexes.¹⁶ Thus it has been estimated that although heme-iron makes up one third of total dietary iron, it represents two-third of absorbed iron.²³ Two mammalian heme

importers have been identified; *HRG-1* was identified first by its ortholog in *C. elegans*, and will be discussed further in later sections. The other heme importer, *Hcp1* was identified using expression analysis in mice.²⁴ However, subsequent analysis demonstrated that while it does import heme ($K_m \approx 125 \mu\text{M}$), it transports folate with much higher affinity ($K_m \approx 1.3 \mu\text{M}$), rendering a physiological role for this transporter uncertain.²⁵

Similarly, heme export has been recognized irrespective of a role in intercellular trafficking due to the fact that heme efflux represents a viable mechanism for attenuation of heme hyper accumulation in cells. The first recognized heme exporter, FLVCR, was serendipitously identified in cats. Although it was a predicted member of the major facilitator superfamily of secondary permeases based on homology, its physiological substrate was unknown.²⁶ FLVCR acts as the cell surface receptor for the retrovirus feline leukemia virus, subgroup C (FeLV-C).²⁶ When infected, felines develop profound anemia, exhibit an arrest of erythropoiesis, and feline embryonic fibroblasts hyperaccumulate heme.²⁷ Since FeLV-C envelope surface unit protein was shown to have a dominant negative effect on FLVCR²⁸, it was postulated these phenotypes may be due to a loss of function of FLVCR.²⁶ Ectopic expression of FLVCR in renal epithelial cells reduced cellular heme levels, and was capable of inducing export of radiolabeled heme and the fluorescent heme analog Zinc Mesoporphyrin (ZnMP) in renal epithelial and K562 cells, suggesting that FLVCR is capable of heme efflux.¹⁶ FLVCR1 knock-out mice lacked definitive erythropoiesis, and died in midgestation.²⁹ FLVCR1 was also necessary for export of heme-iron from bone marrow derived macrophages.²⁹ Subsequent work identified two isoforms for FLVCR1 in mice. Immunofluorescence and subcellular

fractionation showed that FLVCR1a localizes to the plasma membrane, while FLVCR1b lacks the first exon and localizes to the mitochondrion.³⁰ Deletion of the first exon did not result in anemia, but siRNA against FLVCR1b impaired erythroid differentiation, implying that loss of FLVCR1b but not FLVCR1a is responsible for the observed erythropoietic defects of FLVCR possibly by playing a role in mobilizing synthesized heme from the mitochondria.^{22,30} FLVCR2 has been proposed to act as a heme importer, but rigorous studies exploring its potential role have not been conducted.³¹

Given heme's capacity for ROS generation and intercalation into lipids, direct chaperoning of heme by heme-binding proteins has long been proposed in sequestration of heme for storage, or to mediate its delivery to transporters as a mechanism to prevent cytotoxicity associated with free heme.¹⁶ Demonstration of heme-binding itself is not convincing given that heme has been shown to associate with proteins non-specifically.¹

The Need for an Animal Model: Enter *C. elegans*

Although previous efforts have identified many mechanisms capable of trafficking heme, a major shortcoming has been the failure to adopt an appropriate system for targeted genetic screening. Instead, progress has often relied on serendipitous discovery exemplified by the finding of FLVCR. A classic approach to pathway discovery is to change a system's environmental availability for a substrate and then examine how the system is adapting to maintain homeostasis. For heme, this has been difficult to conduct as most model systems are capable of heme synthesis, and upon heme challenge it is difficult to differentiate between components contributing to trafficking and synthesis. One strategy to overcome this is to chemically inhibit heme synthesis, but

this has many pleiotropic effects making the identification of changes specifically associated with heme trafficking problematic.

A potential model system emerged with the finding that *Caenorhabditis elegans* lacks enzymes necessary for heme synthesis rendering them heme auxotrophs.³² This necessitated that worms take heme up from the diet and into enterocytes. Since heme is required in a wide range of fundamental cellular processes already described, it also implies that dietary heme taken up in the intestine must be made available to all extra-intestinal tissues. Thus components regulating the trafficking of heme must coordinate the uptake of heme into the intestine, its intracellular trafficking and eventual export from the intestine, as well as its uptake and utilization by all extra-intestinal tissues. This makes *C. elegans* uniquely suited animal model for elucidating pathways that control heme trafficking. Additionally, normal heme trafficking would be required for *C. elegans* viability. Loss of a vital component of the heme trafficking pathway could be lethal, an excellent genetic readout for conducting forward genetic screens.

Among subsequent efforts to identify functional components of heme uptake, a microarray study was conducted on worms grown axenically in low, optimal, and high heme. This approach identified 288 genes whose expression was changed ≥ 1.6 fold across the three conditions and subsequently classified as heme responsive genes (*hrg*).³³

HRG-1 and its Paralogs

Proof of concept emerged with the identification of the first *bona fide*, conserved heme importer *hrg-1*.¹ Both *C. elegans* and human HRG-1 are capable of inducing heme dependent current in *Xenopus laevis* oocytes implying a direct capability to bind and transport heme.³⁴ Early evidence indicated that *hrg-1* function is conserved in metazoans

as both *C. elegans* and human HRG-1 co-localize in human cell lines. Morpholino knockdown of *hrg-1* in zebrafish results in morphological defects including impaired erythropoiesis, and these phenotypes are rescued by heterologous expression of *C. elegans hrg-1*.³⁴ The discovery of this conserved heme importer in *C. elegans* validated the approach of using worms as a model for discovery of novel components and pathways of heme trafficking which may be conserved in higher order metzoans.

In *C. elegans*, *hrg-1* has three paralogs: *hrg-4*, *hrg-5*, and *hrg-6*.³⁴ Low heme transcriptionally upregulates *hrg-1* and *hrg-4*, and both are down regulated in high heme. In contrast, *hrg-5* and *hrg-6* remain transcriptionally active at high heme.^{34,35} HRG-1::GFP localizes to intracellular vesicles, while HRG-4::GFP is localized exclusively to the apical membrane of enterocytes.^{35,36} Feeding of a toxic heme analog, gallium protoporphyrinIX (GaPPIX), results in embryonic lethality in the progeny of exposed adults.³² Interestingly, RNAi of *hrg-4* but not *hrg-1* reduced toxicity associated with GaPPIX exposure, indicating *hrg-4* function may be more critical for uptake of porphyrins.³⁴ Pulsing with Zinc Mesoporphyrin (ZnMP), a fluorescent heme analog, resulted in accumulation of ZnMP in intracellular vesicles within the intestine. Treatment with RNAi against *hrg-4* resulted in a loss of ZnMP accumulation, while RNAi of *hrg-1* resulted in an increase of ZnMP accumulation.³⁴ Interestingly, HRG-1::GFP showed significant co-localization with ZnMP vesicles.³⁶ These data support a model where HRG-4 acts to mediate heme uptake at the apical membrane, while HRG-1 mediates import from an intracellular compartment. In HeLa cells and yeast, HRG1 co-localizes with V-ATPase subunits³⁷ and the interaction of HRG1 with heme *in vitro* requires low pH³⁸, perhaps due to the fact that heme has enhanced solubility below physiological pH.

These data indicate that the identity of HRG-1 compartments is likely acidified organelles of the endolysosomal system.^{34,38} Loss of either *hrg-1* or *hrg-4* is not lethal, and loss of both results in only a mild growth phenotype; thus it seems that intestinal heme uptake in *C. elegans* is highly redundant. This also means that screening for suppression of loss of intestinal import may not be ideal since it would require scoring a non-lethal phenotype.

The characterization of *hrg-1* also led to the construction of a heme sensor strain (IQ6011), consisting of a transcriptional fusion of the *hrg-1* promoter with GFP.³⁴ In this strain, intestinal GFP levels are inversely correlated with heme availability.^{34,39} Subsequently, a genome-wide RNAi screen knocked down 18,533 genes (93% of the genome)⁴⁰ by RNAi in IQ6011 sensor worms and 177 genes resulted in significant alteration of *P_{hrg-1}::GFP* activity.⁴¹ The identification of *hrg-1* as a conserved heme importer^{34,36,42} validated *C. elegans* as an invaluable model organism for the discovery of novel components of heme trafficking relevant in higher organisms.

HRG-3

HRG-3 was identified as an intercellular heme chaperone in *C. elegans*.⁴³ The previously described microarray study indicated *hrg-3* to be upregulated >70 fold in low heme.⁴³ Null mutants in *hrg-3* have no overt phenotypes in normal growth conditions, but in conditions where environmental heme is relatively low, *hrg-3* mutant progeny exhibited embryonic lethality and early larval arrest.⁴³ Fitting with this observation, subsequent qRT-PCR demonstrated that *hrg-3* transcript is only detectable in low heme conditions ($\leq 6 \mu\text{M}$ heme in axenic mCeHR-2). A transcriptional GFP fusion indicated that *hrg-3* is expressed in the intestine, with the highest signal in the anterior intestine. Thus it was surprising when an HRG-3 fusion protein was shown to be localized

primarily to extra-intestinal tissues including the uterus, coelomocytes (extra-intestinal macrophage-like cells in the pseudocoelom), and gonadal sheath cells when driven either from its own promoter or the constitutive, intestinal specific promoter *vha-6*. These results show that HRG-3 is secreted from the intestine and taken up into extra-intestinal tissues.⁴³

Subsequent spectroscopic analysis demonstrated that HRG-3 binds heme with a stoichiometry of two parts HRG-3 to one part heme regardless of heme-iron's oxidation state⁴³, fitting with later studies showing that HRG-3 dimerizes, and histidines are important for dimerization and heme binding.⁴⁴ Analysis of *hrg-3* mutants expressing a non-integrated HRG-3 transgene where transgene transmission to progeny was ~40% indicated that in low heme conditions, P₀ lacking the transgene laid progeny exhibiting either embryonic lethality or larval arrest; however, P₀ expressing the rescue transgene yielded progeny without defect, regardless of F₁ segregation of the rescue transgene.⁴³ These experiments indicate that in heme limiting conditions, HRG-3 is secreted and taken up by extra-intestinal tissues. Critically, it mobilizes maternal heme to progeny.⁴³

MRP-5

While *hrg-3* demonstrated a pathway of intestinal heme efflux, several lines of evidence indicated that *hrg-3* independent pathways must exist. The fact that null mutants lack a phenotype in normal growth conditions and that *hrg-3* is only transcriptionally active in very low heme⁴³ imply the necessity for a pathway mediating intestinal efflux under heme sufficient growth conditions. An early candidate appeared in the form of *mrp-5*, an ABC transporter homologous to human CFTR. Previously described microarrays showed that *mrp-5* is induced over three fold in response to low heme⁴⁰, and

bioinformatic analysis showed that its putative promoter contains the 23bp heme responsive element responsible for *hrg-1* heme dependent regulation.^{39,40} Subsequent RNAi against 288 *hrgs* in IQ6011 (*P_{hrg-1}::GFP*) demonstrated that loss of *mrp-5* results in a perceived heme deficiency which persisted even with high heme supplementation ($\geq 500 \mu\text{M}$).⁴⁰

Interestingly, RNAi against *mrp-5* results in embryonic lethality, which can be rescued by heme supplementation. RNAi against seven other *mrp* genes (besides *mrp-5*) and five putative homologs of FLVCR in *C. elegans* did not phenocopy *mrp-5*, indicating that *mrp-5* plays a unique and critical role in *C. elegans* heme homeostasis.⁴⁰ Tissue specific RNAi demonstrated that although *mrp-5* appears to be transcribed in several tissues, only intestinal loss of *mrp-5* recapitulates the lethality phenotype, indicating that a crucial site of *mrp-5* activity was in the intestine.⁴⁰ An intestinal MRP-5::GFP fusion protein localized to the basolateral membrane as well as intracellular compartments.⁴⁰ RNAi against *mrp-5* also resulted in an increased accumulation of ZnMP in intestinal vesicles, as well as resistance to GaPPIX toxicity, suggesting that *mrp-5* could be exporting porphyrins from the intestine.

Although direct heme binding by MRP-5 has not been demonstrated, heterologous expression of MRP-5 decreased viability of the heme synthesis deficient yeast strain *Ahem1*, and reporter assays indicated MRP-5 expression results in a re-partitioning of heme from the cytoplasm to intracellular organelles.⁴⁰ This implies that MRP-5 either directly transports heme or a substrate that influences cellular heme. Mammalian MRP5 has also been shown to promiscuously transport a range of substrates including glutamate conjugates and analogs.⁴⁵ The function of vertebrate MRP5 is

unclear. In zebrafish, morpholino knockdown of *mrp-5* resulted in anemia and reduced blood cell formation.⁴⁰ However, *Mrp5* knockout mice have no overt phenotypes.⁴⁰ In MEFs, *Mrp5* localized to the plasma membrane (co-localized with WGA), Golgi (co-localized with galactosyltransferase), and early/recycling endosomes (co-localized with Rab4, Rab5, Rab9, and Rab11), raising the possibility that in mammals MRP5 may mediate heme transport into intracellular organelles.^{39,40,46} These data indicate that while lethality phenotypes are not conserved between *C. elegans* and higher vertebrates, the mechanism for heme trafficking may be conserved.

The fact that loss of *mrp-5* can be suppressed by supplementation of dietary heme implies the presence of another lower affinity pathway for heme export from the intestine. The severe embryonic lethality associated with loss of *mrp-5* in normal growth conditions presented an easy to score phenotype for a forward genetic suppressor screen.

Trafficking of Heme Homeostatic Components

Several of the identified proteins important in heme homeostasis are transmembrane proteins, such as importers HRG-1 and its paralogs, and the exporter MRP-5. Although the signals required for their normal trafficking have not been well studied, maintaining proper localization is critical to their function in partitioning of intestinal heme.

In silico motif analysis revealed a semi-conserved acidic di-leucine based sorting signal at the C-terminus⁴⁰ (ETDLLI in humans at position 1363, GTDKLI in *C. elegans*), and tyrosine (YRAF in *C. elegans* at position 172, YRAD in humans)³⁴ and di-leucine (ESQPLL in *C. elegans* at position 178, DISILS in humans) based sorting signals in the carboxy terminus of HRG-1.^{34,36,47} In *C. elegans*, the *hrg-1* paralogs HRG-4 and HRG-5

lack a hydrophobic residue (\emptyset) in the final position of the tyrosine based sorting motif (YLNK, YSNQ, respectively); the HRG-6 sorting signal fits the canonical motif, although it is distinct from that of HRG-1 (YGKL).³⁵ Given that tyrosine based sorting motifs are generally degenerate in nature, computational analysis is insufficient to determine the role of these motifs in membrane sorting.⁴⁸ With the exception of HRG-1, the other paralogs all lack the di-leucine based sorting motif (*hrg-4*: TASEDG; *hrg-5*: ILKSEI; *hrg-6*: KSIIHP). The discrepancies between sorting signals in HRG-1 and its paralogs fits with the purely apical localization seen in the intestine for HRG-4 and HRG-6 and supports that the endolysosomal localization of HRG-1 is directed by recognition of these motifs, particularly its acidic di-leucine based sorting motif.³⁴⁻³⁶

Sorting events require recognition of these cytosolic sorting signals by trafficking adaptors; adaptor binding mediates the formation and budding of coated vesicles containing the specified cargo. Recognition of these sorting motifs is mediated by adaptor protein complexes (APs)⁴⁷, a family of heterotetrameric complexes. In mammals, there are currently five APs identified⁴⁹⁻⁵¹. However, there are only three in *C. elegans*, *D. melanogaster*, *S. cerevisiae*, and *S. pombe*. Thus the extent of functional conservation in mammals and other model organisms is uncertain.^{51,52} Tyrosine based sorting motifs are proposed to require μ AP subunit binding, while di-leucine based motifs can bind either μ or β AP subunits.⁴⁷

Sorting signals fitting the YXX \emptyset motif (where *X* is any amino acid and \emptyset is an amino acid with a bulky hydrophobic side chain)^{53,54} mediate sorting of transmembrane proteins to endosomes⁴⁷, lysosomes^{47,55}, as well as the basolateral membrane of polarized epithelial cells⁵⁶ though interactions with the μ domains of corresponding

heterotetrameric adaptor protein complexes⁴⁷. Binding to one of the AP complexes then specifies a destination compartment for the YXXØ containing cargo.⁵⁷ The same sorting signal being responsible for sorting to distinct destinations raises an issue of specificity. However, studies utilizing mammalian orthologs of AP complex μ subunits have demonstrated that while the four mammalian μ subunit homologs recognize the YXXØ motif, distinctions arise in preference for the identity of “X” or “Ø”.⁵⁸

The conserved tyrosine and di-leucine based sorting signals in the carboxy terminus of HRG-1 are likely important for its endolysosomal localization. The acidic di-leucine based sorting signal in MRP-5 is likely an important factor for its normal localization. Recognition of MRP-5’s sorting signal for endocytic recycling is typically AP-2 dependent⁵⁹, however sorting of cargo with di-leucine based sorting motifs can also be influenced by recognition of GGAs which play a critical role in sorting cargo from the trans-golgi in mammals⁴⁷. There are reports of a single ortholog in *C. elegans*, but the extent of their functional conservation has not been explored.^{60,61} The acidic di-leucine based sorting signal of MRP-5 may also mediate its basolateral sorting in polarized intestinal cells, a process where recognition of the sorting signal by AP-1 is necessary for normal polarized sorting in *C. elegans*, mice, and zebrafish.⁶²⁻⁶⁵

Whereas AP-1 and AP-2 play major roles in the trafficking of a large number of cargoes, AP-3 seems to mediate the trafficking of a smaller subset of cargoes to lysosome related organelles (LROs).⁵¹ In mammals trafficking to these compartments are mediated by AP-3 as well as BLOC-1 (Biogenesis of Lysosome-related Organelles Complex-1), BLOC-2, and BLOC-3. In humans, mutations in these genes result in a Hermansky-Pudlak syndrome, which is characterized disrupted formation of platelet dense granules

and melanosomes.⁶⁶⁻⁶⁹ In *C. elegans*, only orthologs of AP-3 and BLOC-1 subunits have been identified, and result in aberrant formation of an intestinal specific LRO known as gut granules.^{70,71} Gut granules are characterized by their accumulation of autofluorescent and birefringent material⁷², and are important sites of storage for micronutrients such as zinc.⁷³

Gaps in Knowledge of *C. elegans* Heme Trafficking

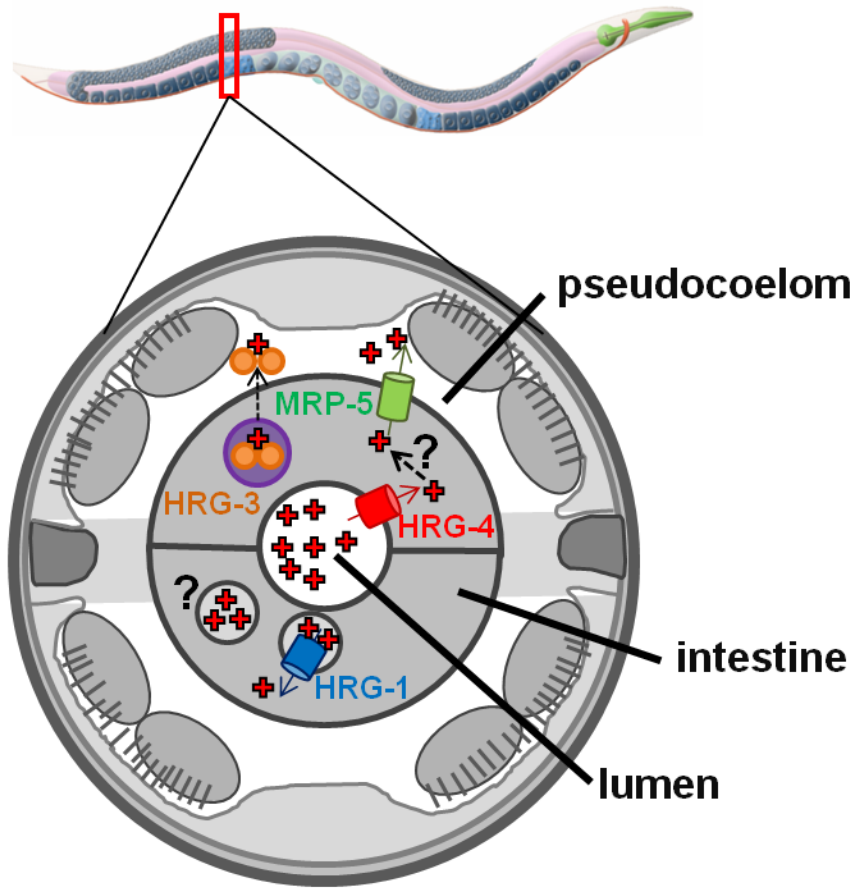
Despite the advances in our understanding of heme trafficking pathways in the past decade using *C. elegans* as a model, the identification of many putatively necessary components in this pathway have remained elusive (Figure 1).^{34,40,43,74-76}

Fitting with the intestinal localization of ZnMP³⁴, work using genetically encoded HRP reporters indicated that in high heme, the intestine continues to accumulate heme after heme levels in other tissues saturate⁷⁷ and that the intestine may play a role in heme storage. However, identification of functional components for heme storage as well as an intestinal site of storage has been unsuccessful.

Additionally a precise mechanism for intracellular heme chaperoning between transporters are unknown. Previous studies have indicated that importers *hrg-1* and *hrg-4* transport heme to the cytosol, but how cytosolic heme is delivered to MRP-5 is unknown. The intent of this project was to conduct a forward genetic suppressor screen to uncover mechanisms by which loss of *mrp-5* may be genetically suppressed. Identification of these mechanisms may elucidate additional components which directly participate in heme trafficking, or perhaps unknown means of regulation of already identified components.

Figure 1: Summary of *C. elegans* Heme Trafficking

A summary of known and unknown components functioning in *C. elegans* intestinal heme trafficking. Dietary heme in the intestinal lumen must be imported and stored in the intestine, then exported across the basolateral membrane to supply extra-intestinal tissues. The importer HRG-4 is localized to the apical membrane and transports heme from the intestinal lumen to the cytosol, while the importer HRG-1 transports heme from an intracellular compartment to the cytosol. The exporter MRP-5 transports heme from the cytosol to the pseudocoelom. In low heme, HRG-3 dimerizes and is secreted from the intestine, though the details of its heme acquisition are unknown. ZnMP accumulation indicates that heme accumulates in intracellular vesicles, some of which co-localize with HRG-1. The mechanisms of intestinal heme storage and chaperoning are unknown.



Chapter 2: Methods

Growth Conditions

Worms were maintained at 20 °C in axenic liquid mCeHR-2 media⁷⁸ supplemented with 20 µM heme with continuous shaking or on nematode growth medium (NGM) plates seeded with OP50 bacteria grown overnight in Luria Broth (LB). NGM plates contained 3 g/L NaCl, 2.5 g/L peptone, 20 g/L agar, 5 mg/L cholesterol, 0.1 M CaCl₂, 0.1 M MgSO₄, and 25 mM KH₂PO₄. NGM agar was autoclaved for 45 m, and allowed to cool to 60 °C in an oven before addition of cholesterol, CaCl₂, MgSO₄, and KH₂PO₄.

NGM Plate Heme Supplementation

Two approaches were used to supplement NGM plates with hemin chloride, and the method used is specified for each assay. One is to directly add hemin chloride to the NGM agar following cooling to 60 °C, just before plating. The other is to supplement LB Broth used to culture *E. coli* with hemin chloride. The prior approach is preferred because it is difficult to consistently plate the precise volume of agar, thus once LB + hemin is absorbed, the effective concentration of hemin may vary.

Hemin Chloride Prep

130 mg hemin chloride (Frontier CAS# 16009-13-8) was added to 15 mL of 0.3 M NH₄OH. Concentrated HCL was added until the solution had a pH of 8.00 (+/- 0.05). The solution was brought to 20 mL with 0.3 M NH₄OH (pH 8.0) to give a final concentration of 10 mM hemin chloride.

Bleaching

Worms were collected from plates with 0.1 M NaCl. Washing consisted of allowing worms to settle on ice for 10 m, aspiration of the supernatant, and resuspension in 0.1 M

NaCl. Three washes were conducted to remove bacteria, and finally the worm pellet was resuspended in 3 mL 0.1 M NaCl. All downstream steps (except centrifugation) were conducted in a sterile laminar flow hood. In a separate tube, 1 mL of 5 M NaOH was mixed with 2 mL 5% Chlorox bleach solution. Then, 1.5 mL of the NaOH / bleach solution was added to the nematode population. The ratio of worm suspension to bleach/NaOH is 2:1; for very large batches of worms, the total volume was adjusted as needed. The suspension was intermittently vortexed until the cuticles of gravid worms dissolved and the eggs were released, then immediately centrifuged at 800 g for 1 m at 4 ° C. The supernatant was aspirated, and 10 mL sterile water was added to the egg pellet and vortexed for 5 s. The suspension was centrifuged at 800 g for 1 m at 4 ° C. The supernatant was aspirated, and the egg pellet was re-suspended in 10 mL sterile water and vortexed for 5 s. The suspension was centrifuged at 800 g for 1 m at 4 ° C. The supernatant was aspirated, and the pellet was resuspended in 5-10 mL M9 salt solution (86 mM NaCl, 42 mM Na₂HPO₄, 22 mM KH₂PO₄, 1 mM MgSO₄ 7H₂O). The eggs were hatched overnight in the M9 solution at 20 ° C rotating at 70 RPM.

RNAi feeding

Bacterial cultures consisted of *E. coli* HT115(DE3) expressing *elt-1*, *elt-2*, *elt-6* double-stranded RNA from the Ahringer or Orfeome library and all sequences were verified by amplifying regions downstream of the T7 promoter. NGM RNAi plates were prepared as described in Growth Conditions except that after cooling and before plating, carbenicillin (100 µg/mL), tetracycline (12 µg/mL), and IPTG (476.6 µg/mL) were added to NGM agar. Bacterial cultures were prepared with HT115(DE3) grown first overnight in LB supplemented with carbenicillin (100 µg/mL) and tetracycline (12 µg/mL). Overnight

cultures were diluted (80 μ L overnight culture to 1 mL fresh LB carb/tet) and allowed to grow for 5.5 h at 37 ° C. NGM RNAi plates were seeded with 5.5 h cultures and dried, then allowed to sit at 21° C overnight to allow induction of dsRNA production by IPTG. Plates were stored at 4° C for up to a week before use.

Worm strains

Worms strains used in this study are listed in Table I. N2, VC1599, RB662, TU3335, JJ1271[glo-1(zu391)], glo-2(zu445), GH378[pgp-2(kx48)], were obtained from the Caenorhabditis Genetics Center (CGC, USA).

Ethyl Methanesulfonate (EMS) Mutagenesis Screen

Adapted from *Jorgensen et. Al (2002)*.⁷⁹. Synchronized worms were grown axenically in mCeHR-2 media in a T-25 flask. Once worms reached the early L4 stage, media was moved from the flask to a 15 mL conical tube. The worm suspension was washed three times (one wash consists of spinning at 800 g for 5 m, followed by resuspension in 10 mL M9). For the final wash, the worm suspension was resuspended in 2 mL M9. In a laminar flow hood, 0.1 M EMS was made by adding 20 μ L liquid EMS (Sigma #M-0880) to 2 mL M9 buffer. The solution was gently inverted until EMS dissolved. The 2 mL worm suspension and 2 mL 0.1 M EMS was combined for a final volume of 4 mL of 50 mM EMS and worm suspension. The 15 mL conical was closed loosely to allow gas exchange, and put inside a container in a 20 ° C incubator rocking at 70 RPM for 4 h. Following 4 h 50 mM EMS treatment, worms were washed twice with M9 as described above and moved back to a T-25 flask containing mCeHR-2 and allowed to grow. All EMS contaminated material (pipette tips, tubes, gloves, etc.) was soaked in EMS

inactivating solution (0.1 M NaOH, 20% w/v Na₂S₂O₃) for at least 24 h, and all EMS solution were mixed with equal volume EMS inactivating solution for 24 h.

ZnMP treatment

Worms were synchronized as L1s, and placed on 60 mm NGM plates seeded with OP50 supplemented with 30 μ M hemin chloride. Once at the early L4 stage, worms were collected from plates by washing off with 0.1 M NaCl, and were washed three times (settling worms on ice for 10 m, aspirating the supernatant, then re-suspending in 10 mL 0.1 M NaCl); following the final wash, worms were re-suspended to a volume \sim 500 μ L. ZnMP treatment was carried out 12-well plates containing 2 mL of mCeHR-2 per well. Each well contained 1.5 μ M hemin chloride, plus either 0 μ M or 50 μ M ZnMP. Worms were moved into wells at a final density of roughly 250 worms/mL. Worms were treated O/N (\sim 15hs) at 20 ° C, shaking at 70 RPM. Following treatment, worms were removed from wells and allowed to settle on ice for 10 m, then washed twice with 0.1 M NaCl. Worms were then allowed to gently shake for 10 m to flush the gut. Worm pellets were kept on ice until being mounted for microscopy. Worms were mounted on agar pads and treated with 1 mM NaN₃ for imaging.

Mapping:

Mapping cross experiment

Crossing plates consisted of 35 mm NGM plates with a 10 μ L spot of OP50 bacteria seeded in the center of the plate. Heme supplemented crossing plates used both 200 μ M hemin chloride added in the NGM agar, as well as in the LB OP50 culture. The P₀ generation consisted of fifteen Hawaiian *mrp-5(ok2067/o)* males and one late L4 suppressor mutant hermaphrodite. The P₀ were placed on a

heme supplemented crossing plate. The inclusion of an *mrp-5(+/+)* and *mrp-5(ok2067/ok2067)* (non-suppressor) were critical controls for downstream screening of F₂ recombinant lines for *mrp-5* suppression. Once F₁ progeny were laid, P₀ were picked off and genotyped to confirm their *mrp-5* allele, and their respective Hawaiian/N2 backgrounds. Each F₁ animal was picked clonally to 24-well NGM plates supplemented with 200 μM hemin chloride in the NGM. F₁ animals were observed, and the frequency of F₁ males was used as a relative gauge of mating success. Once F₁ hermaphrodites laid F₂ progeny, F₁ were genotyped for N2 and Hawaiian backgrounds as described. *Bona fide* cross progeny (heterozygous for Hawaiian and N2 background) were identified, and ~300 F₂ from true F₁ cross progeny were picked out clonally to 24-well NGM plates without heme supplementation. F₂ animals were allowed to grow and subsequently wells were screened for *mrp-5* suppression, indicated by hatching/growing F₃ animals. Around 50 recombinant F₂ lines and their F₃ progeny were pooled for sequencing.

Genomic DNA Extraction

Worms were collected from plates with M9; all pipetting of worms was done with glass Pasteur pipettes. Collected worm pellets were washed with 10x volume of TE five times to remove bacteria, and aspirated to a final volume of 100 μL. The pellet was sonicated with a Bioruptor on high setting, 30 s on, 30 s off for two 15 minute cycles. Next, 50 μL of Proteinase K (10 mg/mL) was added followed by incubation at 65 °C for one hour, until the solution was clear. Next, 20 μL of RNaseA (10 mg/mL) was added and then the solution was incubated at 37 °C for

30 m. Following incubation, the DNA purified with the Qiagen PCR purification kit, and eluted with 30 μ L TE. Quantification of DNA was done with PicoGreen (ThermoFisher).

Library Prep

Library construction was done with the NuGen Ovation SP+ Ultralow DR kit, using 50 ng sheared genomic DNA samples. Library integrity was checked by Agilent High Sensitivity DNA Assay Kit.

Sequencing

Sequencing was performed by Harold Smith at the NIDDK Genomics Core on an Illumina HiSeq 2500; at least 20x genome coverage (read depth) was obtained for each sample to ensure accurate variant calling. In addition to the three suppressors analyzed, the two parental strains were also sequenced (The N2; *mrp-5(ok2067/ok2067)* pre-mutagenesis strain to allow identification of novel EMS induced mutations, as well as Hw; *mrp-5(ok2067/ok2067)* background which contains the paternal contribution for the mapping cross).

Sequencing Analysis

All downstream analyses of the gripped FASTQ files were performed using CloudMap⁸⁰. First, FASTQ files were concatenated for each sample sequenced. Variants present in **either** parental strains [Hawaiian; *mrp-5(ok2067/ok2067)* (paternal strain) or N2; *mrp-5(ok2067/ok2067)* (pre-mutagenesis strain)] were subtracted using “CloudMap Subtract Variants workflow (1 set candidates, 2 sets variants to subtract)” workflow published by gm2123⁸⁰ to constrain the set of variants to those induced by EMS. Using the output from this workflow, all other

analysis was conducted using the “CloudMap Hawaiian Variant Mapping with WGS and Variant Calling workflow” published by gm2123⁸⁰.

Genotyping

All genotyping used the same single worm PCR protocol. Single Worm Lysis Buffer was prepared as a stock (50 mM KCl, 10 mM Tris-HCL pH 8.3, 2.5 mM MgCl₂, 0.45 % NP-40, 0.45 % Tween 20, 0.01 % Gelatin). Proteinase K was freshly added to lysis buffer to the final concentration of 1 mg/mL, and 5 µL of this solution was added to a 0.2 ml PCR tube. A worm was added to the lysis buffer in the tube, then placed at 80 °C for at least 2 h (can be stored at this step), then incubated for 65 °C for one hour, and then 95 °C for 30 m. For each PCR reaction, 2 µL of lysate was used as a template; if multiple reactions were necessary, lysate was diluted with sterile dH₂O up to 10 µL. General PCR conditions were 2 mM MgCl₂, 2 mM dNTPs, and 0.8 µM primers (each). Taq was used for polymerization.

Reaction steps:

1. 95 ° C, 2 m
2. 95 ° C, 30 s
3. 58 ° C, 30 s
4. 72 ° C, 90 s
5. 72 ° C, 10 m
6. 10 ° C, forever

Steps 2-4 were repeated for a total of 35 cycles.

- *mrp-5(ok2067)*

Primers:

1. 5' flank *mrp-5(ok2067)*: 5' – GAT GGC TCA AGA
AAG GAC ACG – 3'
2. 5' internal *mrp-5(ok2067)*: 5' – GGT ATT TGT TTC
ATG CTT CCG TGC – 3'
3. 3' flank *mrp-5(ok2067)*: 5' – AGC ATG ACT GTC
AAA AGT GCG – 3'

Two PCR reactions were used to genotype the *mrp-5(ok2067)* allele. The first reaction used primers 1 and 3, and yielded a 1412bp fragment for *mrp-5(+)* and a 245bp fragment for *mrp-5(ok2067)*. The second reaction used primers 2 and 3 and yielded a 327bp fragment for *mrp-5(+)*, and no product for *mrp-5(ok2067)*.

Below is a summary in tabular form.

	5' flank + 3' flank	5' internal + 3' flank
<i>mrp-5(+)</i>	1412 bp	327 bp
<i>mrp-5(ok2067)</i>	245 bp	no product

○ *apb-3(ok429)*

Primers:

1. 5' flank *apb-3(ok429)*: 5' – GAA TTG GAG TGC TGC
TTG GT – 3'
2. 5' internal *apb-3(ok429)*: 5' – AAC CGA TTT TAG
GGT AGC ACA A – 3'

3. 3' flank *apb-3(ok429)*: 5' – GCC CGT TTC CTT CAA
TTA CA – 3'

Two PCR reactions were used to genotype the *apb-3(ok429)* allele. The first reaction used primers 1 and 3, and yielded a 1688bp fragment for *apb-3(+)* and a 622bp fragment for *apb-3(ok429)*. The second reaction used primers 2 and 3 and yielded a 407bp fragment for *apb-3(+)*, and no product for *apb-3(ok429)*. Below is a summary in tabular form.

	5' flank + 3' flank	5' internal + 3' flank
<i>apb-3(+)</i>	1688 bp	407 bp
<i>apb-3(ok429)</i>	622 bp	no product

○ **N2, Hawaiian genotyping for mapping cross**

Protocol for genotyping Hawaiian background from N2 background by snip-SNPs was adapted from Davis, et. Al.⁸¹ Specifically, an N2 specific snip-SNP on clone T24B8 (CHII at position 9,052,466; wormbase ID: snp_T24B8[1]) and a Hawaiian specific snip-SNP on clone F56C9 (CHIII at position 7,320,107; wormbase ID: snp_F56C9[1]) were used. Described primers⁸¹ were used, and PCR was conducted as described except that 0.4 μM each primer was used, the annealing temperature was 60 °C (step 3), and elongation time was 1 minute (step 4). A 16 μL digestion which consisted of 1.6μL 10x CutSmart (NEB), 0.1μL

DraI (NEB), 4.3μL sterile dH₂O, and 10μL PCR product (directly from PCR reaction, no cleanup) was incubated overnight at 37°C. Both digested and un-digested (PCR product) products were analyzed by 2% agarose gel. The N2 specific snip-SNP snp_T24B8[1] reaction produces a 494bp fragment, which upon DraI digestion yields 373bp and 121bp fragments. The Hawaiian specific snip-SNP snp_F56C9[1] reaction yields a 486bp fragment, and upon DraI digestion results in 354bp and 132bp fragments.

	N2	Hawaiian	N2/Hawaiian
snp_T24B8[1]	373bp + 121bp	494bp	494bp + 373bp + 121bp
snp_F56C9[1]	486bp	354bp + 132bp	486bp + 354bp + 132bp

Assay for RNAi suppression of *mrp-5(ok2067/ok2067)* lethality

RNAi was conducted as specified, except that RNAi was conducted for a generation on high heme, and the progeny were moved to the same RNAi conditions with no added heme. In detail, P₀ gravid worms were picked clonally onto RNAi plates with 200 μM heme added to the NGM (after cooling, before pouring). The worms were allowed to lay eggs (F₁) overnight and the P₀ gravid worms were picked off. The F₁ generation was allowed to grow until gravid, yielding adult F₁ worms grown for an entire generation

under high heme RNAi conditions. Adult F₁ worms were picked clonally onto fresh RNAi plates of the same condition, but without added heme. The worms were allowed to lay F₂ progeny overnight, and then the F₁ were removed. Plates were observed until F₃ worms reached adulthood, and then the entire population was analyzed by COPAS BioSort (Union Biometrica).

Combinatorial RNAi

Combinatorial RNAi was conducted the same as described, except that following 5.5 hour cultures of HT115(DE3), equal volumes of the two cultures (each containing bacteria designed to target a specific gene) were combined, mixed by vortex, then the normal volume of combined culture was used to seed the NGM RNAi plates. Worm strains used for these experiments all contained the RNAi hypersensitivity mutation *lin-15B(n744)*.

Worm Growth Assay

Populations of bleached and synchronized L1 worms were plated onto 10 cm NGM plates without any bacteria seeded. Three L1 worms (P₀) were picked into each well of a 12-well plate. Once gravid F₁ worms were observed in the positive control growth condition (either vector or vector +Heme, specified in figure description), all populations were analyzed as described by ReFLx on a COPAS BioSort (Union Biometrica).

Transcriptional Reporter under RNAi

Approximately 40 synchronized L1 worms of the indicated strain were placed into each well of a 12-well plate. Once gravid, populations were analyzed by ReFLx on a COPAS BioSort (Union Biometrica). For each individual event, the integral GFP was normalized to Time of Flight (TOF) to obtain the average intensity of GFP along the length of the

worm. All of the values for individuals in a given replicate (well) were then averaged, and the averages of the three replicates were averaged to give the value for one biological replicate.

ReFLx Analysis by COPAS BioSort (Union Biometrica)

Worms were washed from plates with ~1 mL M9 and transferred with a 9" glass Pasteur pipette to 1.7 mL eppendorf tubes. Worms were allowed to settle on ice for 15 m; the supernatant was then aspirated, and an additional 1 mL of M9 was added to the pellet; this constitutes one wash. Worm suspensions were washed once more, and then the supernatant aspirated to a remaining volume of ~100 μ L. These worm suspensions were then moved to a well in a 96-well plate. Samples of worm suspension were separated by three "blank" wash wells containing M9 only. All hits were filtered for EXT>30 to filter out debris. All conditions were tested in triplicate (three individual wells), and the arithmetic mean of these constituted one biological replicate.

Confocal

Confocal images were taken with a Zeiss LSM710 confocal microscope with a 63x oil immersion objective. Autofluorescence was visualized with excitation at 405nm, and emission through a DAPI filter. ZnMP and mCherry were visualized with excitation at 561nm and emission through a rhodamine filter. To calibrate DAPI filter settings for visualization of autofluorescence, N2 worms were used. Laser power was set at 1.0 and the gain was adjusted until intestinal cells showed autofluorescent punctae just below signal saturation. To calibrate rhodamine filter settings for visualization of ZnMP, N2 worms treated with vehicle (0 μ M ZnMP, NH₄OH) were used. Laser power was set at 1.0, and gain was adjusted until no signal was present. To calibrate rhodamine filter

settings for visualization of HRG-1-mCherry, IQ6112 worms treated with *hrg-1* RNAi as described were used. Laser power was set at 1.0, and the gain was adjusted until no signal was present.

Chapter 3: Results

A system of *mrp-5* deficiency

The first step towards conducting a forward genetic screen for suppression of deficiency of *mrp-5* was to identify a system of *mrp-5* deficiency which elicited a strong lethality phenotype. RNAi mediated knockdown of *mrp-5* in the parental generation results in heme dependent embryonic lethality in F₁ progeny, a phenotype exacerbated for embryos laid later (Figure 1). However, RNAi is not a suitable system to conduct a forward genetic screen because any gene capable of impacting the RNAi pathway could erroneously be classified as an *mrp-5* suppressor.

A deletion allele, *mrp-5(ok2067)*, was already available through the CGC (Figure 2). The *mrp-5* genetic locus is situated on the right arm of the X chromosome, between 14,945kb and 14,938kb. The *mrp-5(ok2067)* allele harbors a 1,167bp deletion which spans four exons. RT-PCR confirmed that this results in a truncated mRNA with an in frame 528bp deletion. Bioinformatic analysis of the truncated mRNA sequence indicated that the deletion of 176 amino acids contains three transmembrane domains. Wildtype MRP-5 consists of two membrane spanning domains each consisting of six transmembrane helices, as well as two ATP Binding Cassettes (ABCs) which must physically interact to catalyze ATP hydrolysis, allowing transport of a substrate. Topology modeling of the truncated MRP-5 shows that the second ABC would be flipped to the opposite side of the membrane from the first ABC, preventing interaction of the two cassettes making the truncated protein incapable of ATP hydrolysis. Thus, the resultant mutant protein would be unable to function in energy dependent transport.

In support of the assertion that *mrp-5(ok2067/ok2067)* worms would show phenotypes associated with *mrp-5* deficiency, worms homozygous for the deletion allele were non-viable, and the deletion was maintained as a balanced heterozygote as the strain VC1599. Subsequent isolation of *mrp-5(ok2067/ok2067)* worms under high heme conditions recapitulated heme-dependent lethality seen with RNAi of *mrp-5*. To further investigate the precise heme requirements of *mrp-5(ok2067/ok2067)* worms, homozygous mutants or their wildtype broodmate were grown in various levels of supplemented heme, and the viability of their offspring was scored by checking for embryonic lethality (Figure 3A). Embryonic lethality was observed at $\leq 80 \mu\text{M}$ supplemented heme, and total embryonic lethality was observed at $\leq 50 \mu\text{M}$ heme. It was also apparent that in addition to the viability defect of offspring, *mrp-5* deficiency resulted in delayed development (Figure 3B). By 93 h, F₁ embryos were already laid at $\geq 100 \mu\text{M}$ heme, while F₁ embryos did not appear on plates supplemented with $40 \mu\text{M}$ heme until 117 h. At the final time point of 167 h, worms with no supplemented heme were still at the L4 stage. The wildtype broodmate showed F₁ progeny hatching by 67 h regardless of heme supplementation (Figure 3B). Importantly, this assay also provided the growth conditions under which a forward genetic screen for suppression of lethality could be conducted. With heme supplementation $\leq 50 \mu\text{M}$, *mrp-5(ok2067/ok2067)* worms will not lay viable progeny.

A Forward Mutagenesis Screen for Suppression of *mrp-5(ok2067)* Lethality

EMS has been used extensively as a mutagen in forward screens in *C. elegans*⁸². It is an alkylating agent capable of inducing random single base pair transitions, as well as small indels, and even large intragenic deletions.⁸³ However, the majority of EMS

induced mutations consist of simple guanine (G) to adenine (A) transitions.⁸² EMS mutagenesis was conducted on ~20,000 early L4 P₀ *mrp-5(ok2067/ok2067)* worms, inducing germ line mutations (Figure 4). These germ line mutations were propagated through self-fertilization in the P₀, and appeared somatically as heterozygous mutations in the ~80,000 F₁, representing ~160,000 haploid genomes, or an eight-fold genomic coverage.⁸² Self-fertilization in the F₁ and subsequent screening of the F₂ on NGM plates supplemented with 30 μM heme yielded 32 suppressors which laid viable F₃ progeny (Figure 4).

Given the relatively large number of suppressor lines isolated, a strategy was necessary to prioritize the mapping of suppressor mutants. Typically when a genetic screen reaches saturation, there is a potential for the generation of allelic suppressors. Independently mapping allelic suppressors would be a waste of resources, and testing for genetic complementation is a straightforward means of identifying allelic suppressors and prioritizing mapping to identify suppressor alleles in unique genes.^{82,84} This assumes suppression is recessive, and involves intercrossing of suppressor lines to check if heterozygous progeny for paternal/maternal suppressor alleles maintain or lose suppression; if suppression is maintained, one possible conclusion is that the two suppressor alleles are in the same gene. It quickly became clear that this approach would not be pragmatic in the case of analyzing these mutants, due to the fact that *mrp-5(ok2067/O)* males are defective in mating (Figure 5). As hermaphrodites, *mrp-5(ok2067/ok2067)* worms mate normally with wildtype males (Figure 5A-B), indicating the defect is paternal. Furthermore, there are no issues with self-fertilization indicating that their sperm are functional. Although *mrp-5(ok2067/O)* males display well

characterized mating behaviors⁸⁵, there is a possibility that there is a defect in sperm motility or the male mating apparatus. Indeed, *mrp-5(ok2067/O)* males exhibit stunted fan formation, reduced number of rays, and potentially defective spicule retraction (Figure 5C). Interestingly, although suppressor mutants are capable of suppressing *mrp-5(ok2067)* associated lethality, they are still deficient in mating and heme supplementation does not rescue the mating defect (Figure 5B). It is possible that *mrp-5* plays additional roles outside of its capacity in intestinal heme homeostasis and that genetic suppressors or heme supplementation do not overcome this function. It is also possible that the male tail defects are due to a background mutation which has remained linked to *mrp-5(ok2067)* though twelve backcrosses. Given that testing for genetic complementation among suppressors was not feasible, we adopted other means to prioritize mapping of suppressor mutants.

One obvious property to sort *mrp-5* suppressor mutants was to gauge the strength of their ability to suppress *mrp-5* growth deficiency (Figure 6). Worm viability in heme supplementation ranging from 0, 10, 20, and 30 μ M was assayed over several generations (P_0 , F_1 , F_2). Suppressor mutants were grouped by the lowest level of heme supplementation where hatching F_2 progeny were observed three days after P_0 removal. These parameters were chosen to given the highest level of stratification among the strongest suppressors.

Suppressor strains were named IQ1xxx. The first x indicates the lowest level of heme supplementation where viable F_2 were observed (10 μ M). The next two xx digits indicate an arbitrary designation within that group. IQ1001 is not necessarily a stronger suppressor than IQ1005, but both are stronger than IQ1301. The stronger phenotypes

would be preferable for initial mapping due to the fact that a strong suppression would be most evident in a mapping cross experiment. Subsequent analysis of suppressor strains prior to mapping was therefore generally restricted to stronger suppressors.

Since *mrp-5* suppressor mutants exhibit the ability to grow in low heme conditions insufficient for *mrp-5* mutant growth, we reasoned that this is due to a rescue of heme efflux from the intestine. Previous work demonstrated that loss of *mrp-5* results in reduced toxicity when exposed to a toxic heme analog, gallium protoporphyrin IX (GaPPIX), indicating that MRP-5 is capable of effluxing GaPPIX and that retention of GaPPIX in the intestine attenuates its toxicity.⁴⁰ Presumably, rescue of intestinal heme efflux would also result in a reversion to wildtype lethality upon GaPPIX exposure. A GaPPIX lethality growth curve was conducted to establish ideal conditions, and GaPPIX lethality in suppressor mutants was tested (Figure 7B). All *mrp-5* suppressors tested showed a reversion of GaPPIX lethality to wildtype levels. Interestingly, stronger suppressors (IQ10xx) showed higher lethality than most intermediate suppressors with the exception of IQ1207 (IQ11xx, IQ12xx) indicating that *mrp-5* suppression is due to a restored efflux of heme from the intestine and the degree to which heme efflux is rescued is also reflected in the toxicity of GaPPIX. It is possible that IQ1207 is a strong suppressor in terms of the rescue of porphyrin efflux, but that there is another background mutation which is limiting its growth. The readout of these assays depend on whether intestinal porphyrin efflux is occurring by assaying phenotypes associated with delivery to extra-intestinal tissues, but make no differentiation in the mechanism of this intestinal efflux. A phenotypic readout which depends on an intermediate step in

intestinal porphyrin efflux would be more likely to highlight distinct mechanisms of suppression in these mutants.

One such assay is metabolic labeling with the fluorescent heme analog, zinc mesoporphyrin (ZnMP). ZnMP treatment has been used in *C. elegans* and other systems as a proxy to visualize heme trafficking.^{26,34,40,86,87} *C. elegans* accumulates ZnMP in intracellular punctae within the intestine. Loss of *hrg-1* or *mrp-5* increases the intensity of accumulation at these sites, while loss of *hrg-4* results in a loss of ZnMP signal.^{34,40} ZnMP treatment was carried out in *mrp-5(ok2067/ok2067)*, *mrp-5(+/+)*, and *mrp-5* suppressor mutant worms (Figure 8). As previously reported⁴⁰, *mrp-5(ok2067/ok2067)* worms show an increase in accumulation of ZnMP as compared to *mrp-5(+/+)* worms. Interestingly, of the five suppressors tested, there were two general phenotypes observed. IQ1003, IQ1004, and IQ1005 all showed a total loss of any ZnMP signal. In contrast, IQ1001 and IQ1002 both retained high levels of ZnMP accumulation (Figure 8). This result suggests that while all strains tested rescue heme efflux sufficiently to grow without heme supplementation, they appear to do so by at least two distinct mechanisms. In addition, it would be ideal to map suppressors of both phenotypes to maximize the likelihood of identifying non-allelic suppressors.

Hawaiian Variant Mapping of *mrp-5* Suppressor Mutants

With a small group of suppressors prioritized, the next step was to map suppressor mutations to a genetic locus. SNP-based deep sequencing offered a relatively high throughput means for identifying mutations in strains isolated from a forward genetic screen, and is widely used and well established in *C. elegans*⁸². The Hawaiian strain CB4856 (subsequently referred to as Hawaiian or Hw) as a mapping strain due to its high

level of sequence divergence among *C. elegans* wild isolates⁸⁸ (Figure 9). There is an average of one SNP per 1kb between the N2 and Hawaiian strains.^{82,89}

First, the *mrp-5(ok2067)* allele was introgressed from the N2 strain to the Hawaiian background through nine backcrosses, yielding a Hw; *mrp-5(ok2067/ok2067)* mapping strain. The mapping cross required crossing of this mapping strain and a suppressor mutant; however, this task was complicated by the fact that as previously stated, *mrp-5(ok2067/O)* males mate with a very low frequency. To circumvent this issue, all F₁ progeny of the mapping cross were clonally picked and subsequently genotyped for Hw/N2 SNPs. Only *bona fide* F₁ cross progeny which were heterozygous for Hw/N2 SNPs were used (Figure 10). We chose to map IQ1003, IQ1004, and IQ1005 due to the fact that they're all strong suppressors, and share a similar ZnMP phenotype (Figure 8).

We picked ~300 F₂ recombinant lines clonally to plates without added heme. F₂ worms were allowed to self-fertilize, and plates were screened for hatching of the F₃ generation. Under these low heme conditions, only worms capable of suppressing *mrp-5* lethality would lay viable F₃ animals. Each of the three suppressor mutants exhibited slightly less than 25% suppression of *mrp-5* embryonic lethality among recombinant F₂ lines as expected of a recessive suppressor. One possible explanation for this is that there are known incompatibilities between Hawaiian and N2 alleles. A well studied example is the *zeel-1, peel-1* interaction on the left arm of chromosome I where embryos homozygous for a naturally occurring deletion in *zeel-1* arrest if the paternal contribution contains a Hawaiian variant in *peel-1*. This is an unintentional selection and results in a bias towards N2 recombinants in this region.⁸⁸ Another, less likely explanation is that all three *mrp-5*

suppressor mutants are in fact multigenic rather than containing only a single suppressor allele.

At least 49 recombinant F₂ lines were pooled; greater than 50 recombinant F₂ lines have a minimal contribution in increasing the resolution of the mapping interval.^{82,90} Pooled recombinant F₂ lines were sequenced along with the paternal mapping strain (Hw; *mrp-5(ok2067/ok2067)*) and the original pre-mutagenesis strain (N2; *mrp-5(ok2067/ok2067)*). The online mutant analysis pipeline CloudMap⁸⁰ was used to analyze NGS data and construct mapping plots (Figure 11).

Identification of a region containing the putative suppressor allele, or mapping interval, requires the observation of a region of unexpected N2 linkage. Since the suppressor allele is linked to the N2 background, and only worms homozygous for this allele should survive screening, the suppressor allele region should show complete N2 linkage. In all *mrp-5* suppressor mutant sequences analyzed, there was a strong region of N2 linkage on the right arm of the X Chromosome at the *mrp-5* locus (~15Mb), fitting with, the fact that the *mrp-5* allele in this region was introgressed from the N2 background (Figure 11A-C). A putative mapping interval should be a region of complete N2 linkage of roughly two Mb (due to the number of recombinant lines sequenced).^{82,89,90} All mutants also showed a slight N2 linkage on the left arm of Chromosome I around 2.5Mb (Figure 11A-C), which corresponds to the previously described *zeel-1*, *peel-1* locus.⁸⁸ These regions were expected sites of N2 linkage and were initially not considered as regions containing suppressor alleles.

IQ1003 did not have any other regions of N2 linkage. In addition, the left arm of chromosome I showed a stronger bias than the other two mutants, and the peak of N2

linkage was around 1Mb rather than 2.5Mb near the *zeel-1*, *peel-1* locus (Figure 11A). For these reasons the mapping interval for the *mrp-5* suppressor allele *ih1003* was chosen as the first 2Mb on the left arm of chromosome I (Figure 11D).

IQ1004 showed a region of strong N2 linkage centered at 4Mb on chromosome II (Figure 11B). The mapping interval for the *mrp-5* suppressor allele *ih1004* was chosen as 3-5Mb on chromosome II (Figure 11D).

IQ1005 showed no strong linkages to N2 anywhere except the X chromosome (Figure 11C). In addition to the *mrp-5* locus ~15Mb, there was a region of strong N2 linkage on the left arm of the X chromosome centered around 1Mb; neither of the other two mutants analyzed showed any linkage on the X chromosome besides the *mrp-5* locus. Thus the mapping interval for the *mrp-5* suppressor allele *ih1005* was chosen as the first 2Mb of the X chromosome (Figure 11D).

The next step was to construct a list of candidate suppressor alleles in each of these regions (Figure 11E). The snpEff function in the workflow used for mutant sequence analysis⁸⁰ predicts the effect of a SNP at the protein level. Effects most likely to disrupt normal protein function were prioritized as candidates, including mutations categorized as missense, nonsense, frameshift, or those likely to have an effect on mRNA splicing. IQ1004 had six candidate alleles, IQ1005 had four candidate alleles, and IQ1003 only had a single candidate allele in their respective mapping intervals. Interestingly, all three suppressor mutant candidate alleles included a unique subunit of adaptor protein complex 3 (AP-3), indicating a strong likelihood that all three suppressor mutants were in fact in the same class of *mrp-5* suppressors (Figure 11E).

The most straightforward means to identify which mutant allele is responsible for suppression of *mrp-5* was to conduct RNAi knockdown against each candidate in the original pre-mutagenesis strain, *mrp-5(ok2067/ok2067)*, under low heme conditions. Assuming that the suppressor allele is a loss of function mutation, RNAi knockdown of the true suppressor allele will recapitulate the suppression of *mrp-5* lethality in low heme, but no other candidate gene RNAi will have an effect. Although unlikely, it is possible that a gain of function mutation could be recessive. If this were the case, RNAi knockdown of the true suppressor allele in the suppressor strain would result in a loss of *mrp-5* suppression, but not in any other candidate. The former strategy was adopted first because it is more likely that a recessive suppressor allele is a loss of function. RNAi knockdown of the suppressor alleles in *mrp-5(ok2067/ok2067)* worms over two generations resulted in a suppression of *mrp-5* lethality for subunits of all four subunits of AP-3, but not in any other candidate gene (Figure 12). Although only three subunits of AP-3 (*apd-3*, *apm-3*, *aps-3*) were candidates, the fourth (*apb-3*) was included. The details of the molecular lesions in suppressor alleles *apd-3(ih1004)*, *apm-3(ih1005)*, and *aps-3(ih1003)* are described (Figure 13A-C). Mutants have previously been generated and are available from the CGC for *apd-3*, *apb-3*, and *apm-3*; however, this is the first reported mutant allele of *aps-3*. Likely, this is because its small genomic locus (619bp) makes it an unlikely target of random mutagenesis (Figure 13A).

AP-3 suppression of general *mrp-5* deficiency

The candidate verification in *mrp-5(ok2067/ok2067)* worms showed that RNAi induced deficiency of genes encoding AP-3 subunits was capable of suppressing lethality associated with *mrp-5(ok2067/ok2067)*, and that the same was true of the suppressor

alleles. To see if this is true of general *mrp-5* deficiency or if these suppressors were informational suppressor alleles, combinatorial RNAi of candidate suppressor genes was conducted with or without *mrp-5* (Figure 14). Subunits of AP-3, but no other candidates, resulted in a significant suppression of *mrp-5* RNAi induced loss of viability (Figure 14A). Additionally, RNAi knockdown of candidate genes in combination with vector had no impact on viability (Figure 14B) indicating that AP-3 subunit mutant alleles identified in our screen were directly responsible for the *mrp-5* suppression. It also indicates that neither AP-3 subunits nor *mrp-5* are allele specific in this regard. Mutant alleles or RNAi of AP-3 are capable of suppressing lethality caused by *mrp-5* deficiency implying that AP-3 subunit mutants are bypass suppressors of *mrp-5* deficiency.

Testing of other Adaptor Protein Complexes

To test whether adaptor protein deficiency suppressing *mrp-5* deficiency was unique to AP-3 or if this was a general feature of adaptins, RNAi of genes encoding AP-2 and AP-1 subunits was conducted in *mrp-5(ok2067/ok2067)* worms (Figure 15). RNAi knockdown of genes encoding AP-2 subunits resulted in suppression of *mrp-5* loss of viability. However, RNAi knockdown of genes encoding AP-1 subunits had no effect on the *mrp-5* phenotype. To test this in a second system of *mrp-5* deficiency as well as to ascertain the impact of knockdown of these subunits alone, combinatorial RNAi was conducted against genes encoding AP-1 and AP-2 subunits with or without RNAi against *mrp-5* (Figure 16). In concordance with the *mrp-5(ok2067)* result, RNAi against genes encoding AP-2 subunits but not AP-1 subunits suppressed *mrp-5* RNAi lethality (Figure 16A). However, combination with vector RNAi demonstrated that knockdown of genes encoding AP-1 subunits is lethal, while knockdown of genes encoding AP-2 subunits

resulted only in mild brood size reduction (Figure 16B). These experiments demonstrate that although only genes encoding subunits of AP-3 were identified in the suppressor screen, RNAi knockdown of genes encoding AP-2 subunits also results in a suppression of *mrp-5* lethality. However these experiments do not sufficiently address whether AP-1 may have the same capacity due to the fact that RNAi of a gene encoding an AP-1 subunit is lethal. This question could potentially be probed in the future by starting AP-1 knockdown later in development rather than from the L1 stage.

Effect of AP-3 Subunit loss on Systemic Heme Status

The fact that loss of AP-3 seems to rescue worm viability as well as reversion to GaPPIX toxicity in the absence of *mrp-5* indicates that loss of AP-3 subunits in an *mrp-5* deficient background results in a restoration of porphyrin efflux from the intestine. To test if heme levels in extra-intestinal tissues are truly restored, we looked for a rescue of tissue specific heme deficiency signals. First, the effect of combinatorial RNAi was examined in an *hrg-1* transcriptional reporter strain, IQ6015 (Figure 17). Despite being transcribed in the intestine, *hrg-1* promoter activity acts as a reporter of whole animal heme status, and is inversely correlated with heme levels.^{39,41} As expected, knockdown of *mrp-5* results in an increase in GFP signal.⁴⁰ Knockdown of genes encoding AP-3 subunits does not have a significant impact on *hrg-1* transcription alone (with vector). Additionally, no subunit is able to significantly suppress the increased signal due to *mrp-5* RNAi, although *aps-3* RNAi resulted in a consistent mild attenuation of *hrg-1* promoter activity, which was statistically insignificant.

To examine the effect of AP-3 subunit deficiency on an extra-intestinal reporter, the same assay was carried out in a strain containing an *hrg-2* translational reporter

driven by the *hrg-2* promoter, IQ8125 (Figure 18). The *hrg-2* promoter is active in the hypodermis, and is negatively regulated by heme.^{40,76} A caveat here is that since this is a fusion protein it is not equitable to the transcriptional reporter if there are any post-translational effects. As expected, *mrp-5* RNAi caused an increase in HRG-2-YFP signal, indicating hypodermal heme deficiency. Dietary supplementation of heme but not knockdown of AP-3 subunits suppressed this hypodermal heme deficiency signal. These experiments indicate that while AP-3 subunit mutants are capable of suppressing macroscopic *mrp-5* phenotypes such as lethality, they do not show suppression of heme responsive reporters. Given that *mrp-5* RNAi growth defects were rescued by supplementing ≥ 50 μ M heme but *P_{hrg-1}::gfp* remained active with ≥ 500 μ M heme supplemented, this result is not unsurprising.⁴⁰

To get a more complete picture of tissue heme status independent of signaling, a similar experiment was conducted on genetically encoded tissue specific HRP reporters. HRP requires heme as a cofactor for activity and HRP activity is a measure of heme availability in the secretory pathway.⁷⁷ IQ6351 contains an ER targeted HRP driven from the constitutive, intestine-specific promoter of *vha-6⁹¹*, and IQ6352 contains the same transgene but driven from the hypodermis-specific promoter of *dpy-7^{77,92}*. Combinatorial RNAi against genes encoding AP-3 subunits and *mrp-5* or genes encoding AP-3 subunits alone (+vector) was carried out in these strains (Figure 19). In the intestine, HRP activity was increased with the knockdown of *mrp-5*, consistent with previous results.⁷⁷ There was a mild increase in HRP activity in the knockdown of some AP-3 subunit genes, and interestingly, all AP-3 subunit genes except *aps-3* showed an additive increase in activity when knocked down in combination with *mrp-5* (Figure 19A). In the hypodermal

reporter, knockdown of *mrp-5* resulted in lower heme loading of HRP which is consistent with previous results.⁷⁷ As in the intestine, knockdown of AP-3 subunits resulted in a similar increase in HRP activity. In combination with *mrp-5* RNAi, knockdown of AP-3 subunits increased HRP activity compared to knockdown of *mrp-5* alone (Figure 19B). This indicates that in fact, AP-3 subunit deficiency does suppress the decrease in activity due to *mrp-5* deficiency. Notably the suppression is relatively mild and remains significantly lower than vector only conditions. This result could be the potential explanation for the lack of suppression of *mrp-5* heme deficiency signals as heme levels in peripheral tissues are restored to a sufficient degree to rescue viability but insufficient to suppress heme responsive reporters. Since the HRP readout is dependent on heme availability to an ER reporter, it is likely dependent on heme availability in the secretory system and may not be representative of total tissue heme status. AP-3 subunits are expressed ubiquitously⁹³, and RNAi knockdown of AP-3 subunit genes is systemic; thus, changes in heme availability in the hypodermis could be the result of mistrafficking of hypodermal heme stores to a secretory compartment rather than a reflection of a change in total hypodermal heme levels due to an increase in intestinal efflux. This could be addressed by tissue specific RNAi of AP-3 subunits in the intestine. These data indicate that loss of AP-3 causes an increase in heme efflux from the intestine which could be due to an increase in heme efflux specifically, or perhaps efflux of all materials is increased non-specifically.

To determine the specificity of AP-3 complexes on micronutrient trafficking, we analyzed *cua-1* mutants. Preliminary work in the Kim lab has demonstrated the copper exporter ATP7A has an ortholog in *C. elegans* which seems to show a conserved role as

an intestinal copper exporter and loss of *cua-1* is lethal.^{94,95} These parallels to heme trafficking and the ease of scoring suppression of a lethal phenotype made copper homeostasis an attractive system to gauge the universality of AP-3 mutant suppression of micronutrient export deficiency. RNAi against *cua-1* was conducted in N2 or *apb-3* mutants and the effect on viability was tested in normal and high copper as well as copper limiting conditions in the presence of BCS, a copper chelator (Figure 20). Vector RNAi conditions suggest that in ideal copper conditions, N2 and *apb-3* mutants show identical growth. However, *apb-3* mutants are less viable than N2 in extreme copper conditions. RNAi knockdown of *cua-1* resulted in decreased viability compared to vector, except with supplementation of copper. Interestingly, *cua-1* knockdown in *apb-3* mutants resulted in a complete loss of viability in any copper growth conditions (Figure 20). The primary interpretation from this result is that unlike in heme homeostasis, *apb-3* deficiency does not suppress loss of viability due to deficiency in intestinal export, but instead sensitizes them. Overall, these results suggest that AP-3 deficiency does not suppress deficiency in intestinal export for all micronutrients.

Gut Granules

The majority of work regarding AP-3 function *C. elegans* deals with its role in the biogenesis of gut granules, an intestine specific lysosome related organelle (LRO). AP-3 subunit mutants do not develop gut granules, an obvious phenotype due to the fact that gut granules are autofluorescent^{72,96} and a prominent feature of the worm intestine. Given that the AP-3 mutant *mrp-5* suppressors isolated from the screen showed a complete loss of ZnMP accumulation (Figure 8), we examined whether the lack of ZnMP vesicles and gut granules were correlated. Since backcrossing the suppressor mutants would be

problematic due to the poor mating of *mrp-5(ok2067/O)* males, we sought to reconstruct an AP-3 mutant *mrp-5* suppressor. An independently generated AP-3 subunit mutant strain RB662 (*apb-3(ok429/ok429)*) which was isolated in a screen for loss of gut granule (*glo*) mutants⁷⁰ was crossed to *mrp-5(ok2067/ok2067)* worms to yield IQ1901, as well as wildtype broodmates (1. *mrp-5(+/+); apb-3(+/+)*, 2. *mrp-5(+/+); apb-3(ok429/ok429)*).

To ascertain if there is a relationship between ZnMP vesicles and gut granules we exposed each of these strains with ZnMP and analyzed them by confocal microscopy (Figure 21). In wildtype worms, there is in fact an overlapping population of gut granules and ZnMP containing vesicles, and in *apb-3(ok429/ok429)* mutants there is no detectable signal for gut granules or ZnMP, irrespective of the *mrp-5* genotype. It has been reported that gut granules represent a terminal endocytic compartment, and that anything taken up through fluid phase endocytosis, such as TRITC-BSA, will localize to these compartments.^{70,97} However, loss of the heme importer *hrg-4* prevents ZnMP accumulation in the intestine, indicating that localization to these sites does not depend on a non-specific endocytic pathway.³⁴ Interestingly, although the *apb-3(ok429/ok429)* mutants have no gut granules, there appears to be autofluorescent material accumulated in the intestinal lumen (Figure 21). This phenotype was originally observed in a genetic screen for *glo* mutants, and the authors hypothesized that as a result of defective gut granule biogenesis, material normally trafficked to these organelles mistraffick to the plasma membrane, releasing their contents into the lumen (apical) or pseudocoelom (basolateral).^{70,97} Given that ZnMP accumulates in these vesicles, this possible mechanism could result in the intestinal efflux of heme in the absence of AP-3 activity in *mrp-5* mutants.

Intrigued by the role gut granules may be playing in intestinal handling of porphyrins, we sought to explore this relationship further. Is the suppression of *mrp-5* due to the loss of gut granules, or some upstream trafficking event mediated by AP-3? If the *mrp-5* suppression phenomenon is a direct result of gut granule loss (*glo*), then mutations in other *glo* genes would also result in a similar phenotype. We therefore tested the viability of *pgp-2*, *glo-1*, and *glo-2* mutants when exposed to *mrp-5* RNAi (Figure 22). While *glo-1* and *pgp-2* localize to gut granules and are required for their normal biogenesis, *glo-2* is a BLOC-1 complex subunit, which in mammalian cell lines has been shown to interact with AP-3 and be required for normal trafficking of AP-3 cargo⁹⁸⁻¹⁰⁰. However, *C. elegans* BLOC-1 seems to have functions in trafficking to gut granules independent of AP-3.⁷¹ As expected, mutations in AP-3 subunits *apd-3* and *apb-3* suppress *mrp-5* lethality without the addition of heme, while other *glo* mutants tested did not suppress *mrp-5* depletion. AP-3 subunit mutants do not show complete suppression; *mrp-5* RNAi results in a smaller population than vector treatment. Most interestingly, supplementation of heme does not improve the viability of AP-3 mutants like it does for N2 or other *glo* mutants (Figure 22).

Role of Other Heme Homeostatic Components in AP-3 Deficiency

Given that several components mediating intestinal heme trafficking have previously been identified^{34,40,41,43}, we determined the role of these when AP-3 is depleted. Given that ZnMP accumulates in gut granules and HRG-1 has been shown to co-localize with ZnMP vesicles³⁶, we examined whether loss of AP-3 may affect HRG-1 localization. IQ6112 worms, which express HRG-1-MCHERRY fusion protein, were exposed to RNAi against genes encoding AP-3/AP-2 subunits, and HRG-1-MCHERRY

localization was examined by confocal microscope (Figure 23). In wildtype worms, HRG-1-MCHERRY localizes to small vesicles near the apical surface, consistent with previous reports.³⁶ However, HRG-1-MCHERRY was not co-localized to autofluorescent vesicles, indicating that ZnMP accumulates in HRG-1 vesicles as well as gut granules and that these represent two distinct sites of ZnMP accumulation. Loss of AP-3 subunits resulted in a slight perturbation of apical concentration of HRG-1-MCHERRY vesicles. However, knockdown of genes encoding AP-2 subunits resulted in a more pronounced mis-localization of HRG-1-MCHERRY to enlarged punctae which were distinct from sites of auto-fluorescence. This result is consistent with our in silico observation that HRG-1 harbors canonical C-terminal sorting signals recognized by adaptins. However, the fact that mis-localization was more dramatic with loss of AP-2 implies that HRG-1 trafficking may be mediated by AP-2, which is generally responsible for trafficking of components from the plasma membrane to recycling endosomes, and suggests that HRG-1 may be recycling between the plasma membrane and an endocytic compartment.⁵¹ Interestingly, studies in other model organisms have indicated that in polarized cells, AP-2 mediates recycling from the basolateral plasma membrane⁵¹, which contradicts the generally conserved apical association of HRG-1 proteins.³⁴⁻³⁶ This could represent a functional divergence in *C. elegans* regarding a role of adaptins in mediating apical sorting, as indicated by the requirement of AP-1 for the normal apical sorting of PAR-6.¹⁰¹

Given that loss of adaptors appears to alter the function of heme homeostatic components, we determined if any known components are uniquely important in suppression of *mrp-5* lethality by AP-3 mutants. To test this, RNAi against *hrg-1*, *hrg-4*,

hrg-3, and *hrg-7* was conducted in the *apb-3;mrp-5* mutant strain IQ1901 and its three wildtype broodmates, and viability was assayed (Figure 24). As expected, loss of any component except *mrp-5* did not impact viability in wildtype worms (Figure 24A).^{36,40,41,43} Interestingly, *apb-3* mutants showed a general loss of viability when supplemented with high heme, indicating loss of AP-3 subunits results in susceptibility to heme toxicity (Figure 24B). This raises the possibility that loss of *apb-3* results in increased heme efflux, and that this efflux is unregulated, such that in high environmental heme *apb-3* mutants are incapable of attenuating efflux resulting in toxicity.

In *mrp-5* mutant worms (Figure 24C), viability is restored with supplementation of dietary heme. Unexpectedly, loss of *hrg-4* in *mrp-5* mutants causes a complete loss of viability which cannot be rescued by heme supplementation. The synthetic lethality between *hrg-4* and *mrp-5* which cannot be rescued by heme is the first report of a lethal *hrg-4* phenotype³⁶, and suggests a clear distinction between heme imported by HRG-1 and HRG-4. This is also unexpected due to the high level of redundancy of intestinal heme import in *C. elegans*. It appears that *hrg-1* and its paralogs *hrg-5* and *hrg-6* are not sufficient to act as heme importers in the absence of *hrg-4* if *mrp-5* is lost. A potential complication arises from the high homology between *hrg-1*, *hrg-4*, *hrg-5*, and *hrg-6*. If RNAi transitivity against *hrg-4* resulted in generation of secondary siRNA¹⁰² complementary to other *hrg* paralogs, it could result in an unintended knockdown of other *hrg-1* paralogs. In fact, previous work has indicated that *hrg-4* RNAi results in a decrease in *hrg-6* promoter activity³⁵. To differentiate between this being an *hrg-4* deficiency phenomenon and not an artifact of RNAi, *mrp-5* RNAi could be conducted in *hrg-4* mutants. However, the fact that *hrg-1* RNAi has no effect implies that RNAi

transitivity does not play a role in the off target knockdown of *hrg-4* by *hrg-1* RNAi treatment.

Surprisingly, *mrp-5; apb-3* double mutants (Figure 24D) showed a loss of viability with RNAi knockdown of *hrg-4*, *hrg-3*, and *hrg-7* in low heme. A possible explanation is that *hrg-3* and *hrg-7* have been reported to effect viability in low heme conditions.^{41,43} Thus lethality without heme supplementation could simply be due to the fact that simultaneous deficiency of AP-3 subunits and *mrp-5* results in relatively heme starved worms based on analysis of systemic heme status. Nonetheless, heme does not reverse the lethality due to *hrg-4* RNAi.

Figure 1: *mrp-5* RNAi embryonic lethality is increased later in a brood

(A) A protocol schematic for Figure 1B. (B) Approximately 10 synchronized L1 N2 worms (P_0) obtained from bleaching were placed onto 35 mm plates pre-seeded with HT115(DE3) bacteria expressed dsRNA against knockdown vector control or *mrp-5*. P_0 worms were moved to a fresh plate of the same conditions every 24 h following the observation of F_1 embryos.

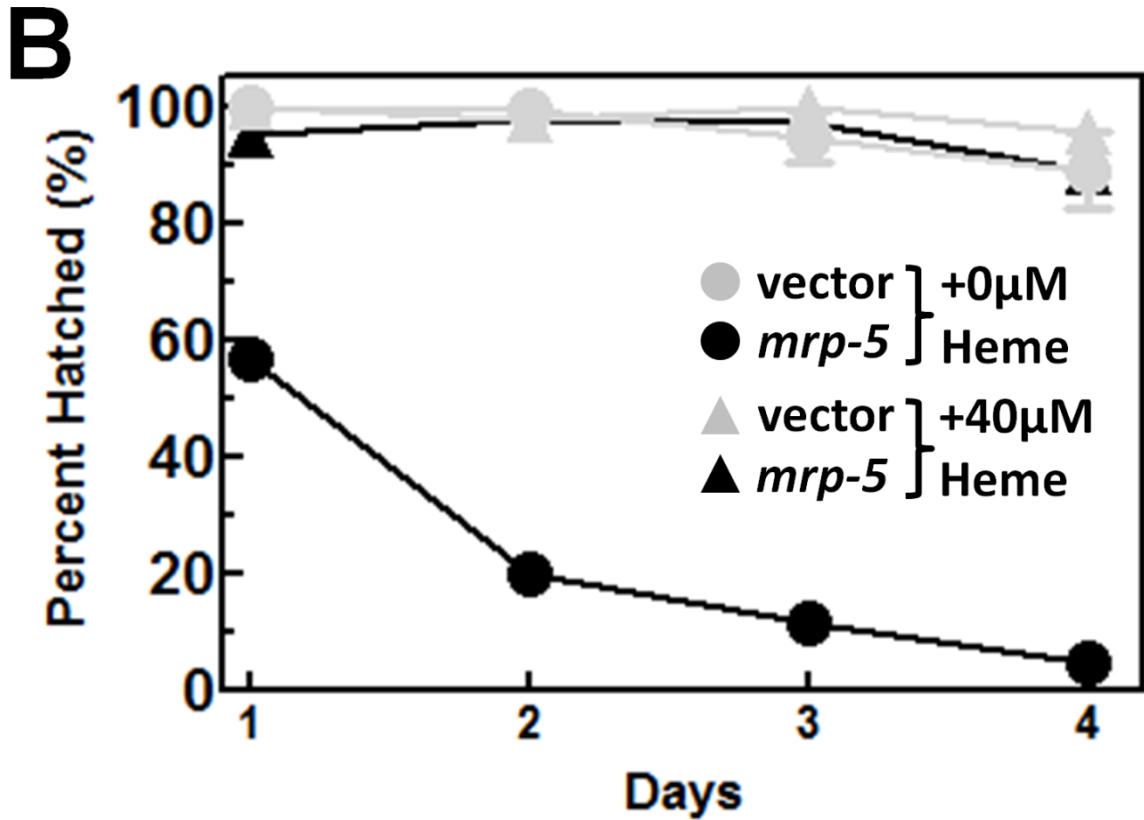
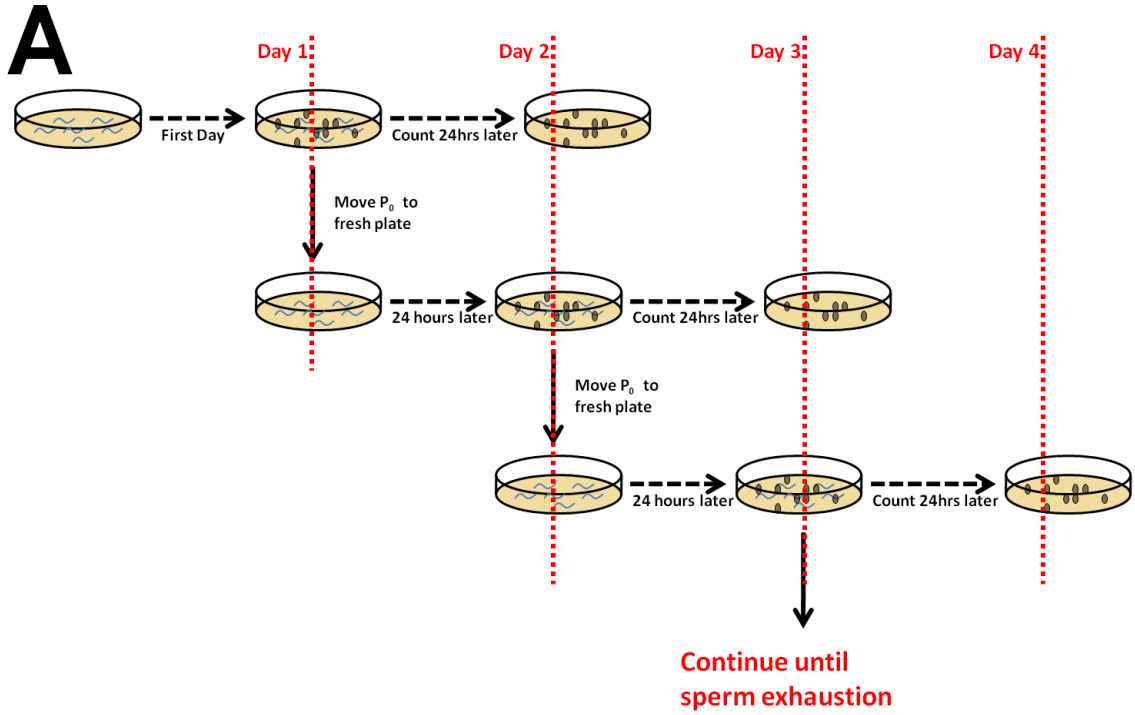


Figure 2: Genomic structure of *mrp-5(ok2067)* and putative protein topology

Picture of genetic locus was adapted from material obtained from www.wormbase.org; membrane protein topologies were generated using TMHMM 2.0¹⁰³ and drawn using TOPO2 (<http://www.sacs.ucsf.edu/TOPO2>). Deletion sequence was confirmed by RT-PCR.⁴⁰

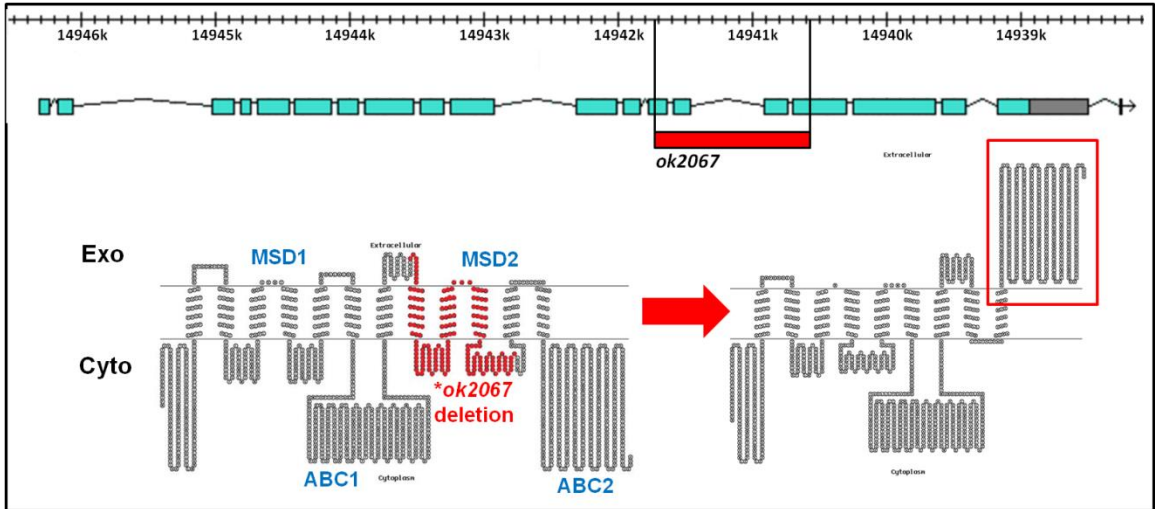


Figure 3: *mrp-5(ok2067/ok2067)* heme growth curve

(A) NGM agar plates were seeded with OP50 grown overnight in LB supplemented with the indicated concentration of hemin. Worms were maintained for one generation on 200 μ M heme NGM plates, and their progeny were synchronized. Approximately 50 synchronized L1 (P_0) were seeded onto each plate and observed daily. Once F_1 embryos were observed on a plate, P_0 were removed and hatching was scored 24 h later. No embryos were observed at 10 or 20 μ M heme. (B) During the course of the experiment described in Figure 3A, the P_0 generation duration was scored by duration between seeding of P_0 and observation of F_1 embryos.

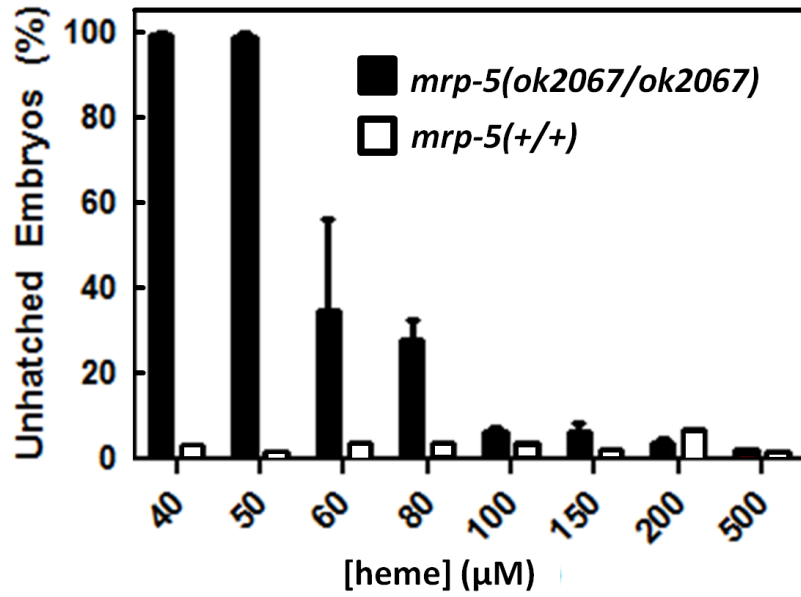
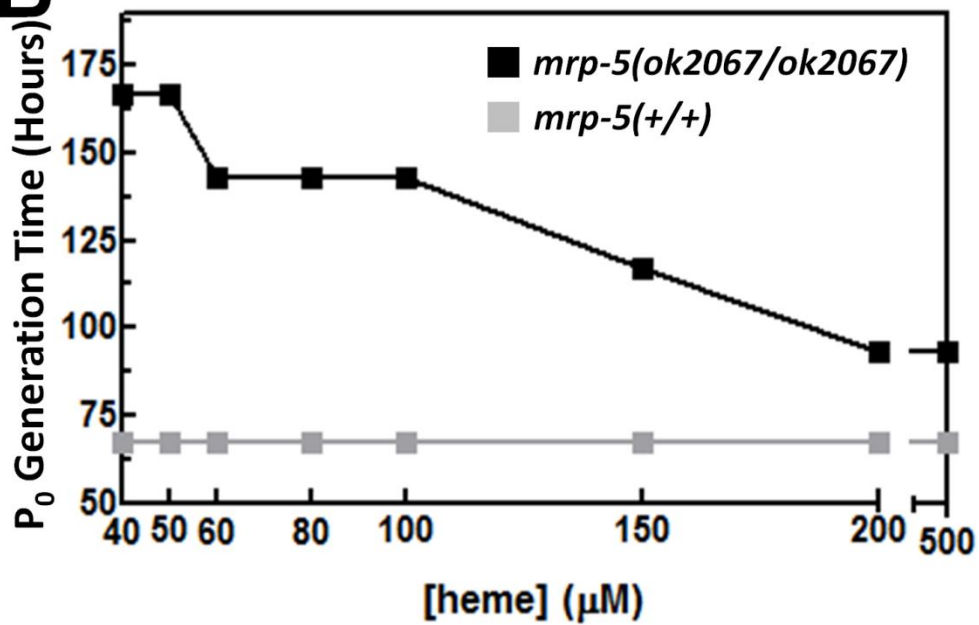
A**B**

Figure 4: EMS screen schematic

N2; *mrp-5(ok2067ok2067)* worms were maintained in axenic mCeHR-2 media supplemented with 200 μ M hemin. Following EMS treatment (see methods), mutagenized P₀ animals were moved back to axenic mCeHR-2 media supplemented with 200 μ M hemin and allowed to lay F₁ progeny. Gravid F₁ were bleached to isolate and synchronize the F₂ generation, which were then placed on 38 10 cm plates supplemented with 30 μ M heme. Viable F₃ were picked to fresh NGM plates seeded with 30 μ M heme OP50. Only lines capable of laying viable progeny after seven days were called *mrp-5* suppressors.

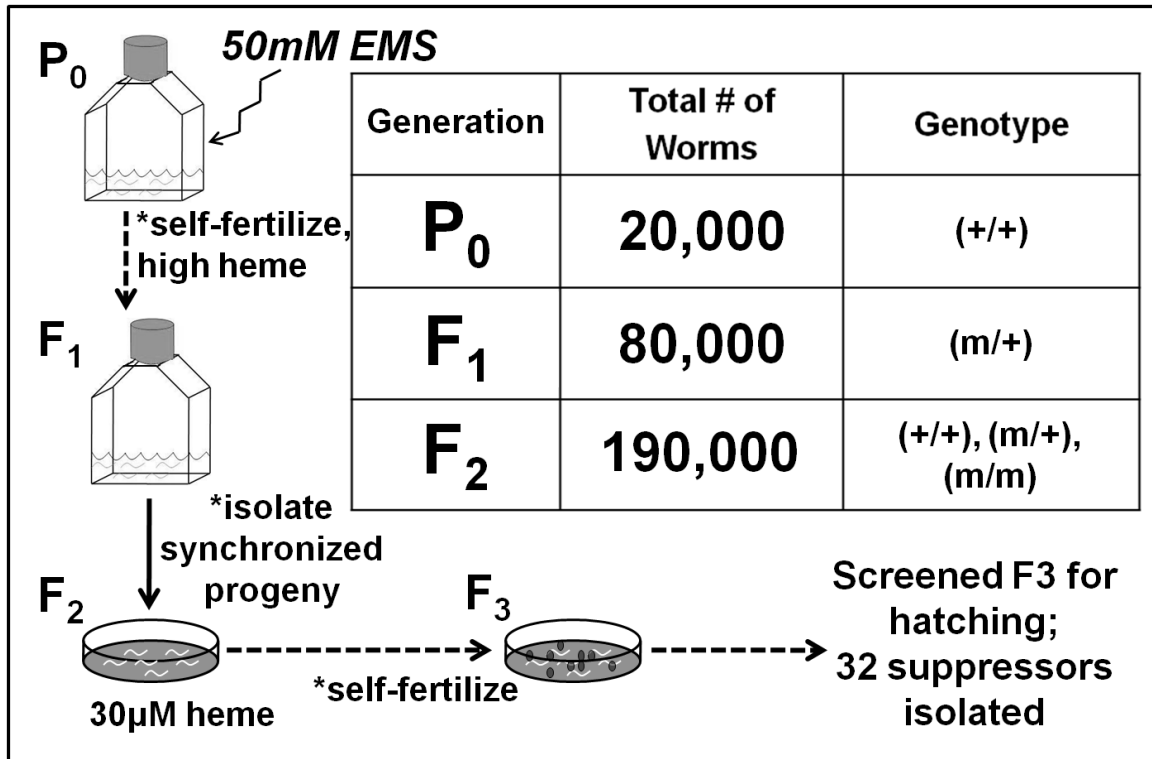


Figure 5: Mating deficiency in *mrp-5(ok2067/o)* males

(A) Mating plates consisted of 35mm NGM plates with a 10 μ L spot of 200 μ M hemin OP50 culture. Seven males of the indicated strain were picked onto a plate with one sperm exhausted N2 hermaphrodite. Presence of progeny was used as a measure of mating success due to the fact that hermaphrodites were sperm exhausted. (B) Mating plates consisted of 35 mm NGM plates where 200 μ M hemin chloride was supplemented directly to the NGM, and were seeded with a 10 μ L spot of 200 μ M hemin OP50 culture. Six males of the indicated strain were picked onto a plate with one virgin *unc-119* hermaphrodite, which have a high mating success due to their relative lack of locomotion. Once progeny were observed, all parents were removed from the plate by aspiration. Mating success was scored by checking if progeny contained males. (C) Males of both strains were grown for at least one generation on NGM agar plates directly supplemented with 100 μ M hemin. Males were placed onto agar pads with M9 and 1mM NaN₃. Images were taken using a DMIRE2 epifluorescence microscope (Leica) connected to a Retiga 1300 cooled mono 12-bit camera.

A

Male Strain	# with Progeny	# with No Progeny	Total
<i>mrp-5(ok2067/o)</i>	0	7	7
IQ1001	1	16	17
<i>mrp-5(+/+)</i>	12	1	13

B

Male Strain	# successful	# unsuccessful	Total
<i>mrp-5(ok2067/o)</i>	1 (<10% progeny)	18	19
<i>mrp-5(+/+)</i>	4	0	4

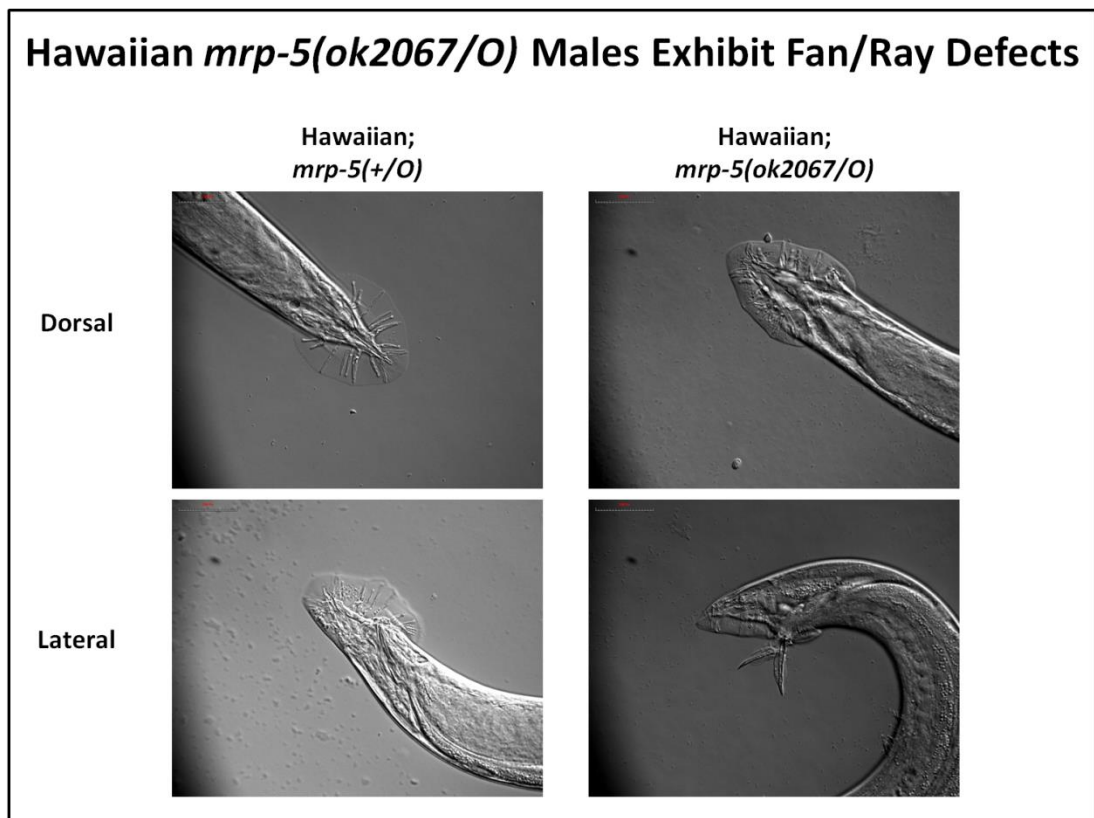
C

Figure 6: Suppression strength assay

(A) P₀ worms were grown on plates seeded with 100 μM hemin OP50. Three P₀ animals were moved as L4 larvae to plates supplemented with 0 μM, 10 μM, 20 μM, or 30 μM hemin. Once F₁ progeny were laid, P₀ worms were removed. Three days following removal of the P₀, the growth of the F₁ and hatching of F₂ was scored. Suppressor strains were categorized by the lowest concentration of heme supplementation where hatching F₂ progeny were observed three days following P₀ removal. (B) Representative photographs of IQ1001 (red in Figure 6A), *mrp-5(+/+)*, *mrp-5(ok2067/ok2067)*.

A

[heme] (μM)	Mutant #
0	IQ1001 , IQ1002, IQ1003, IQ1004, IQ1005
10	IQ1101, IQ1102, IQ1103
20	IQ1201, IQ1202, IQ1203, IQ1204, IQ1205, IQ1206, IQ1207
30	IQ1301, IQ1302, IQ1303

Mutants with no viable (hatched) F2 at 30 μM heme: IQ1401, IQ1402, IQ1403, IQ1404, IQ1405, IQ1406, IQ1407, IQ1408, IQ1409, IQ1410, IQ1411, IQ1412, IQ1413, IQ1414

B

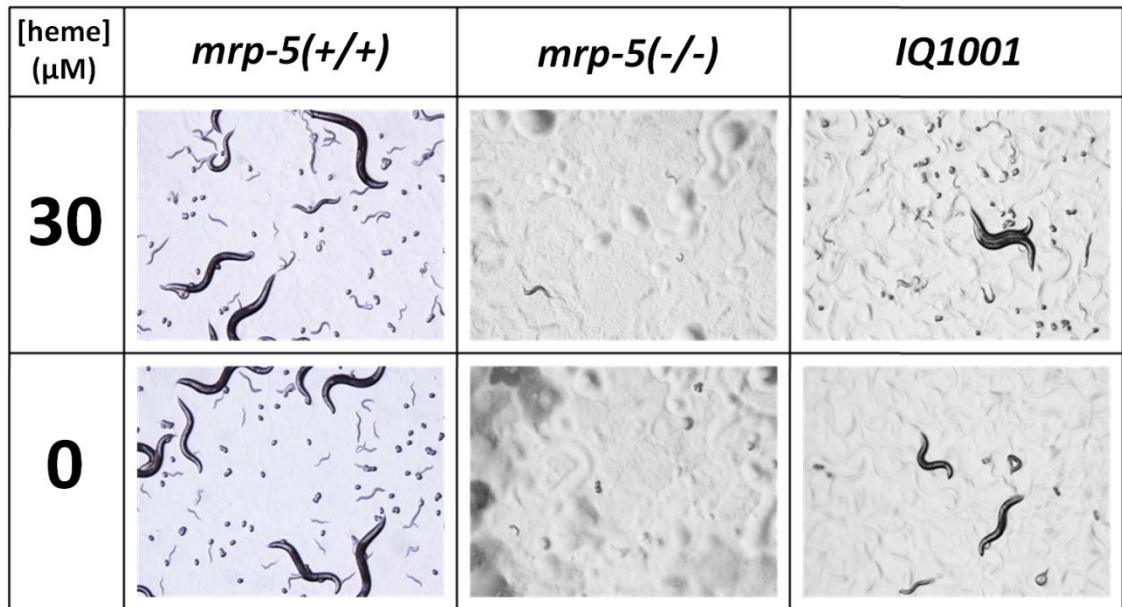


Figure 7: GaPPIX lethality in *mrp-5* suppressor mutants

(A) Gallium Protoporphyrin IX (GaPPIX) was directly supplemented to 35mm NGM agar plates, which were then seeded with 200 μ L OP50. Approximately 50 synchronized L1 worms were placed on plates at time 0, and lethality was scored at the indicated time points. Lethality was determined by a complete lack of movement and failure of a worm to respond to tactile stimulus. (B) Plates were prepared as described. All strains were maintained for one generation on NGM plates supplemented with 100 μ M heme, and their progeny were synchronized by bleaching and placed onto GaPPIX plates for the lethality assay.

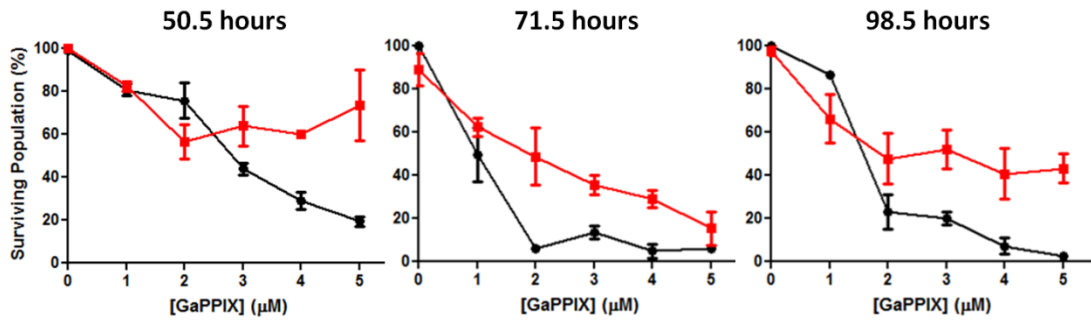
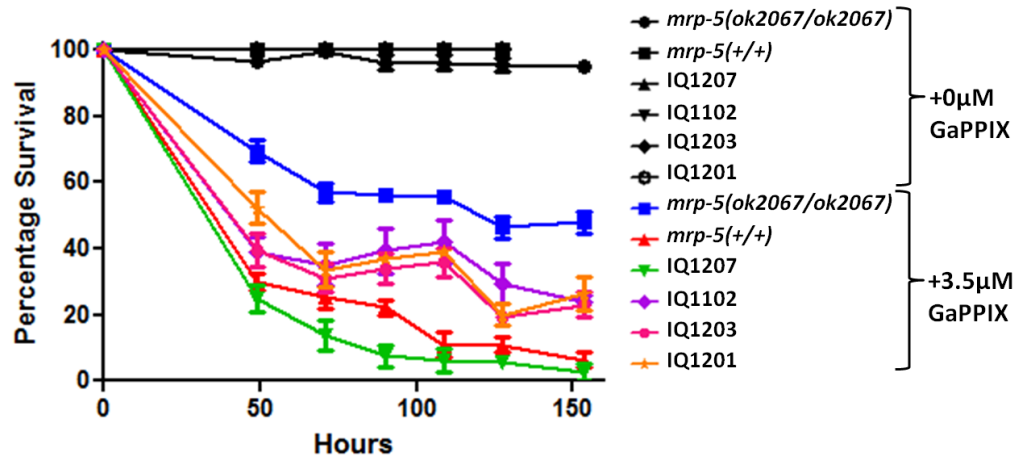
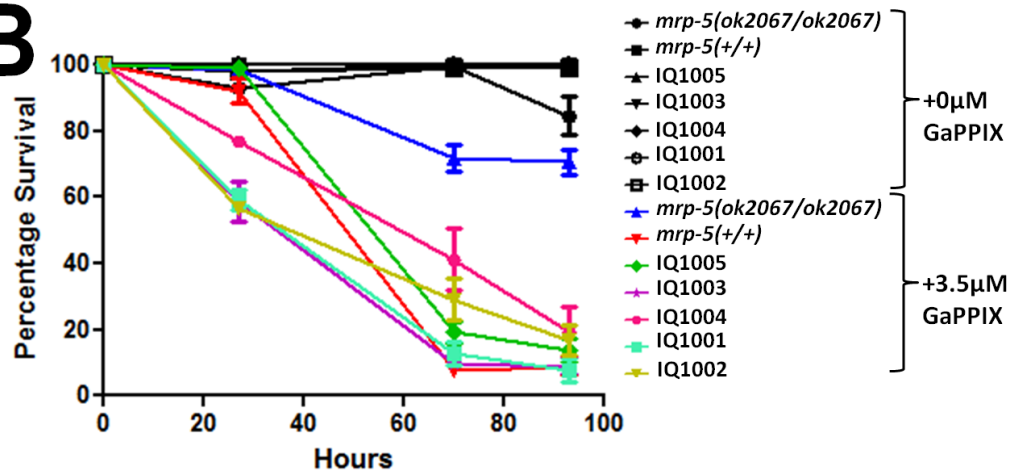
A**B**

Figure 8: ZnMP uptake in *mrp-5* suppressor mutants

The indicated strains were grown and treated with ZnMP as described. WT refers to the *mrp-5(+/+)* broodmate of *mrp-5(ok2067/ok2067)*, while *mrp-5* refers to *mrp-5(ok2067/ok2067)*. Images were taken using a DMIRE2 epifluorescence microscope (Leica) connected to a Retiga 1300 cooled mono 12-bit camera, and ZnMP signal was detected by rhodamine filter. Exposure time was calibrated with worms not exposed to ZnMP. Scalebar = 50 μ m.

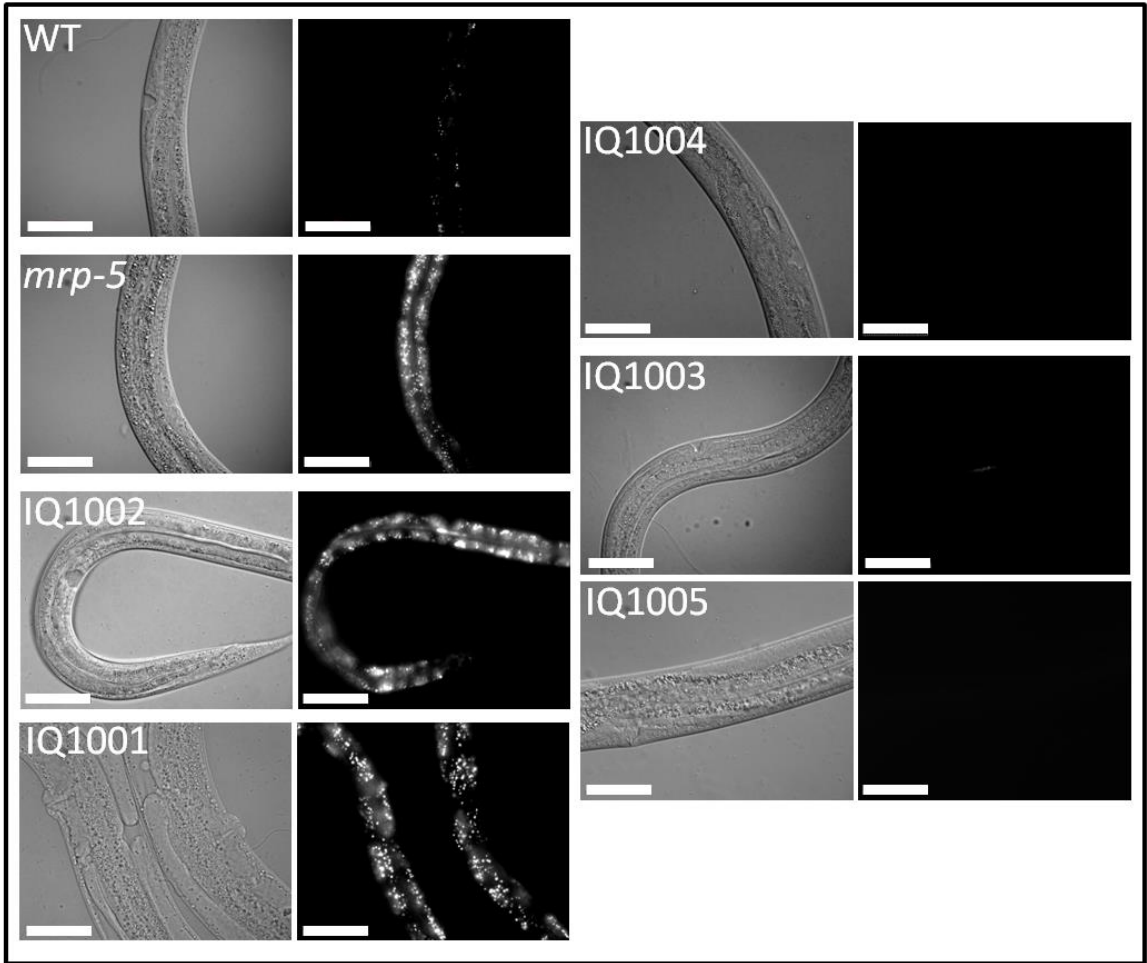


Figure 9: Hawaiian Variant Mapping Strategy

A general scheme for the Hawaiian Variant Mapping approach assuming the simplest case of a recessive suppressor. Paternal mapping strain (Hw; *mrp-5(ok2067/O)*) is crossed to a hermaphrodite suppressor mutant. F₂ progeny are picked clonally to low heme. Only F₂ recombinant lines homozygous for the suppressor allele will lay viable F₃. Pooling of recombinant F₂ lines and subsequent sequencing should reveal no bias towards either background at unlinked loci; linked loci should include *mrp-5* and the suppressor allele.

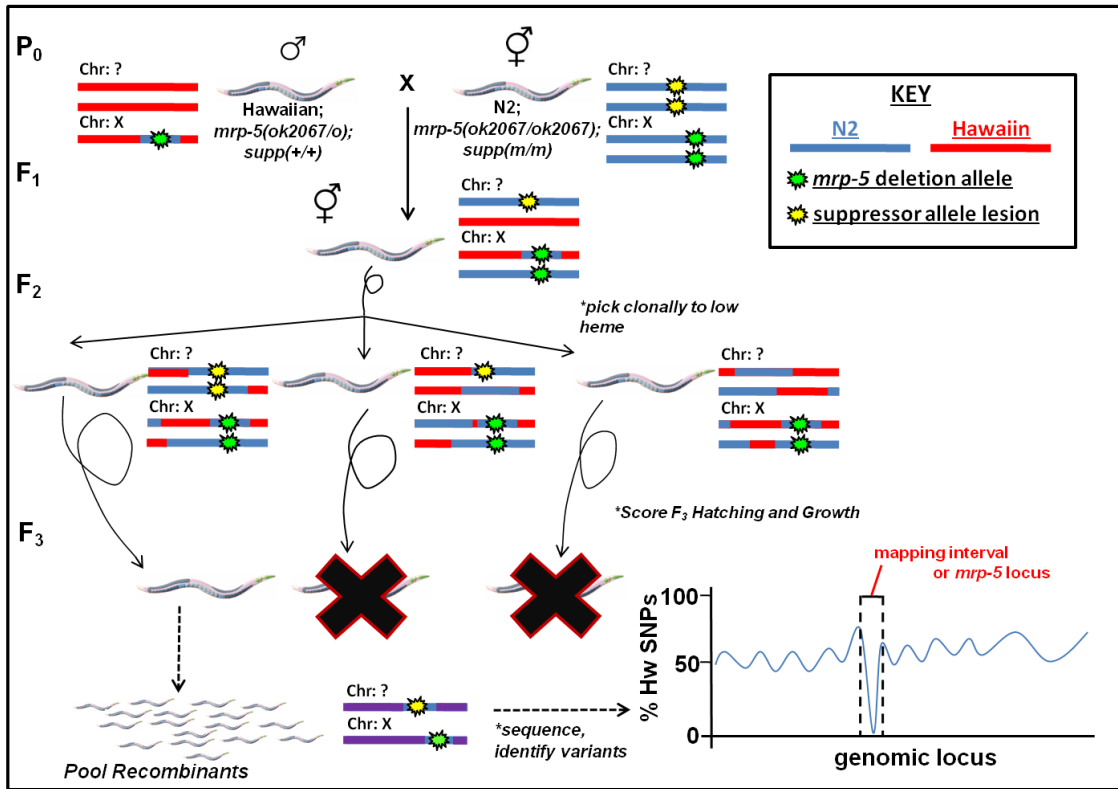
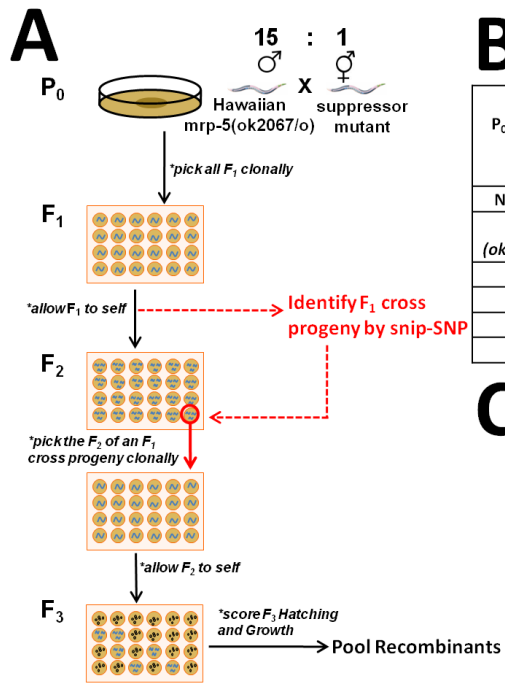


Figure 10: Hawaiian Variant Mapping – F₁, F₃ screening

(A) A schematic of the strategy for ensuring F₁ are the product of the indicated cross rather than self-progeny of the hermaphrodite. Genotyping for the background strain using snip-SNPs was conducted as described. (B) A report of screening of the F₁ screening containing the observed ratio of males and *bona fide* cross progeny confirmed by heterozygosity for Hawaiian and N2 SNPs. (C) A report of the ratio of suppression of *mrp-5* lethality for clonally picked F₂ recombinant lines.



B

P ₀ Herm. Strain	% Male of F ₁ Generation	# of F ₁ Herm. Genotyped	# of F ₁ Herm. Cross Progeny	% Cross Progeny of Genotyped F ₁
N2 <i>mrp-5(+/+)</i>	0%	9	0	0%
N2 <i>mrp-5(ok2067/ok2067)</i>	6.5%	38	4	10.5%
IQ1002	0%	9	0	0%
IQ1005	34%	28	28	100%
IQ1004	44%	7	7	100%
IQ1003	47%	13	12	92.3%

C

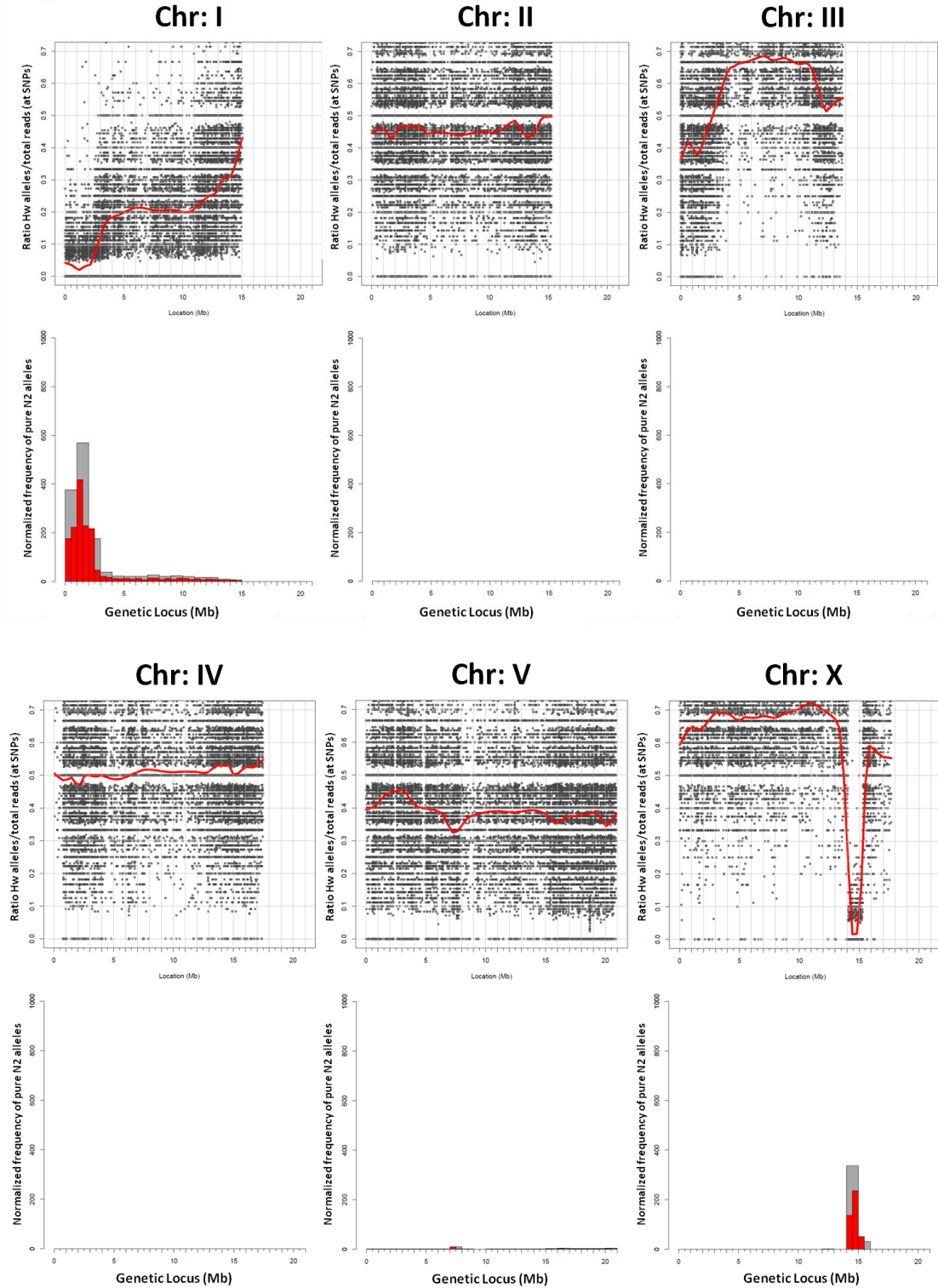
P ₀ Herm. Strain	# F ₂ wells growing	# F ₂ wells screened	% suppression of F ₂ Generation
N2 <i>mrp-5(ok2067/ok2067)</i>	0	242	0%
IQ1003	51	284	18.0%
IQ1005	49	287	17.1%
IQ1004	53	276	19.2%

Figure 11: Hawaiian variant mapping results – IQ1003, IQ1004, IQ1005

(A-D) All mapping plots were generated using “CloudMap Hawaiian Variant Mapping with WGS and Variant Calling workflow” published by gm2123⁸⁰ on the Galaxy web server. For a given chromosome (linkage group, LG), the top plot represents the ratio of Hawaiian to N2 versions of a SNP, where each black dot represents an individual SNP. The red line represents an LOESS regression line of the frequency of Hawaiian SNPs as a function of genetic locus. The bottom plot represents the frequency of pure N2 alleles over a given interval. Red bars represent bin size of 0.5Mb and grey bars represent bin size of 1Mb. The mappings plots for (A) IQ1003, (B) IQ1004, and (C) IQ1005 are shown. (D) The mapping intervals for each strain are summarized. (E) Candidate genes generated by compiling all genes containing missense, nonsense, frameshift, or splicing variants (predicted by snpEff function of “CloudMap Hawaiian Variant Mapping with WGS and Variant Calling workflow” published by gm2123⁸⁰) within the indicated mapping intervals for each suppressor mutant.

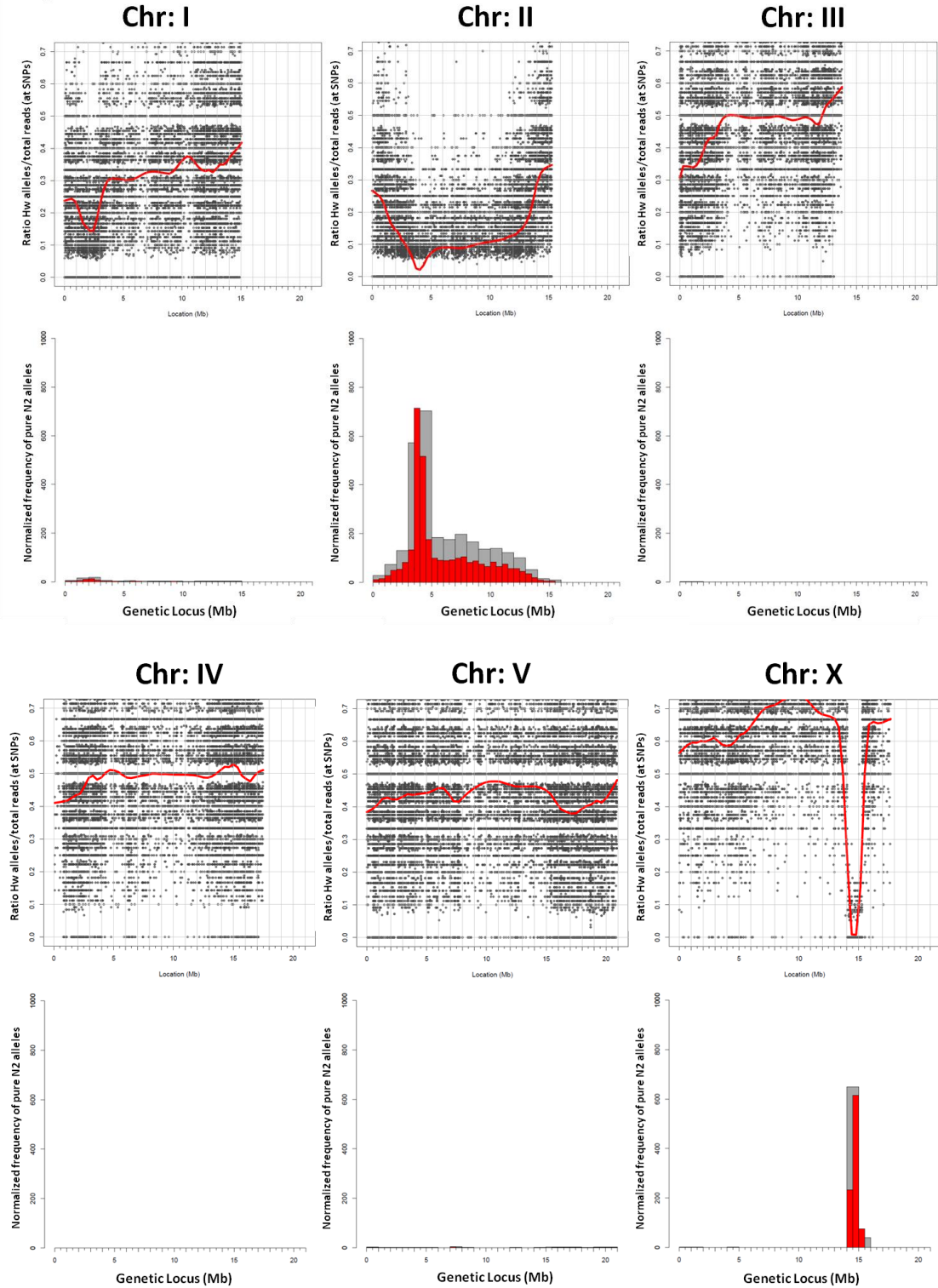
A

IQ1003



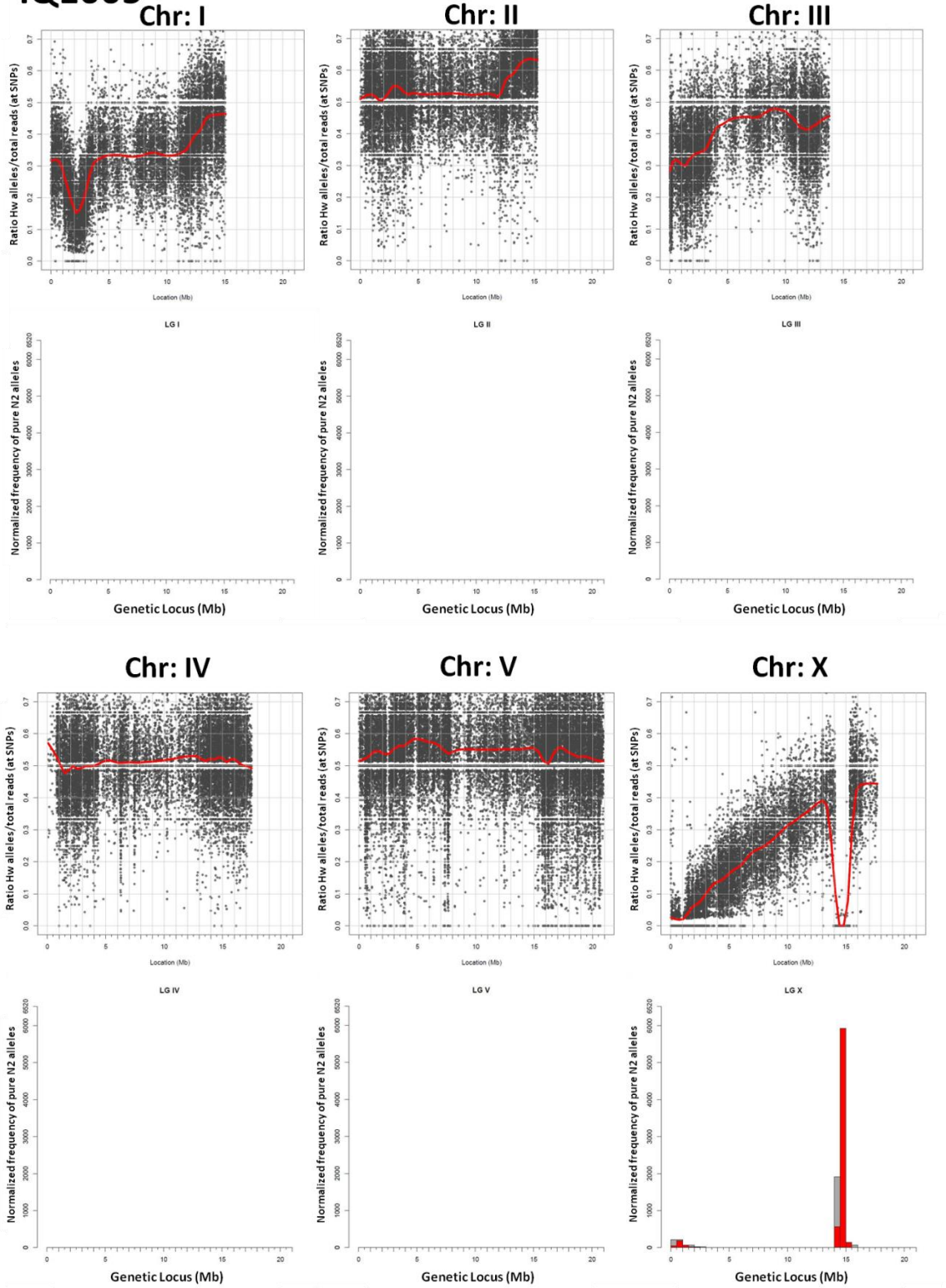
B

IQ1004

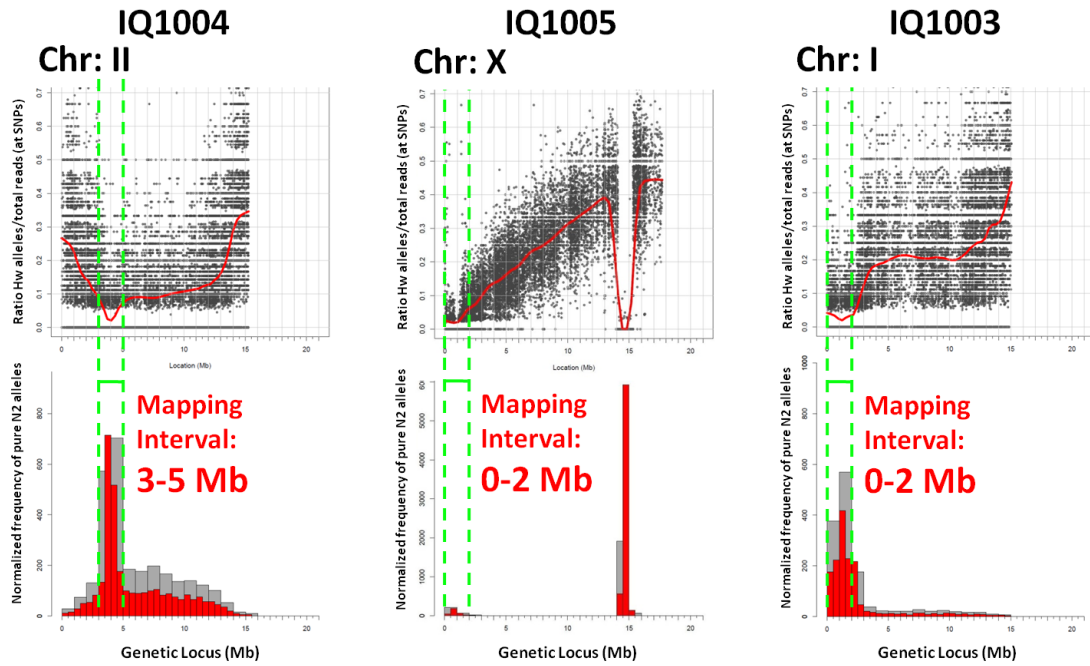


C

IQ1005



D



E

Candidate gene(s):

IQ1004

- *apd-3* – delta subunit of AP-3
- *W10G11.19*
- *F19B10.10*
- *C17A2.7*
- *F56D3.1*
- *lat-2* – latrophilin receptor

IQ1005

- *nas-38* – astacin like metalloprotease
- *apm-3* – mu subunit of AP-3
- *H11E01.3*
- *F07G6.3*

IQ1003

- *aps-3* – sigma subunit of AP-3

Figure 12: Candidate testing by RNAi in *mrp-5(ok2067/ok2067)*

RNAi against candidate genes was conducted for a generation on 200 μ M heme NGM plates, and these adults were moved clonally to the same RNAi conditions without heme supplementation, allowed to lay progeny overnight, then removed. The positive control condition was observed until the second generation reached adulthood, and then the entire population for all treatments was analyzed by COPAS BioSort (Union Biometrica). Data represents averages of three technical replicates from two independent experiments, where all populations were normalized as a percentage of the vector +200 μ M Heme condition. Indicated significant differences compared to the vector treatment were obtained by post-hoc multiple means comparisons utilizing Bonferroni correction *** $p < 0.001$, ** $p < 0.01$. * $p < 0.05$.

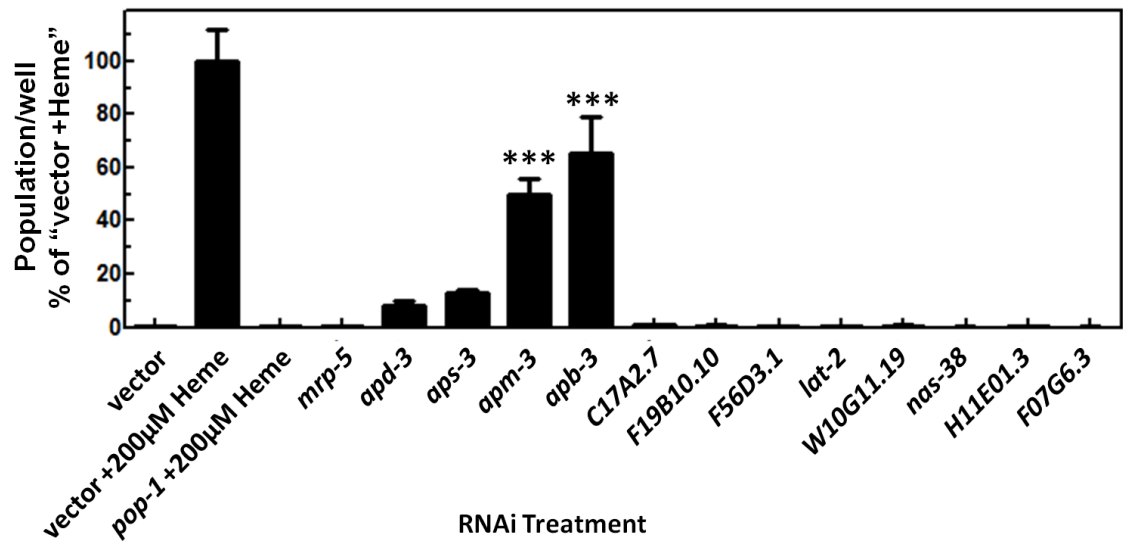
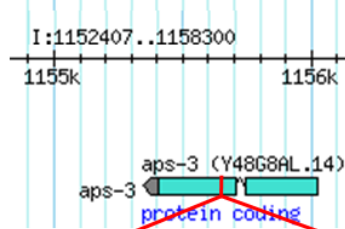


Figure 13: AP-3 subunit suppressor alleles

(A) The *aps(ih1003)* allele contains a substitution at nucleotide position 383 from a C to a T. This is predicted to result in a nonsense mutation of codon 115 from R to a stop, and result in a C-terminal truncation of 79 amino acids. (B) The *apm-3(ih1005)* allele contains a substitution at nucleotide position 1967 from a G to an A. The mutated guanine is predicted to act as a 5' nucleophilic splice donor for the excision of intron 9. An effect on transcript splicing has not been confirmed. (C) The *apd-3(ih1004)* allele contains a substitution at nucleotide position 7,853 from a C to a T. This is predicted to result in a nonsense mutation of codon 761 from a Q to a stop, and result in a C-terminal truncation of 492 amino acids. (D) The genomic sequence of *aps(ih1003)* is reported. (E) The genomic sequence of *apm-3(ih1005)* is reported. (F) The genomic sequence of *apd-3(ih1004)* is reported. Nucleotide positions refer to genomic sequence. Position 1 is the translational start site (A in ATG start codon). Genomic sequences contain the indicated mutation in red as well as up to 500bp of flanking sequence. Images of genomic loci are adapted from wormbase.org. Interpretation of coding effects based only on genomic sequences.

A

aps-3(ih1003)

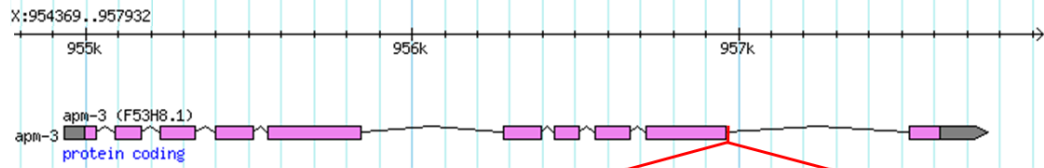


GTG.GAT.(C→T)GA

- PTC
- Loss of 79 C-terminal AAs

B

apm-3(ih1005)

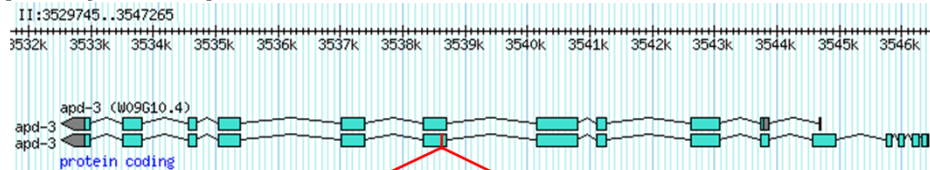


- Loss of splice site donor

TGTCCGGATTAAA(G→A)gtagctttat

C

apd-3(ih1004)



ATG.GAG.(C→T)AA

- PTC
- Loss of 492 C-terminal AAs

D

>Y48G8AL.14(ih1003)

ATGATAAAAGCGATACTTGTTCATCAACAATCACGGAAAACCAAGACTTTTAAAAATTTTATCAA
CATTATCCAGAGGAGAAGCAACAGCAAATCGTTCGAGAAACCTTCCAACCTGGTGTCAAAGCG
CGACGATAACGTCTGCAATTTTCTGGAAGGAGGAACTCTCATCGATGGAAATGACTATCGATT
AATCTACAGGCATTATGCCACATTGTATTTTCATATTTTGTGTTGATTCTTCTGAAAGTGAACCTT
GGAATCCTCGATTTGATTTCAGGTAAGCTATCCTATTTTTAAAAATCGATTAAGTGTTCAGGTC
TTCGTTGAAACTCTCGACCGCTGCTTCGAAAACGTGTGCGAGCTGGATCTAATCTTCCACGTG
GATTGAGTTACCACATTCTCGGCGAAATCGTGATGGGCGGTATGGTTCGAGACGAACATG
AACGAGATCCTTCAACGCATCCAGGAACAGGACAAAATCCAGAAGCAAGAGGCTGGAATCAC
TGCGGCGCCGCCCCTGCGGCTCAAGAATATGAACATTTCCCAGCAGTTGAAGGA
CATCAAGCTGCCAGATTTACCGTCGCTTTCGAATTTGAAAAATGCATTTTGA

E

>F53H8.1(ih1005)

...AAATAAAGCGATTATGGCTACTGATAATCTCTATCAATTTGTAATTGTAGTGAATATCGGAT
TGCAAAATTGTTTAGTTCTGTGCACCTCTAAAGATTTAAATACAAAATTATAAATAAACCAAA
TGAAAATATTTAATAATATAACTTTCACACCACCAATTTGGGTGCTGACGTTTTGAACTA
GCATGTGTTCTGGAGGTA AAAAATTTGAAAAATATTTGGAAATATTAAGAATATATTCATCTT
ATCCTTGACAAATTTTCAGGTTGACGTTTGTGTAAACTGTCCGGAATGCCTGATCTCACAATG
ACCTTATCAACCCAAGACTTCTAGATGATGTATCCTTCCATCCATGTGTGATACAAGCGCT
GGGAGGTAAACCGCTCATAACATTTATATCTTAATCACAATTTTTTTCAGAACGAGAAGGTTCT
TTCATTTGTTCCCTCCAGATGGCAACTTTTCGTCTGTTGTCCTATCATATTGCTGCACAAAAGTAA
TGATTTTCATTCTACAGATAAAAATTTCTATAACTTAATTAATTTTCAGTATGGTTGCCATTCCAA
TCTACGTTAGACAAGTGATCTCCTTGAAACCAAATGCTGGAAAACCTTGACCTCACAGTTGGAC
CAAAGCTAAGCATGGGTAAAGTGGTGTGTTTTTCGAAGATCTAAATCACAATCCCTCTAAACAAA
AACGATGTTAAGCTGGAAGACGTTGTTCTTGAATTCACAATGCCAAAATGTGTACAAAACATGC
AATTTGGTGGCGAGTCACGGAAGAATCGCGTTCGACCCGACGACTAAACTATTGCAATGGAC
CATTGGAAAAATTGAAGTCGGAAAACCATCAACACTCAAAGGATCAGTTGCTGTGAGCGGAA
CTACTGTTGCAGAGAATCCACCAATTTCACTGAAATTCAAAATTAACCAGTTGGTTCTGTCCG
GATTA AAAGTTAGCTTTATCAGCTTGAAGTGAATACCCCTATACTTGCAAAGTAAA...

F

>W09G10.4a(ih1004)

...CTCGGCACGACAATTTTTTGTAAAATACCAACGAGCATGCGCCTTTAAAGAGTACTGTAAC
AGGAGTTTTCCATCGATTTTTTCATAGTATTTTATTTAAAAATTTATATTTATAAGGCTATTTTT
TAAAGATAAAGAAGTACTTGGCTCAATGGATGGAGGAAATTTTTTTAGATTA AAAAAAATATTC
TAAAAAATTTATATTAATTTTGTGACATTTTTCAATTTTTTTCCGATATTTTATCGATTTTTTA
TTTTCAGAATAAACAGTTTTTGTGACATTTTTAATGAAAAATTCATAAATTTGGCTCCTAAAATG
CTGAAATTTGAAAAAAAAGTTCTACAATTTTTTCTAAATTTCCAGGGCTCAGCAACTGCTCC
AAAACGTCCAACACGTTTCGGCAACCCTCTCGAACGCGTAGAAATTTGTCGAAAAAGAAAAAG
AAATTC AATCAACCACTGGAAATTTCCGGGTGTAGTTGGGCTCCACCGGTATATGGAGTAAACAAG
ACTCGACGTTGAGCTGGAAAAAAGCGAAAGAGGATGATATAATTGGTGGTGGAAAAAAGAA
GAAATCGACGAAAAAAGATGGAAAAAAGAATGGGAAGAAAAAGTGGAAAAAAGCGAAGAAC
AACGAGTACAAGTAGTGAAGAAGAGGATCGAATTTGTGCATAAAGTTAATCGAAATGATGGAG
AAATGCCTGAAGGAGCCAAGTCAACGGATGATGAGGATGAGAAAAGTACGGAAAATTTGAGGA
TTTTTCAGAGAAATTTGGAGAAAAAATTTGTCCAAAAAAGGGAAATTTTTTTTTTTGGGAATTTGGG
CAATTTTTTGGCATATTTACAAAAAATCCAAAACATGTGCAATTTTACCAAAAAAATGTCCA
GTTTTTGGCGAAAAATGTTTACCTAAAAAAGTCAATTTGTTTACCAAAAAATGTCAAATTTTTTAC
CAAAAAAGTGCAATTTTTTGGCAAAAAAATGTCAATTTTTTACCGAATAATTTCAAAAAA...

Figure 14: Candidate testing by combinatorial RNAi

The IQ6015 RNAi hypersensitive strain was synchronized and three L1s (P₀) were placed onto NGM plates for combinatorial RNAi against the indicated gene(s); either *mrp-5* and a candidate gene (A), or vector control and a candidate gene (B). Once the F₁ generation reached gravid in the positive control treatment, total populations for each condition were analyzed by COPAS BioSort (Union Biometrica). Data represents the averages of three technical replicates from two independent experiments, where all populations were normalized as a percentage of the positive control treatment. Indicated significant differences compared to the vector treatment were obtained by post-hoc multiple means comparisons utilizing Bonferroni correction *** $p < 0.001$, ** $p < 0.01$. * $p < 0.05$.

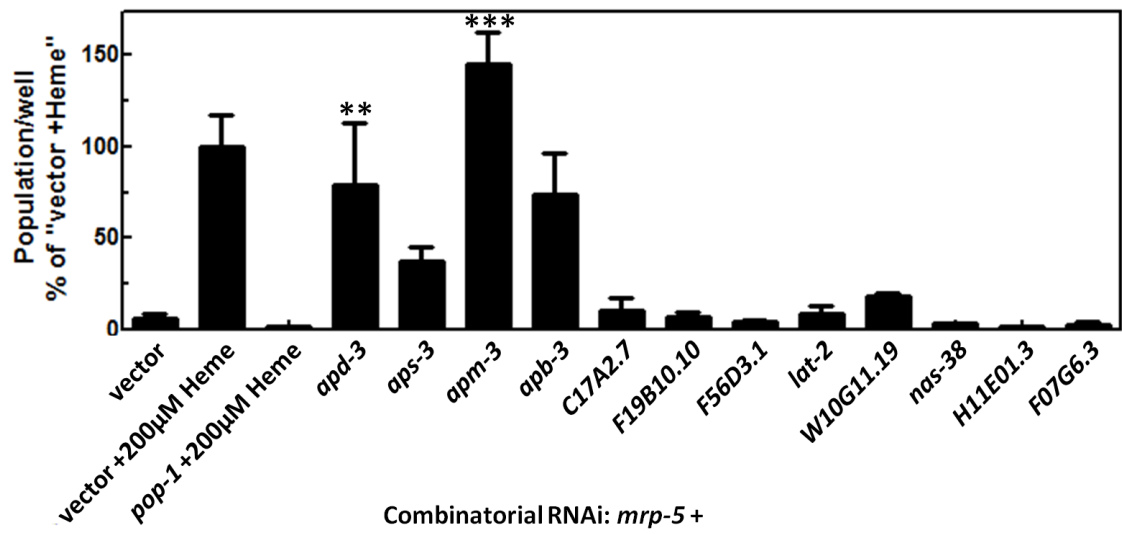
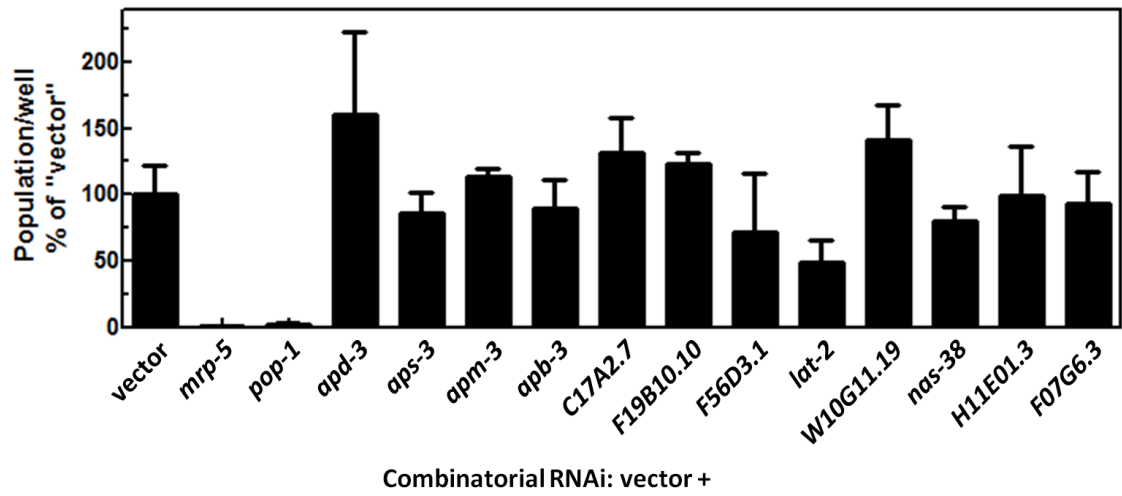
A**B**

Figure 15: RNAi against AP-1 or AP-2 subunit genes in *mrp-5(ok2067/ok2067)*

RNAi against genes encoding subunits of adaptor protein complexes was conducted for a generation on 200 μ M heme NGM plates, and these adults were moved clonally to the same RNAi conditions without heme supplementation, allowed to lay progeny overnight, then removed. The vector +200 μ M heme positive control condition was observed until the second generation reached adulthood, and then the entire population for all treatments was analyzed by COPAS BioSort (Union Biometrica). Data represents averages of three technical replicates from two independent experiments, where all populations were normalized as a percentage of the vector +200 μ M Heme condition. Indicated significant differences compared to the vector treatment were obtained by post-hoc multiple means comparisons utilizing Bonferroni correction *** $p < 0.001$, ** $p < 0.01$. * $p < 0.05$.

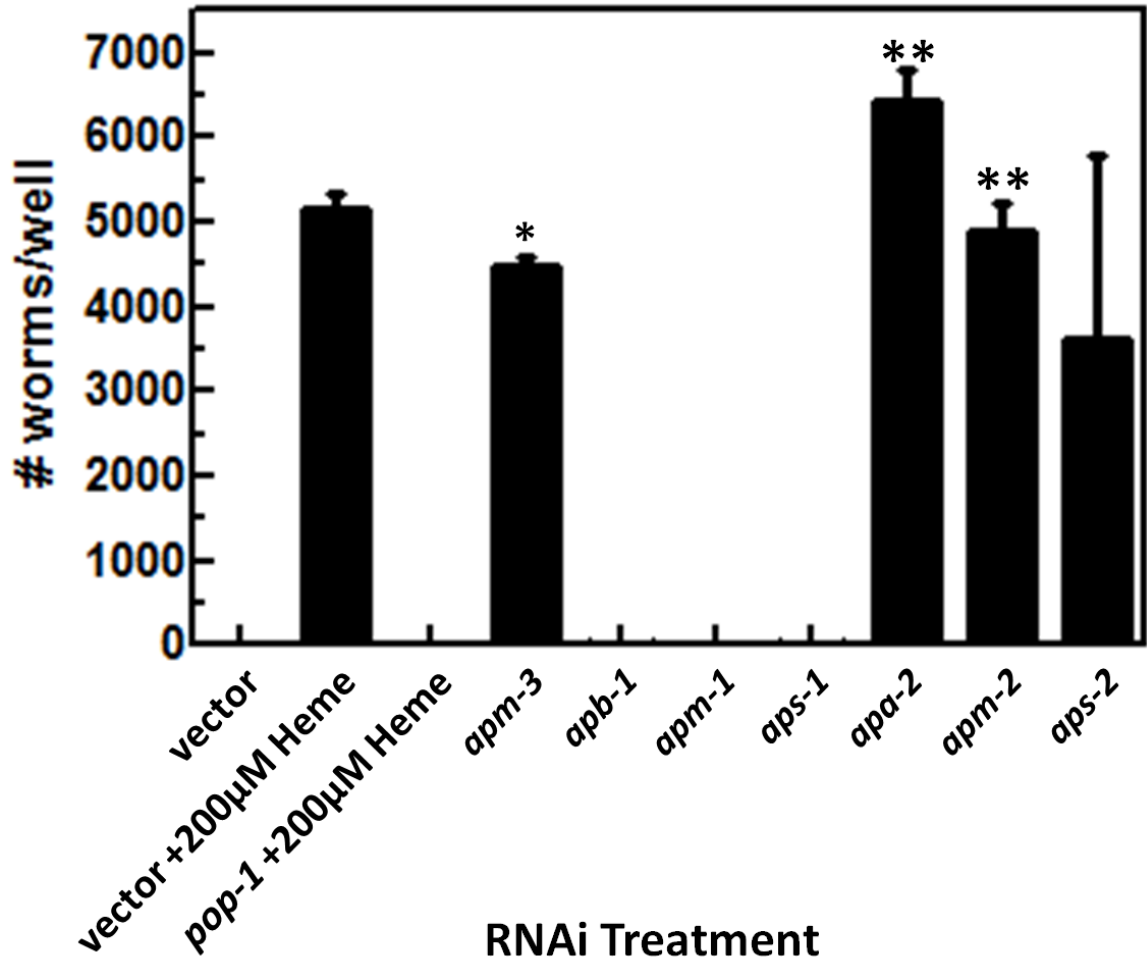


Figure 16: Combinatorial RNAi against AP-1 or AP-2 and vector or *mrp-5*

The IQ6015 RNAi hypersensitive strain was synchronized and three L1s (P₀) were placed onto NGM plates for combinatorial RNAi against the indicated gene(s); either *mrp-5* and a gene encoding an AP subunit (A), or vector control and a gene encoding an AP subunit (B). Once the F₁ generation reached gravid in the positive control treatment, total populations for each condition were analyzed by COPAS BioSort (Union Biometrica). Data represents the averages of three technical replicates from two independent experiments, where all populations were normalized as a percentage of the positive control treatment. Indicated significant differences compared to the vector treatment were obtained by post-hoc multiple means comparisons utilizing Bonferroni correction *** p < 0.001, ** p < 0.01. * p < 0.05.

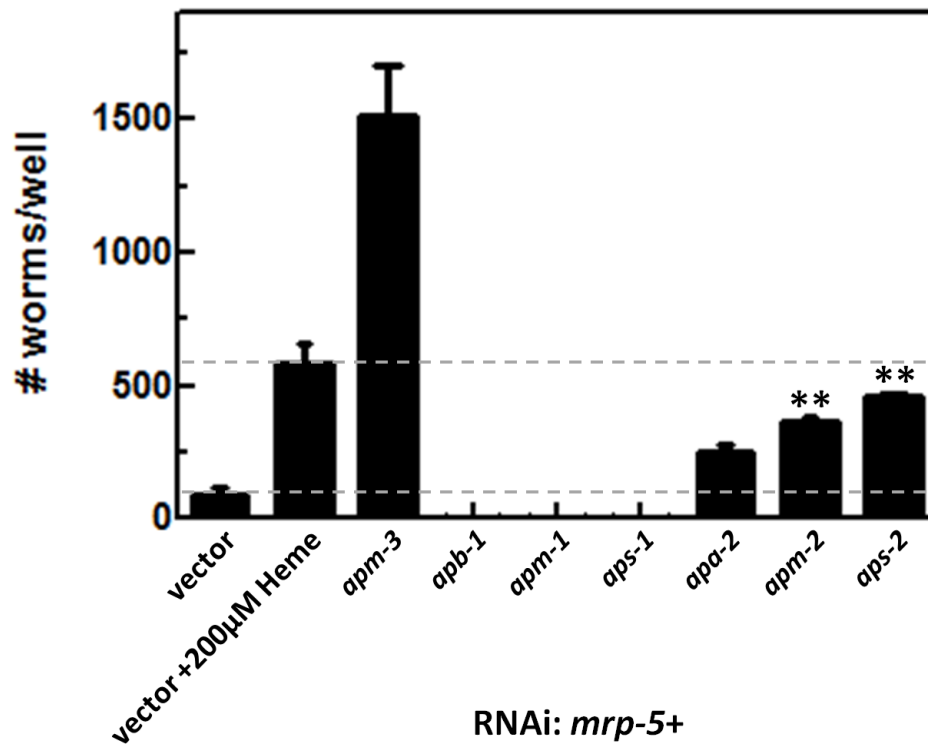
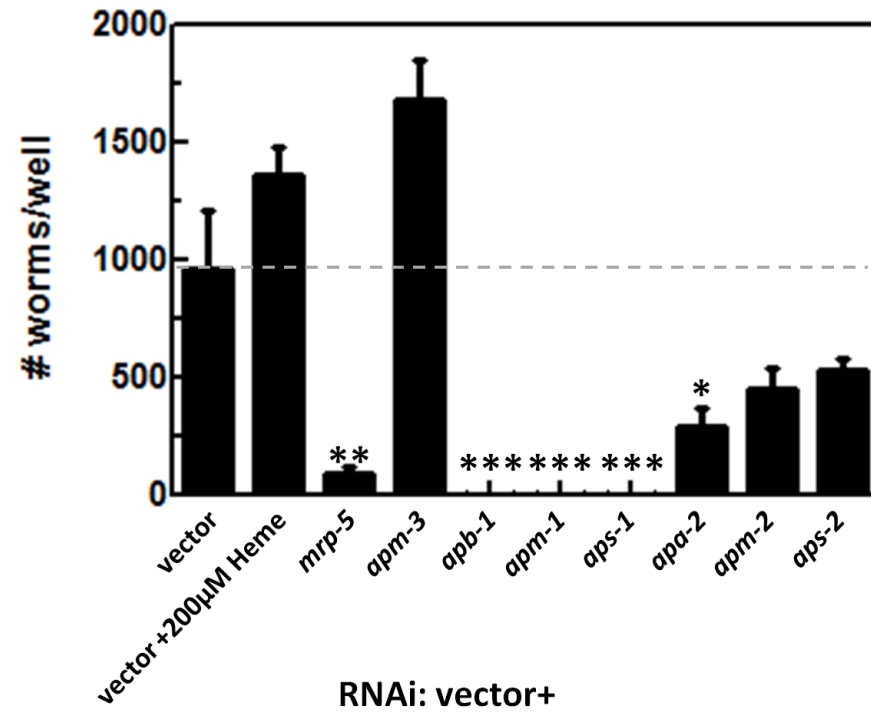
A**B**

Figure 17: AP-3 subunit RNAi in *P_{hrg-1}::GFP::unc-54 UTR*; *lin-15B(n744/n744)*

IQ6015 (*P_{hrg-1}::GFP::unc-54 UTR*; *lin-15B(n744/n744)*) worms were synchronized, and 40 L1s were placed onto NGM plates seeded with HT115(DE3) bacteria for combinatorial RNAi against either vector and genes encoding AP-3 subunits, or *mrp-5* and genes encoding AP-3 subunits. Integral GFP signal was obtained by analysis with COPAS BioSort (Union Biometrica) using a ~13mW 488nm laser for excitation, and a 510(+/- 23)nm filter to detect emission. Integral GFP signal of each worm was normalized to the worm's size (TOF), and the average of all adults in that technical replicate were averaged, then normalized to vector treatment. Data represents the averages from three independent experiments, where each experimental average is the mean of three technical replicates. Indicated significant differences are as compared to the vector + vector treatment unless indicated by a grey line, and were obtained by post-hoc multiple means comparisons utilizing Bonferroni correction *** $p < 0.001$, ** $p < 0.01$. * $p < 0.05$.

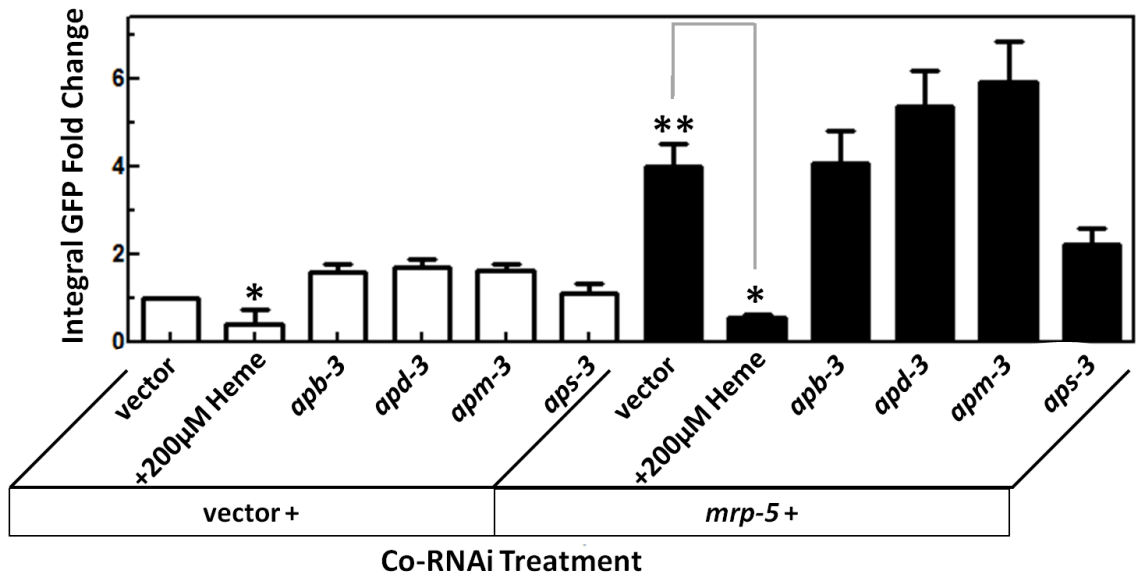


Figure 18: AP-3 subunit RNAi in *P_{hrg-2}::HRG-2-YFP::unc-54 UTR*

IQ8125 (*P_{hrg-2}::HRG-2-YFP; lin-15B(n744/n744)*) worms were synchronized, and 40 L1s were placed onto NGM plates seeded with HT115(DE3) bacteria for combinatorial RNAi against either vector and genes encoding AP-3 subunits, or *mrp-5* and genes encoding AP-3 subunits. Integral GFP signal was obtained by analysis with COPAS BioSort (Union Biometrica) using a ~13mW 488nm laser for excitation, and a 543(+/- 22)nm filter to detect emission. Integral GFP signal of each worm was normalized to the worm's size (TOF), and the average of all adults in that technical replicate were averaged, then normalized to vector treatment. Data represents the averages of three technical replicates from two independent experiments. Indicated significant differences are as compared to the vector + vector treatment unless indicated by a grey line, and were obtained by post-hoc multiple means comparisons utilizing Bonferroni correction *** $p < 0.001$, ** $p < 0.01$. * $p < 0.05$.

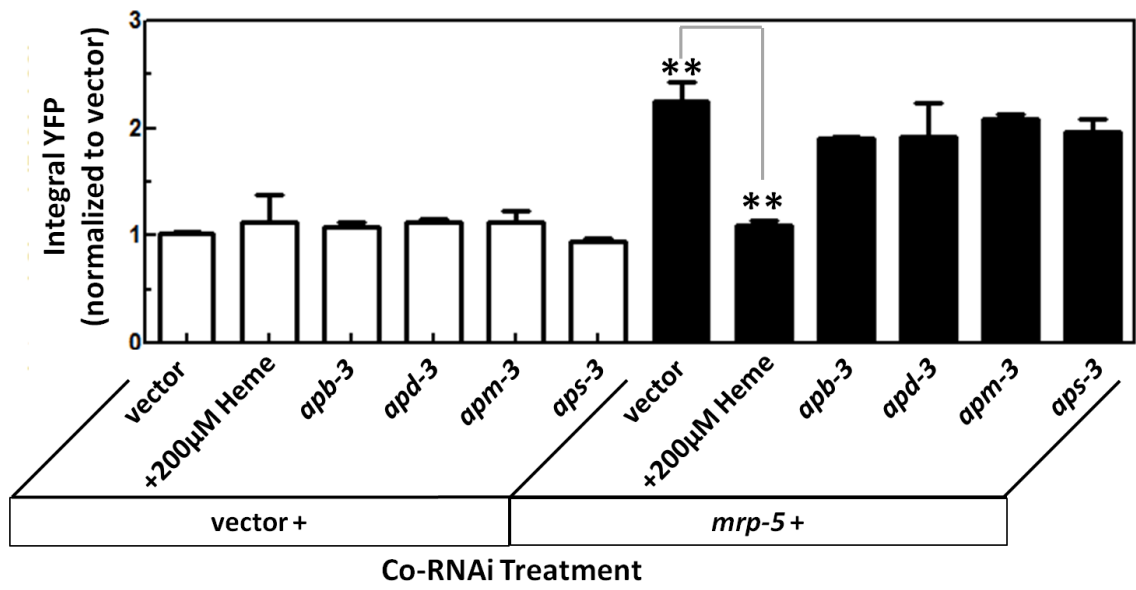


Figure 19: HRP activity Assay in RNAi model of *mrp-5* suppression

Worms were bleached from stock plates (NGM, OP50) and ~10,000 synchronized L1s were plated to 10 cM plates seeded with 1.5mL of HT115(DE3) for combinatorial RNAi against the indicated genes. Worms were allowed to grow until at the young adult stage, washed twice with M9 and lysed in 100 μ L buffer (150 mM NaCl, 20 mM HEPES, 0.5% Triton X-100, with Protease Inhibitor Cocktail Set III) and Lysing Matrix C beads (MP Biomedicals) in a FastPrep-24 Beadbeater (MP Biomedicals). Lysates were kept on ice at all times. A volume of (x) μ L worm lysate (for IQ6311, x=2; for IQ6312, x=5) was mixed with (200-x) μ L fresh peroxidase assay buffer (0.1 mg/mL o-dianisidine, 0.02% H₂O₂ in 0.1M NaH₂PO₄/Na₂HPO₄ buffer, pH 6) in 96-well plate; absorbance at 440nm (OD₄₄₀) and 600nm (OD₆₀₀) were immediately measured using a plate reader (SynergyHT, BioTek). Protocol adapted from described methods.⁷⁷ Experiment was conducted with (A) IQ6351 (*vha-6::ER-HRP-mcherry::unc-54 UTR; lin-15b(n744/n744)*) or (B) IQ6352 (*dpy-7::ER-HRP-mcherry::unc-54 UTR; lin-15b(n744/n744)*) strains. Data represents the averages of three technical replicates. Indicated significant differences are as compared to the vector + vector treatment unless indicated by a grey line, and were obtained by post-hoc multiple means comparisons utilizing Bonferroni correction *** p < 0.001, ** p < 0.01. * p < 0.05.

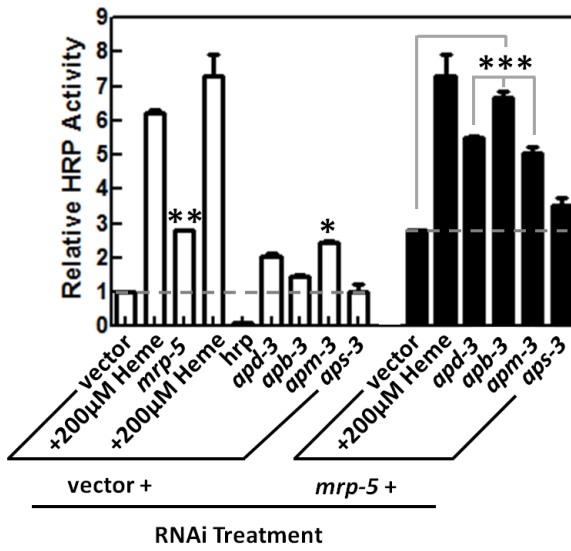
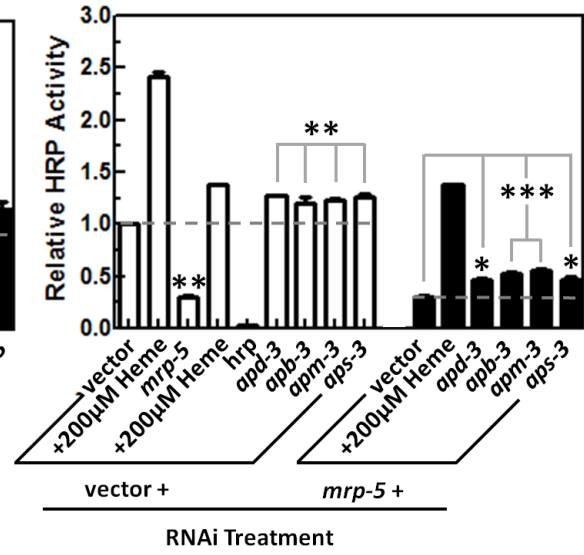
A*vha-6::HRP-mcherry::unc54-UTR***B***dpy-7::HRP-mcherry::unc54-UTR*

Figure 20: *cua-1(ok904)* suppression assay

Preceding the experiment, P₀ worms of either N2 or *apb-3(ok429/ok429)* strain were synchronized as L1s and plated onto NGM plates seeded with HT115(DE3) for RNAi against either vector or *cua-1*. Once gravid, P₀ worms were bleached, and F₁ were synchronized as L1 progeny. Three F₁ L1s/well were placed onto NGM plates supplemented with BCS or CuCl₂ and seeded with HT115(DE3) bacteria for RNAi against the indicated genes. The F₁ of P₀ grown on vector were used for vector or *pop-1* RNAi conditions, while the F₁ of P₀ grown on *cua-1* were placed to *cua-1* RNAi conditions. F₁ worms were allowed to lay F₂. Once F₂ worms reached gravid for the vector, no supplementation treatment, all worms of that strain were analyzed by COPAS Biosort (Union Biometrica). Data represents the averages of three technical replicates.

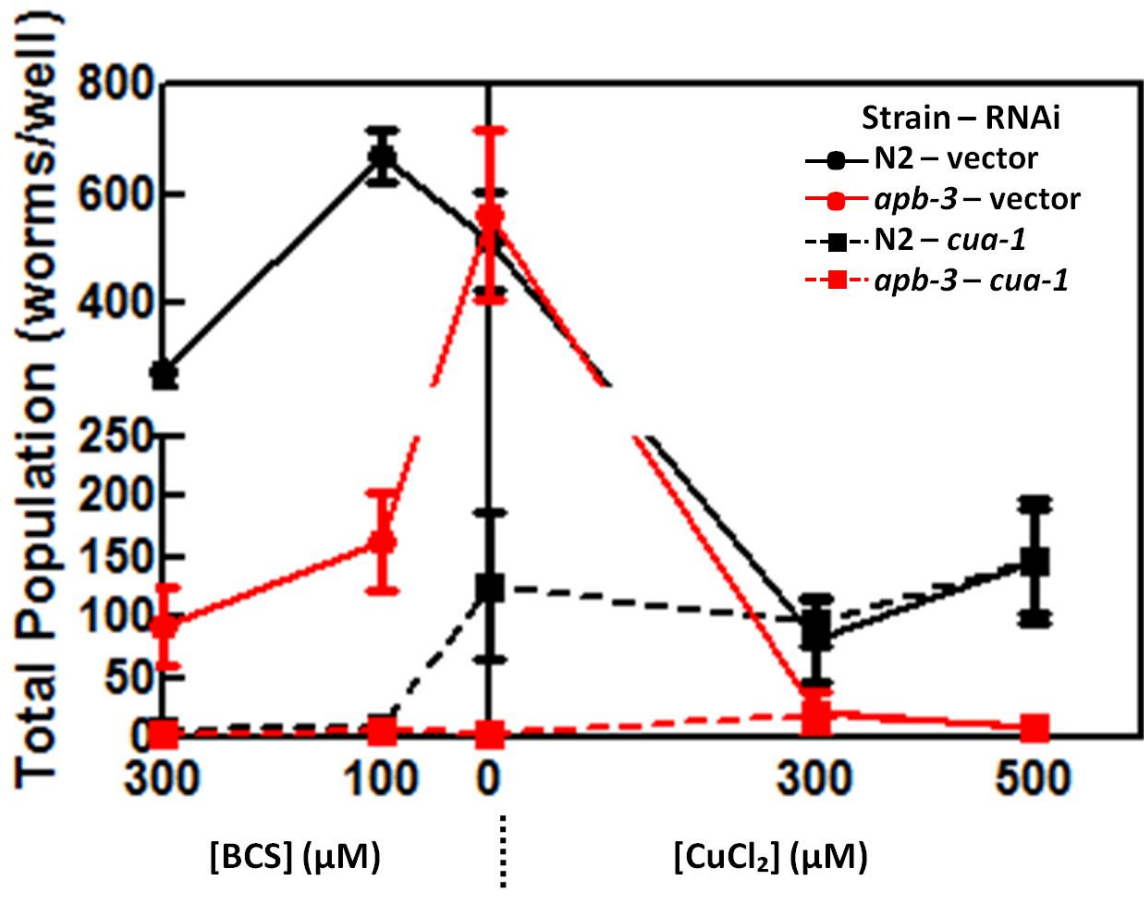


Fig 21: ZnMP Treatment in suppressor mutants

IQ1901(*mrp-5(ok2067/ok2067);apb-3(ok429/ok429)*), RB662(*mrp-5(+/+);apb-3(ok429/ok429)*), and WT(*mrp-5(+/+);apb-3(+/+)*) worms were treated with ZnMP and imaged by confocal microscopy. ZnMP was excited by 561nm laser and emission was visualized by rhodamine filter. Autofluorescence was excited by 405nm laser and emission was visualized by DAPI filter. Scalebar = 10 μ m.

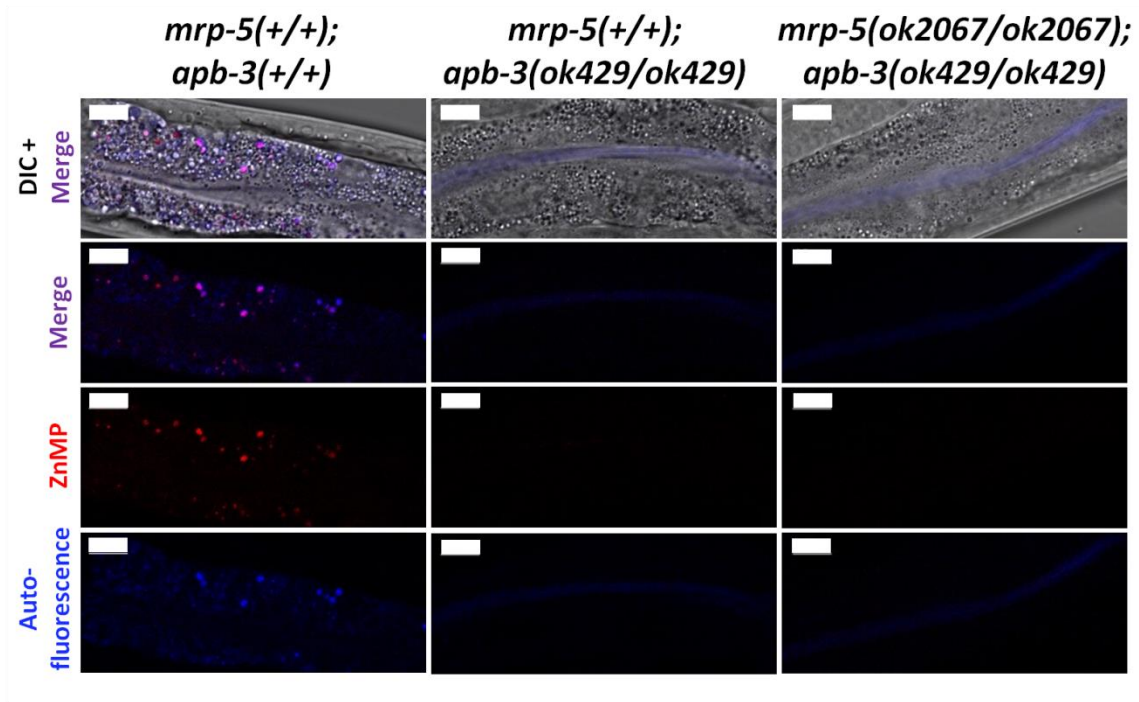


Figure 22: *mrp-5* RNAi Suppression Assay

N2, RB662(*apb-3(ok429/ok429)*), RB2257(*apd-3(ok3058/ok3058)*), JJ1271(*glo-1(zu391/zu391)*), *glo-2(zu445/zu445)*, GH378(*pgp-2(kx48/kx48)*) animals were maintained on NGM with no supplemented heme for one generation and then bleached. Three synchronized L1 (P₀) progeny were placed on NGM seeded with HT115(DE3) for RNAi against the indicated gene. Once F₁ treated with vector control reached gravid, all treatments for that strain were analyzed by COPAS Biosort (Union Biometrica). Data represents the averages of three technical replicates.

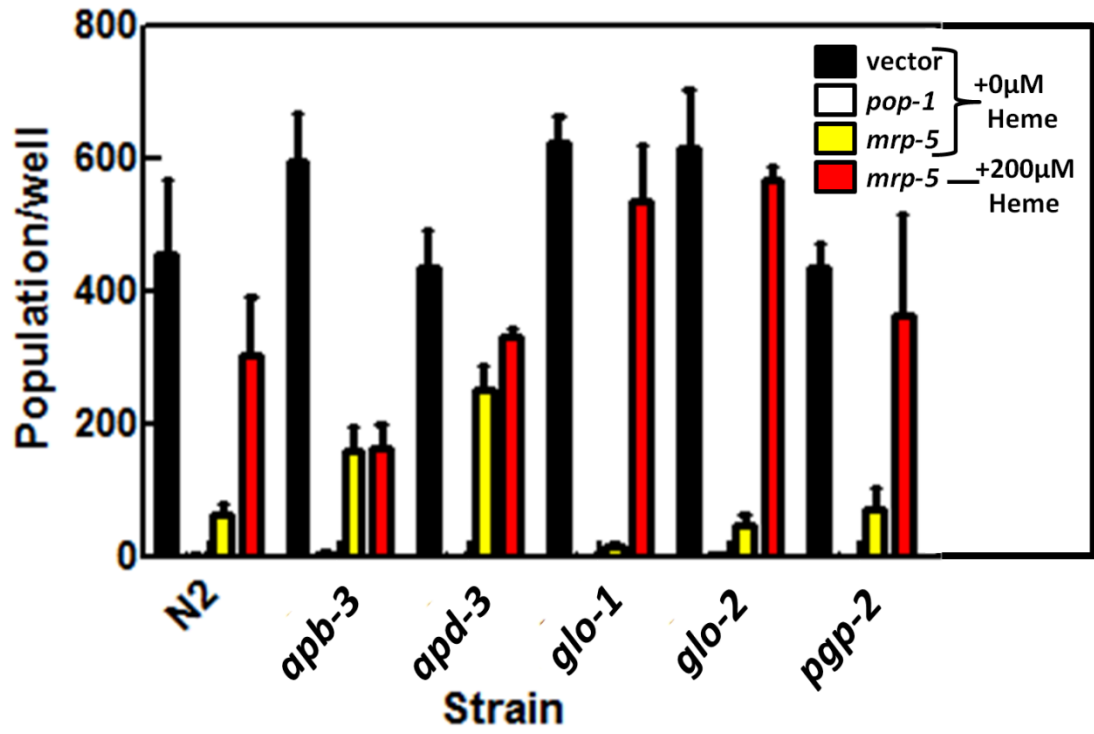


Figure 23: AP-2 and AP-3 RNAi in *P_{vha-6}::HRG-1-mCherry::unc-54 UTR*

RNAi against *apb-3* is representative of *apd-3*, *apm-3*, *aps-3* and RNAi against *apa-2* is representative of *apm-2*, *aps-2*. Synchronized IQ6112 (*P_{vha-6}::HRG-1-mcherry::unc-54 UTR*) L1s were plated onto NGM plates seeded with HT115(DE3) for RNAi against the indicated gene and allowed to grow for until at the young adult stage. Worms were mounted on agar pads with 1mM NaN₃ in M9 buffer and imaged on a Zeiss LSM710 confocal microscope. HRG-1-MCHERRY indicates rhodamine filter, and autofluorescence indicates DAPI filter. Scalebar = 20 μm.

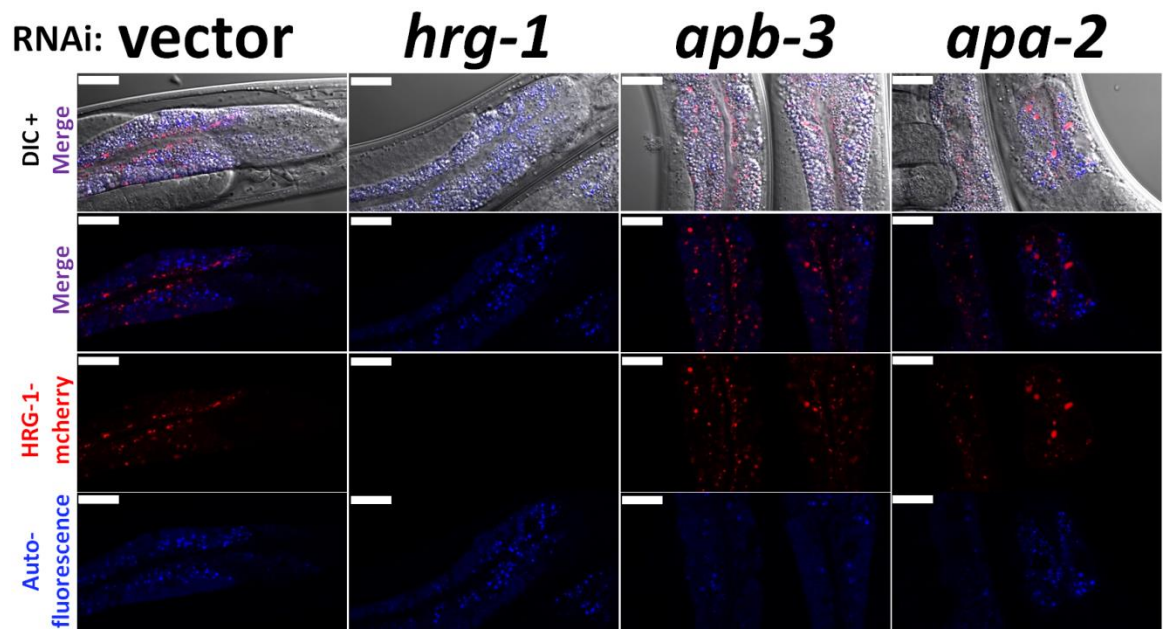
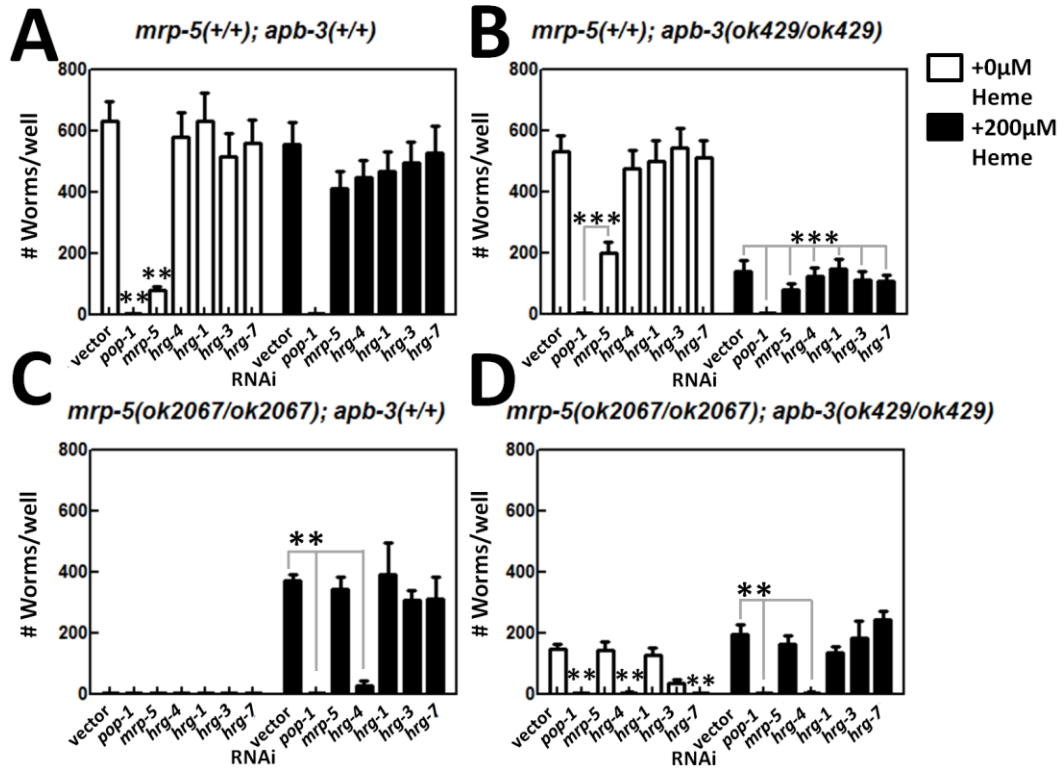


Figure 24: *mrp-5* Suppressor Reversion Assay

Worms of the indicated strain: either (A) WT, (B) *apb-3*, (C) *mrp-5*, or (D) *apb-3;mrp-5* were maintained for one generation on NGM plates supplemented with 100 μ M hemin in the agar, then bleached and their progeny were synchronized as L1s. Three of these synchronized progeny were moved to NGM plates seeded with HT115(DE3) for RNAi against the indicated genes. Once F₁ treated with vector positive control reached gravid all treatments of that strain were analyzed by COPAS BioSort. For *mrp-5(ok2067/ok2067)*; *apb-3(+/+)* vector +200 μ M hemin was used as the positive control. Data represents the averages of three technical replicates from two independent experiments. Indicated significant differences compared to the vector treatment were obtained by post-hoc multiple means comparisons utilizing Bonferroni correction *** $p < 0.001$, ** $p < 0.01$. * $p < 0.05$.



The forward genetic screen described herein sought to uncover additional mechanisms involved in heme homeostasis by screening for bypass suppressors of *mrp-5*, an essential gene for heme export in *C. elegans*. Of the 32 suppressor mutants isolated, three of the strongest suppressors were mapped to distinct subunits of AP-3. The fact that AP-3 controls the trafficking of a large set of transmembrane proteins to several distinct organelles makes a mechanistic interpretation of the mode of suppression difficult. It is possible that suppression is due to the mistrafficking of one specific protein whose trafficking is controlled by AP-3, or it could be a consequence of one of the broader phenotypes associated with loss of AP-3, such as defective biogenesis of lysosome related organelles.

The extra-intestinal accumulation of gut granular contents (Figure 21, “Results”) suggested a possible mechanism for bypass of *mrp-5* deficiency (Figure 1). Material contained in gut granules localizes outside of the intestine⁷⁰, raising the possibility that contents normally trafficking to gut granules (such as porphyrins) are secreted in AP-3 subunit mutants. Previously, defective trafficking to yeast vacuoles or mammalian lysosomes has been shown to result in secretion of that compartment’s contents.^{70,104} If occurring through the basolateral membrane, this would functionally bypass regulated heme efflux by MRP-5. However, other *glo* mutants do not phenocopy *mrp-5* suppression (Figure 22, “Results”). This could be due to the fact that *glo-1* and *pgp-2* mutants play a specific role at the site of gut granules important for their biogenesis, while AP-3 plays a much more general, upstream role in specifying cargo for delivery to gut granules and other compartments in the endolysosomal system.⁴⁷ The lack of suppression by the BLOC-1 subunit *glo-2* indicates that some capacity of AP-3 function upstream of gut

granule biogenesis and distinct from *glo-2* mediated trafficking is important for *mrp-5* suppression. Particularly problematic for this scenario (Figure 1) is the fact that autofluorescent material has been observed to accumulate extra-intestinally in *glo-1*, *glo-2* and *pgp-2* mutants^{70,105} indicating that this *glo* phenotype is not correlated with *mrp-5* suppression, and that the basolateral secretion of gut granule contents (Figure 1) is unlikely. ZnMP treatment of additional *glo* mutants would be useful to gauge how equitable the trafficking phenotypes are between AP-3 subunit mutants and other *glo* mutants.

Based on the characterization of the dynamics of deficiency in AP-3 subunit mediated suppression of *mrp-5* deficiency, we present a model for two plausible mechanisms of suppression (Figure 2).

The first hypothesis involves the regulated trafficking of heme containing vesicles from endosomes to gut granules (Figure 2A). The fact that *mrp-5* phenotypes can be suppressed with dietary supplementation of heme suggests that there is a low affinity mechanism for the efflux of intestinal heme independent of *mrp-5*. ZnMP data indicate that porphyrins are accumulating in vesicles of the endolysosomal system, and that some of these vesicles may eventually fuse with gut granules (Figure 21, “Results”); it could be that the alternative, low affinity pathway is due to the fusion of a subset of heme containing vesicles with the basolateral membrane, resulting in heme efflux into the pseudocoelom. AP-3 subunit mutants, mis-specification of heme containing vesicles could result in an increase of the fusion of these vesicles with the basolateral membrane or other organelles. One inconsistency with this hypothesis is that RNAi against *mrp-5* in AP-3 subunit mutant strains cannot be rescued by heme supplementation (Figure 22,

“Results”). If increased efflux of heme-containing vesicles are responsible for suppression, then increased luminal heme should increase intestinal heme efflux and rescue growth. However the significance of this observation is unclear since loss of viability due to *hrg-3* and *hrg-7* RNAi in *mrp-5; apb-3* double mutants can be rescued with heme (Figure 24D, “Results”). Another complication to this hypothesis is the fact that in the absence of *mrp-5*, loss of *hrg-4* is lethal (Figure 24C-D), implying that in *mrp-5* mutants heme must be imported across the apical membrane into the cytosol. Cytosolic heme would then have to traverse the membrane of the vesicle.

The second hypothesis concerns the mistrafficking of a single transmembrane protein in AP-3 subunit mutants rather than a general defect in vesicular trafficking (Figure 2B). It is not clear how ZnMP and possibly other porphyrins are delivered to endolysosomal vesicles. One possibility is that endocytosis of luminal contents from the apical surface results in the accumulation of porphyrins at these sites. Another possibility is that an unidentified porphyrin exporter localizes in an AP-3 dependent manner to sites of ZnMP accumulation and acts to efflux porphyrins from the cytosol into these vesicles. Loss of AP-3 subunits could result in the mis-localization of this exporter to the plasma membrane, constituting a functional bypass of MRP-5. There is some precedent for this mis-sorting phenomenon. In mammalian cell culture models, AP-3 deficiency results in increased plasma membrane¹⁰⁶ expression of lysosomal membrane proteins Lamp-1, Lamp-2, and CD63.^{93,106}

Tissue-specific HRP reporters indicate in the intestine, loss of AP-3 subunits may increase heme availability in the secretory pathway (Figure 19, “Results”), implying that loss of AP-3 results in general mis-allocation of intracellular heme among organelles.

Combinatorial RNAi of *mrp-5* and genes encoding AP-3 subunits have an additive effect (Figure 19, “Results”). This could be due to the fact that in *mrp-5* mutants, increased ZnMP accumulation (Figure 8) implies higher intestinal heme content. Mis-localization of these increased heme stores would result in a higher content of heme mis-partitioned to the secretory pathway than with loss of AP-3 subunits alone. This is consistent with both hypotheses, as mis-partitioning of intestinal heme could occur through mis-trafficking of heme-containing vesicles or through mis-localization of a heme exporter.

A critical experiment to differentiate these two hypotheses would be treating wildtype, *apb-3* mutants, and *apb-3; mrp-5* double mutants with an excess of exogenously provided substrate such as FITC-Dextran or TRITC-BSA. In wildtype worms, both of these substances are endocytosed and localize to gut granules and extra-intestinally to coelomocytes.⁷⁰ If basolateral secretion of endolysosomal contents is increased in suppressor mutants, these exogenous substrates would likely increase accumulation in coelomocytes. However, if heme is being trafficked through specific recognition of heme by an exporter, intestinal efflux of FITC-Dextran or TRITC-BSA may not be increased.

Validation of the hypothesis regarding mis-localization of an exporter would require identification of such a transporter, and would represent an important gain in our present understand of mechanisms underlying heme homeostasis, but its identification would be challenging. One approach would be to conduct a genetic screen for loss of *mrp-5* suppression in AP-3 subunit mutants; the difficulty of this approach is highlighted by the fact that any gene which disrupts growth in heme limiting conditions (such as *hrg-*

7, *hrg-3*) or block intestinal entry (such as *hrg-4*) results in decreased viability (Figure 24, “Results) and would screen as a false positive for loss of *mrp-5* suppression.

A systemic screening of trafficking components capable of mediating suppression of *mrp-5* deficiency would significantly advance the current understanding of pathways important for this phenotype. Currently, loss of individual subunits AP-3 and AP-2 have been shown as being sufficient for *mrp-5* suppression, an interesting observation given that there is evidence that loss of a single unit results in the formation of hemi-complexes which may retain some functional capacity.^{107,108} Addressing whether loss of other trafficking components ranging from specific trafficking functions^{71,109,110} to more ubiquitous components such as *chc-1* or *rab-5*¹¹¹ result in *mrp-5* suppression would demonstrate what specific pathways, when disrupted, result this phenomenon and may help in ascertaining a molecular mechanism.

Although gut granules are autofluorescent, other markers can be used for their detection such as localization of *glo-1::gfp* or *cdf-2::gfp*; use of these additional markers would strengthen the assertion that ZnMP co-localization with autofluorescent organelles represents gut granule localization, and examination of the dynamics of these reporters when autofluorescence is not present, such as in AP-3 subunit mutants, may offer additional insights into trafficking dynamics in the absence of AP-3 function.

These hypotheses also make the assumption that intestinal AP-3 deficiency is responsible for *mrp-5* suppression; but, this assertion is not demonstrated. Since the *apm-3* subunit is expressed ubiquitously⁹³, there exists a possibility that *mrp-5* suppression depends on an extra-intestinal mechanism. Additionally, *apd-3* and *apb-3* are reported to be expressed in two distinct isoforms but the significance of these splice variants are not

known.⁹³ Specific knockdown of either isoform of these two subunits may yield novel findings regarding the role of these isoforms and potentially give insight into AP-3 mediated suppression of *mrp-5*.

Figure 1: Potential suppression mechanism – global secretion of gut granules

In *mrp-5(ok2067/ok2067); apb-3(ok429/ok429)* worms, autofluorescent material accumulates in the intestinal lumen, and it has been postulated this is due to secretion of gut granular contents. ZnMP treatment indicates that gut granules also accumulate heme (Figure 21, “Results”). If secreted gut granule contents, including heme, were secreted into the pseudocoelom out of the basolateral membrane, it could constitute a functional bypass of *mrp-5* mediated intestinal heme export.

mrp-5(-/-); apb-3(-/-)

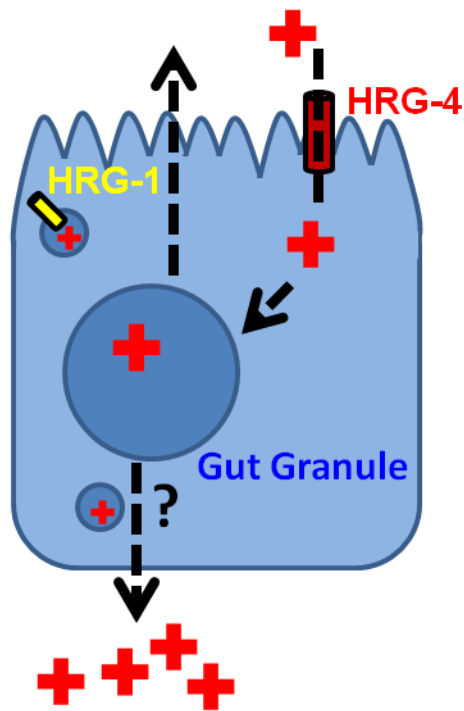
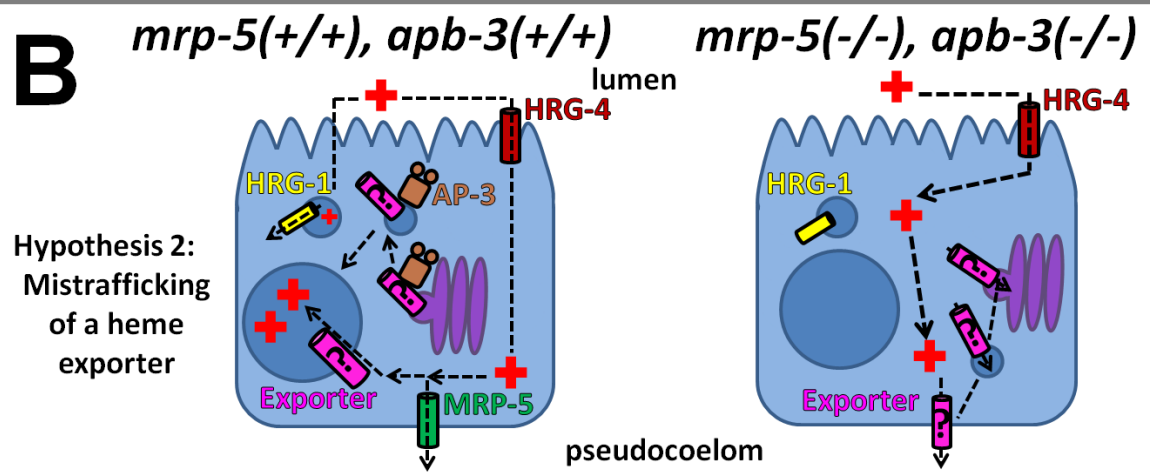
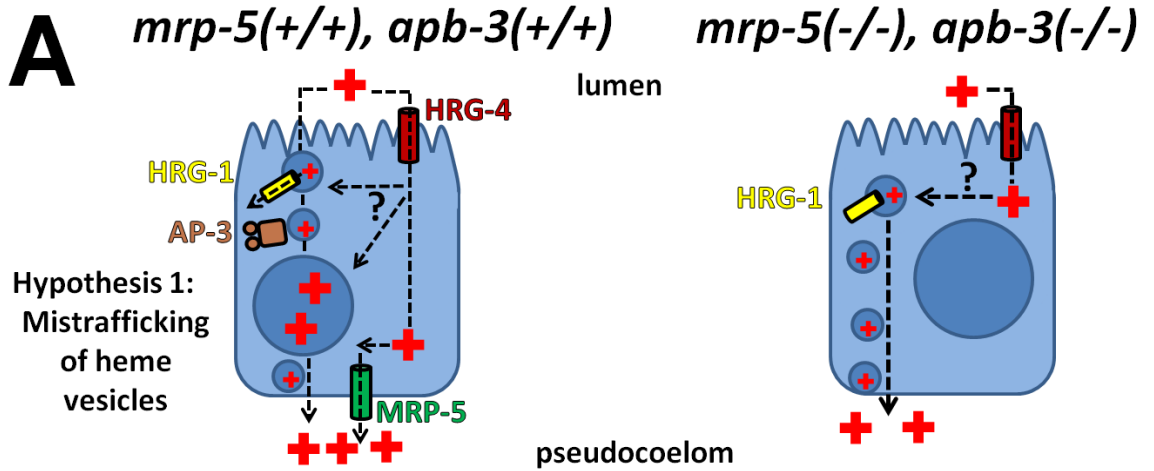


Figure 2: Model for AP-3 mediated suppression of *mrp-5* deficiency

A model describing two potential mechanisms underlying the restoration of intestinal heme efflux in AP-3 subunit mutant, *mrp-5* suppressor mutants. (A) Hypothesis 1: mis-trafficking of heme containing vesicles results in an increase of the fusion of these vesicles with the basolateral membrane as well as other organelles, such as the ER. (B) Hypothesis 2: A heme exporter is normally localized to heme containing vesicles in the endo-lysosomal system in an AP-3 dependent manner; loss of AP-3 results in mis-localization to the plasma membrane, constituting a bypass of *mrp-5*, as well as other organelles such as the ER.



Appendix A: *C. elegans* Strains

Strain Name	Genotype	Description	Obtained by
N2	WT	Used as WT strain	CGC
Hawaiian (CB4856)	WT	WT, used as mapping strain	CGC
VC1599	<i>mrp-5(ok2067/+)</i>	<i>mrp-5</i> balanced heterozygote	CGC
N2; <i>mrp-5(ok2067ok2067)</i>	<i>mrp-5(ok2067/ok2067)</i>	<i>mrp-5(ok2067/ok2067)</i> allele in the N2 background	VC1599 was outcrossed to N2 3x times ⁴⁰
Hawaiian; <i>mrp-5(ok2067/2067)</i>	<i>mrp-5(ok2067/ok2067)</i>	<i>mrp-5(ok2067/ok2067)</i> allele in the Hawaiian background	N2; <i>mrp-5(ok2067ok2067)</i> was outcrossed to Hawaiian 9x times
RB662	<i>apb-3(ok429/ok429)</i> ¹¹²	<i>apb-3</i> mutant	CGC
IQ1901	<i>mrp-5(ok2067/ok2067); apb-3(ok429/ok429)</i>	AP-3, <i>mrp-5</i> suppressor mutant	Crossing N2; <i>mrp-5(ok2067ok2067)</i> to RB662
RB2257	<i>apd-3(ok3058/ok3058)</i>	<i>apd-3</i> mutant	CGC
JJ1271	<i>glo-1(zu391)</i> ¹¹²	<i>glo-1</i> mutant	CGC
	<i>glo-2(zu445)</i> ¹¹²	<i>glo-2</i> mutant	CGC
GH378	<i>pgp-2(kx48)</i> ¹¹³	<i>pgp-2</i> mutant	CGC
CB4845	<i>unc-119(e2498)</i>	<i>unc-119</i> mutant	CGC
TU3335	<i>lin15B(n744); uIs57</i>	RNAi hypersensitive strain	CGC
IQ6112	<i>P_{vha-6}::HRG-1-mCherry::unc-54 UTR</i>	HRG-1 translational reporter, intestinal expression	Bombardment
IQ6011	<i>P_{hrg-1}::GFP::unc-54 UTR</i>	<i>hrg-1</i> transcriptional reporter	Injection ³⁴
IQ6015	<i>P_{hrg-1}::GFP::unc-54 UTR; lin-15B(n744/n744)</i>	<i>hrg-1</i> transcriptional reporter, RNAi hypersensitive	IQ6011 was crossed to TU3335
IQ8031	<i>P_{hrg-3}::GFP::unc-54 UTR</i>	<i>hrg-3</i> transcriptional reporter	Injection, Bombardment ⁴³

IQ8035	<i>P_{hrg-3}::GFP::unc-54 UTR; lin-15B(n744/n744)</i>	<i>hrg-3</i> transcriptional reporter, RNAi hypersensitive	IQ8011 was crossed to TU3335
IQ8122	<i>P_{hrg-2}::HRG-2-YFP::unc-54 UTR</i>	<i>hrg-2</i> translational reporter	Injection, Bombardment ⁷⁶
IQ8125	<i>P_{hrg-2}::HRG-2-YFP::unc-54 UTR; lin-15B(n744/n744)</i>	<i>hrg-2</i> translational reporter, RNAi hypersensitive	IQ8122 was crossed to TU3335
IQ6311	<i>P_{vha-6}::HRP-mcherry::unc-54 UTR</i>	Intestinal HRP(ER) reporter	Bombardment
IQ6351	<i>P_{vha-6}::HRP-mcherry::unc-54 UTR; lin-15B(n744/n744)</i>	RNAi Hypersensitive Intestinal HRP(ER) reporter	Crossing IQ6311 and TU3335
IQ6312	<i>P_{dpy-7}::HRP-mcherry::unc-54 UTR</i>	Hypodermal HRP(ER) reporter	Bombardment
IQ6352	<i>P_{dpy-7}::HRP-mcherry::unc-54 UTR; lin-15B(n744/n744)</i>	RNAi Hypersensitive Hypodermal HRP(ER) reporter	Crossing IQ6312 and TU3335
IQ1001	<i>mrp-5(ok2067/ok2067); supp(ih1001/ih1001)</i>	<i>mrp-5</i> suppressor mutant; unmapped	EMS mutagenesis of N2; <i>mrp-5(ok2067ok2067)</i>
IQ1002	<i>mrp-5(ok2067/ok2067); supp(ih1002/ih1002)</i>	<i>mrp-5</i> suppressor mutant; unmapped	EMS mutagenesis of N2; <i>mrp-5(ok2067ok2067)</i>
IQ1003	<i>mrp-5(ok2067/ok2067); aps-3(ih1003/ih1003)</i>	<i>mrp-5</i> suppressor mutant; mapped	EMS mutagenesis of N2; <i>mrp-5(ok2067ok2067)</i>
IQ1004	<i>mrp-5(ok2067/ok2067); apd-3(ih1004/ih1004)</i>	<i>mrp-5</i> suppressor mutant; mapped	EMS mutagenesis of N2; <i>mrp-5(ok2067ok2067)</i>
IQ1005	<i>mrp-5(ok2067/ok2067); apm-3(ih1005/ih1005)</i>	<i>mrp-5</i> suppressor mutant; mapped	EMS mutagenesis of N2; <i>mrp-</i>

			<i>5(ok2067ok2067)</i>
IQ1101	<i>mrp-5(ok2067/ok2067); supp(ih1101/ih1101)</i>	<i>mrp-5</i> suppressor mutant; unmapped	EMS mutagenesis of N2; <i>mrp-5(ok2067ok2067)</i>
IQ1102	<i>mrp-5(ok2067/ok2067); supp(ih1102/ih1102)</i>	<i>mrp-5</i> suppressor mutant; unmapped	EMS mutagenesis of N2; <i>mrp-5(ok2067ok2067)</i>
IQ1103	<i>mrp-5(ok2067/ok2067); supp(ih1103/ih1103)</i>	<i>mrp-5</i> suppressor mutant; unmapped	EMS mutagenesis of N2; <i>mrp-5(ok2067ok2067)</i>
IQ1201	<i>mrp-5(ok2067/ok2067); supp(ih1201/ih1201)</i>	<i>mrp-5</i> suppressor mutant; unmapped	EMS mutagenesis of N2; <i>mrp-5(ok2067ok2067)</i>
IQ1202	<i>mrp-5(ok2067/ok2067); supp(ih1202/ih1202)</i>	<i>mrp-5</i> suppressor mutant; unmapped	EMS mutagenesis of N2; <i>mrp-5(ok2067ok2067)</i>
IQ1203	<i>mrp-5(ok2067/ok2067); supp(ih1203/ih1203)</i>	<i>mrp-5</i> suppressor mutant; unmapped	EMS mutagenesis of N2; <i>mrp-5(ok2067ok2067)</i>
IQ1204	<i>mrp-5(ok2067/ok2067); supp(ih1204/ih1204)</i>	<i>mrp-5</i> suppressor mutant; unmapped	EMS mutagenesis of N2; <i>mrp-5(ok2067ok2067)</i>
IQ1205	<i>mrp-5(ok2067/ok2067); supp(ih1205/ih1205)</i>	<i>mrp-5</i> suppressor mutant; unmapped	EMS mutagenesis of N2; <i>mrp-5(ok2067ok2067)</i>
IQ1206	<i>mrp-5(ok2067/ok2067); supp(ih1206/ih1206)</i>	<i>mrp-5</i> suppressor mutant; unmapped	EMS mutagenesis of N2; <i>mrp-5(ok2067ok2067)</i>
IQ1207	<i>mrp-5(ok2067/ok2067); supp(ih1207/ih1207)</i>	<i>mrp-5</i> suppressor mutant; unmapped	EMS mutagenesis of N2; <i>mrp-5(ok2067ok2067)</i>
IQ1301	<i>mrp-5(ok2067/ok2067); supp(ih1301/ih1301)</i>	<i>mrp-5</i> suppressor mutant; unmapped	EMS mutagenesis of N2; <i>mrp-5(ok2067ok2067)</i>
IQ1302	<i>mrp-5(ok2067/ok2067);</i>	<i>mrp-5</i> suppressor	EMS mutagenesis of

	<i>supp(ih1302/ih1302)</i>	mutant; unmapped	N2; <i>mrp-5(ok2067ok2067)</i>
IQ1303	<i>mrp-5(ok2067/ok2067); supp(ih1303/ih1303)</i>	<i>mrp-5</i> suppressor mutant; unmapped	EMS mutagenesis of N2; <i>mrp-5(ok2067ok2067)</i>
IQ1401	<i>mrp-5(ok2067/ok2067); supp(ih1401/ih1401)</i>	<i>mrp-5</i> suppressor mutant; unmapped	EMS mutagenesis of N2; <i>mrp-5(ok2067ok2067)</i>
IQ1402	<i>mrp-5(ok2067/ok2067); supp(ih1402/ih1402)</i>	<i>mrp-5</i> suppressor mutant; unmapped	EMS mutagenesis of N2; <i>mrp-5(ok2067ok2067)</i>
IQ1403	<i>mrp-5(ok2067/ok2067); supp(ih1403/ih1403)</i>	<i>mrp-5</i> suppressor mutant; unmapped	EMS mutagenesis of N2; <i>mrp-5(ok2067ok2067)</i>
IQ1404	<i>mrp-5(ok2067/ok2067); supp(ih1404/ih1404)</i>	<i>mrp-5</i> suppressor mutant; unmapped	EMS mutagenesis of N2; <i>mrp-5(ok2067ok2067)</i>
IQ1405	<i>mrp-5(ok2067/ok2067); supp(ih1405/ih1405)</i>	<i>mrp-5</i> suppressor mutant; unmapped	EMS mutagenesis of N2; <i>mrp-5(ok2067ok2067)</i>
IQ1406	<i>mrp-5(ok2067/ok2067); supp(ih1406/ih1406)</i>	<i>mrp-5</i> suppressor mutant; unmapped	EMS mutagenesis of N2; <i>mrp-5(ok2067ok2067)</i>
IQ1407	<i>mrp-5(ok2067/ok2067); supp(ih1407/ih1407)</i>	<i>mrp-5</i> suppressor mutant; unmapped	EMS mutagenesis of N2; <i>mrp-5(ok2067ok2067)</i>
IQ1408	<i>mrp-5(ok2067/ok2067); supp(ih1408/ih1408)</i>	<i>mrp-5</i> suppressor mutant; unmapped	EMS mutagenesis of N2; <i>mrp-5(ok2067ok2067)</i>
IQ1409	<i>mrp-5(ok2067/ok2067); supp(ih1409/ih1409)</i>	<i>mrp-5</i> suppressor mutant; unmapped	EMS mutagenesis of N2; <i>mrp-5(ok2067ok2067)</i>
IQ1410	<i>mrp-5(ok2067/ok2067); supp(ih1410/ih1410)</i>	<i>mrp-5</i> suppressor mutant; unmapped	EMS mutagenesis of N2; <i>mrp-</i>

			<i>5(ok2067ok2067)</i>
IQ1411	<i>mrp-5(ok2067/ok2067); supp(ih1411/ih1411)</i>	<i>mrp-5</i> suppressor mutant; unmapped	EMS mutagenesis of N2; <i>mrp-5(ok2067ok2067)</i>
IQ1412	<i>mrp-5(ok2067/ok2067); supp(ih1412/ih1412)</i>	<i>mrp-5</i> suppressor mutant; unmapped	EMS mutagenesis of N2; <i>mrp-5(ok2067ok2067)</i>
IQ1413	<i>mrp-5(ok2067/ok2067); supp(ih1413/ih1413)</i>	<i>mrp-5</i> suppressor mutant; unmapped	EMS mutagenesis of N2; <i>mrp-5(ok2067ok2067)</i>
IQ1414	<i>mrp-5(ok2067/ok2067); supp(ih1414/ih1414)</i>	<i>mrp-5</i> suppressor mutant; unmapped	EMS mutagenesis of N2; <i>mrp-5(ok2067ok2067)</i>

REFERENCES:

1. Severance S, Hamza I. Trafficking of heme and porphyrins in metazoa. *Chem Rev.* 2009;109:4596-4616.
2. Hamza I, Dailey HA. One ring to rule them all: trafficking of heme and heme synthesis intermediates in the metazoans. *Biochim Biophys Acta.* 2012;1823:1617-1632.
3. Krishnamurthy P, Xie T, Schuetz JD. The role of transporters in cellular heme and porphyrin homeostasis. *Pharmacol Ther.* 2007;114:345-358.
4. Hardison RC. A brief history of hemoglobins: plant, animal, protist, and bacteria. *Proc Natl Acad Sci U S A.* 1996;93:5675-5679.
5. Skoneczny M, Rytka J. Oxygen and haem regulate the synthesis of peroxisomal proteins: catalase A, acyl-CoA oxidase and Pex1p in the yeast *Saccharomyces cerevisiae*; the regulation of these proteins by oxygen is not mediated by haem. *Biochemical Journal.* 2000;350 Pt 1:313-319.
6. Balla J, Vercellotti GM, Jeney V, et al. Heme, heme oxygenase, and ferritin: how the vascular endothelium survives (and dies) in an iron-rich environment. *Antioxid Redox Signal.* 2007;9:2119-2137.
7. Korolnek T, Hamza I. Like iron in the blood of the people: the requirement for heme trafficking in iron metabolism. *Front Pharmacol.* 2014;5:126.
8. Balla G, Vercellotti GM, Muller-Eberhard U, Eaton J, Jacob HS. Exposure of endothelial cells to free heme potentiates damage mediated by granulocytes and toxic oxygen species. *Lab Invest.* 1991;64:648-655.
9. Pischik E, Kauppinen R. An update of clinical management of acute intermittent porphyria. *Appl Clin Genet.* 2015;8:201-214.
10. Bonkovsky HL, Maddukuri VC, Yazici C, et al. Acute porphyrias in the USA: features of 108 subjects from porphyrias consortium. *Am J Med.* 2014;127:1233-1241.
11. Bonkovsky HL, Healey JF, Lourie AN, Gerron GG. Intravenous heme-albumin in acute intermittent porphyria: evidence for repletion of hepatic hemoproteins and regulatory heme pools. *Am J Gastroenterol.* 1991;86:1050-1056.
12. Magness ST, Maeda N, Brenner DA. An exon 10 deletion in the mouse ferrochelatase gene has a dominant-negative effect and causes mild protoporphyria. *Blood.* 2002;100:1470-1477.
13. Dooley KA, Fraenkel PG, Langer NB, et al. montalcino, A zebrafish model for variegate porphyria. *Exp Hematol.* 2008;36:1132-1142.
14. Uc A, Stokes JB, Britigan BE. Heme transport exhibits polarity in Caco-2 cells: evidence for an active and membrane protein-mediated process. *Am J Physiol Gastrointest Liver Physiol.* 2004;287:G1150-1157.
15. Bullen JJ, Rogers HJ, Griffiths E. Role of iron in bacterial infection. *Curr Top Microbiol Immunol.* 1978;80:1-35.
16. Kadish KM, Smith KM, Guillard R. Handbook of porphyrin science : with applications to chemistry, physics, materials science, engineering, biology and medicine vol. 15.
17. Letoffe S, Delepelaire P, Wandersman C. Functional differences between heme permeases: *Serratia marcescens* HemTUV permease exhibits a narrower substrate specificity (restricted to heme) than the *Escherichia coli* DppABCDF peptide-heme permease. *J Bacteriol.* 2008;190:1866-1870.
18. Wandersman C, Stojiljkovic I. Bacterial heme sources: the role of heme, hemoprotein receptors and hemophores. *Curr Opin Microbiol.* 2000;3:215-220.
19. Protchenko O, Rodriguez-Suarez R, Androphy R, Bussey H, Philpott CC. A screen for genes of heme uptake identifies the FLC family required for import of FAD into the endoplasmic reticulum. *J Biol Chem.* 2006;281:21445-21457.

20. Weissman Z, Kornitzer D. A family of *Candida* cell surface haem-binding proteins involved in haemin and haemoglobin-iron utilization. *Mol Microbiol.* 2004;53:1209-1220.
21. Weissman Z, Shemer R, Conibear E, Kornitzer D. An endocytic mechanism for haemoglobin-iron acquisition in *Candida albicans*. *Mol Microbiol.* 2008;69:201-217.
22. Fleming MD, Hamza I. Mitochondrial heme: an exit strategy at last. *J Clin Invest.* 2012;122:4328-4330.
23. Conrad ME, Umbreit JN. Iron absorption and transport-an update. *Am J Hematol.* 2000;64:287-298.
24. Shayeghi M, Latunde-Dada GO, Oakhill JS, et al. Identification of an intestinal heme transporter. *Cell.* 2005;122:789-801.
25. Qiu A, Jansen M, Sakaris A, et al. Identification of an intestinal folate transporter and the molecular basis for hereditary folate malabsorption. *Cell.* 2006;127:917-928.
26. Quigley JG, Yang Z, Worthington MT, et al. Identification of a human heme exporter that is essential for erythropoiesis. *Cell.* 2004;118:757-766.
27. Abkowitz JL, Holly RD, Grant CK. Retrovirus-induced feline pure red cell aplasia. Hematopoietic progenitors are infected with feline leukemia virus and erythroid burst-forming cells are uniquely sensitive to heterologous complement. *J Clin Invest.* 1987;80:1056-1063.
28. Weiss RA, Taylor CS. Retrovirus receptors. *Cell.* 1995;82:531-533.
29. Keel SB, Doty RT, Yang Z, et al. A heme export protein is required for red blood cell differentiation and iron homeostasis. *Science.* 2008;319:825-828.
30. Chiabrando D, Marro S, Mercurio S, et al. The mitochondrial heme exporter FLVCR1b mediates erythroid differentiation. *J Clin Invest.* 2012;122:4569-4579.
31. Khan AA, Quigley JG. Heme and FLVCR-related transporter families SLC48 and SLC49. *Mol Aspects Med.* 2013;34:669-682.
32. Rao AU, Carta LK, Lesuisse E, Hamza I. Lack of heme synthesis in a free-living eukaryote. *Proc Natl Acad Sci U S A.* 2005;102:4270-4275.
33. Severance S, Rajagopal A, Rao AU, et al. Genome-wide analysis reveals novel genes essential for heme homeostasis in *Caenorhabditis elegans*. *PLoS Genet.* 2010;6:e1001044.
34. Rajagopal A, Rao AU, Amigo J, et al. Haem homeostasis is regulated by the conserved and concerted functions of HRG-1 proteins. *Nature.* 2008;453:1127-1131.
35. Ben Saidan HB. Multiple HRG-1 paralogs regulate heme homeostasis in *C. elegans*. MOCB. Vol. M.S. College Park: Maryland; 2014:85.
36. Yuan X, Protchenko O, Philpott CC, Hamza I. Topologically conserved residues direct heme transport in HRG-1-related proteins. *J Biol Chem.* 2012;287:4914-4924.
37. O'Callaghan KM, Ayllon V, O'Keefe J, et al. Heme-binding protein HRG-1 is induced by insulin-like growth factor I and associates with the vacuolar H⁺-ATPase to control endosomal pH and receptor trafficking. *J Biol Chem.* 2010;285:381-391.
38. Kadish KM, Smith KM, Guillard R. Handbook of porphyrin science : with applications to chemistry, physics, materials science, engineering, biology and medicine. vol. 26.
39. Sinclair J, Hamza I. A novel heme-responsive element mediates transcriptional regulation in *Caenorhabditis elegans*. *J Biol Chem.* 2010;285:39536-39543.
40. Korolnek T, Zhang J, Beardsley S, Scheffer GL, Hamza I. Control of metazoan heme homeostasis by a conserved multidrug resistance protein. *Cell Metab.* 2014;19:1008-1019.
41. Sinclair J, Beardsley S, Pinter K, Samuel T, Yuan X, Zhang J, Meng K, Yun S, Krause M, Hamza I. Long-range signaling at the neural-intestinal axis promotes organismal heme homeostasis. Manuscript Submitted. 2016.
42. White C, Yuan X, Schmidt PJ, et al. HRG1 is essential for heme transport from the phagolysosome of macrophages during erythrophagocytosis. *Cell Metab.* 2013;17:261-270.

43. Chen C, Samuel TK, Sinclair J, Dailey HA, Hamza I. An intercellular heme-trafficking protein delivers maternal heme to the embryo during development in *C. elegans*. *Cell*. 2011;145:720-731.
44. Marciano O, Moskovitz Y, Hamza I, Ruthstein S. Histidine residues are important for preserving the structure and heme binding to the *C. elegans* HRG-3 heme-trafficking protein. *J Biol Inorg Chem*. 2015;20:1253-1261.
45. Jansen RS, Mahakena S, de Haas M, Borst P, van de Wetering K. ATP-binding Cassette Subfamily C Member 5 (ABCC5) Functions as an Efflux Transporter of Glutamate Conjugates and Analogs. *J Biol Chem*. 2015;290:30429-30440.
46. Stenmark H. Rab GTPases as coordinators of vesicle traffic. *Nat Rev Mol Cell Biol*. 2009;10:513-525.
47. Bonifacino JS, Traub LM. Signals for sorting of transmembrane proteins to endosomes and lysosomes. *Annu Rev Biochem*. 2003;72:395-447.
48. Bonifacino JS, Dell'Angelica EC. Molecular bases for the recognition of tyrosine-based sorting signals. *Journal of Cell Biology*. 1999;145:923-926.
49. Hirst J, Barlow LD, Francisco GC, et al. The fifth adaptor protein complex. *PLoS Biol*. 2011;9:e1001170.
50. Hirst J, Irving C, Borner GH. Adaptor protein complexes AP-4 and AP-5: new players in endosomal trafficking and progressive spastic paraplegia. *Traffic*. 2013;14:153-164.
51. Boehm M, Bonifacino JS. Adaptins: the final recount. *Molecular Biology of the Cell*. 2001;12:2907-2920.
52. Boehm M, Bonifacino JS. Genetic analyses of adaptin function from yeast to mammals. *Gene*. 2002;286:175-186.
53. Canfield WM, Johnson KF, Ye RD, Gregory W, Kornfeld S. Localization of the signal for rapid internalization of the bovine cation-independent mannose 6-phosphate/insulin-like growth factor-II receptor to amino acids 24-29 of the cytoplasmic tail. *J Biol Chem*. 1991;266:5682-5688.
54. Ohno H, Aguilar RC, Yeh D, Taura D, Saito T, Bonifacino JS. The medium subunits of adaptor complexes recognize distinct but overlapping sets of tyrosine-based sorting signals. *J Biol Chem*. 1998;273:25915-25921.
55. Guarnieri FG, Arterburn LM, Penno MB, Cha Y, August JT. The motif Tyr-X-X-hydrophobic residue mediates lysosomal membrane targeting of lysosome-associated membrane protein 1. *J Biol Chem*. 1993;268:1941-1946.
56. Honing S, Hunziker W. Cytoplasmic determinants involved in direct lysosomal sorting, endocytosis, and basolateral targeting of rat Igp120 (lamp-I) in MDCK cells. *Journal of Cell Biology*. 1995;128:321-332.
57. Mardones GA, Burgos PV, Lin Y, et al. Structural basis for the recognition of tyrosine-based sorting signals by the mu3A subunit of the AP-3 adaptor complex. *J Biol Chem*. 2013;288:9563-9571.
58. Traub LM, Bonifacino JS. Cargo recognition in clathrin-mediated endocytosis. *Cold Spring Harb Perspect Biol*. 2013;5:a016790.
59. Kelly BT, Owen DJ. Endocytic sorting of transmembrane protein cargo. *Current Opinion in Cell Biology*. 2011;23:404-412.
60. Jeon KW. International review of cell and molecular biology, Volume 320. Oxford: Academic; 2015.
61. Boman AL. GGA proteins: new players in the sorting game. *Journal of Cell Science*. 2001;114:3413-3418.
62. Bonifacino JS. Adaptor proteins involved in polarized sorting. *Journal of Cell Biology*. 2014;204:7-17.

63. Shafaq-Zadah M, Brocard L, Solari F, Michaux G. AP-1 is required for the maintenance of apico-basal polarity in the *C. elegans* intestine. *Development*. 2012;139:2061-2070.
64. Hase K, Nakatsu F, Ohmae M, et al. AP-1B-mediated protein sorting regulates polarity and proliferation of intestinal epithelial cells in mice. *Gastroenterology*. 2013;145:625-635.
65. Clemens Grisham R, Kindt K, Finger-Baier K, Schmid B, Nicolson T. Mutations in *ap1b1* cause mistargeting of the Na⁽⁺⁾/K⁽⁺⁾-ATPase pump in sensory hair cells. *PLoS One*. 2013;8:e60866.
66. Di Pietro SM, Dell'Angelica EC. The cell biology of Hermansky-Pudlak syndrome: recent advances. *Traffic*. 2005;6:525-533.
67. Cullinane AR, Curry JA, Carmona-Rivera C, et al. A BLOC-1 mutation screen reveals that *PLDN* is mutated in Hermansky-Pudlak Syndrome type 9. *Am J Hum Genet*. 2011;88:778-787.
68. Huizing M, Helip-Wooley A, Westbroek W, Gunay-Aygun M, Gahl WA. Disorders of lysosome-related organelle biogenesis: clinical and molecular genetics. *Annu Rev Genomics Hum Genet*. 2008;9:359-386.
69. Sitaram A, Marks MS. Mechanisms of protein delivery to melanosomes in pigment cells. *Physiology (Bethesda)*. 2012;27:85-99.
70. Hermann GJ, Schroeder LK, Hieb CA, et al. Genetic analysis of lysosomal trafficking in *Caenorhabditis elegans*. *Molecular Biology of the Cell*. 2005;16:3273-3288.
71. Hermann GJ, Scavarda E, Weis AM, et al. *C. elegans* BLOC-1 functions in trafficking to lysosome-related gut granules. *PLoS One*. 2012;7:e43043.
72. Coburn C, Gems D. The mysterious case of the *C. elegans* gut granule: death fluorescence, anthranilic acid and the kynurenine pathway. *Front Genet*. 2013;4:151.
73. Roh HC, Collier S, Guthrie J, Robertson JD, Kornfeld K. Lysosome-related organelles in intestinal cells are a zinc storage site in *C. elegans*. *Cell Metab*. 2012;15:88-99.
74. Khan AA, Quigley JG. Control of intracellular heme levels: heme transporters and heme oxygenases. *Biochim Biophys Acta*. 2011;1813:668-682.
75. Sinclair J, Hamza I. Lessons from bloodless worms: heme homeostasis in *C. elegans*. *Biometals*. 2015;28:481-489.
76. Chen C, Samuel TK, Krause M, Dailey HA, Hamza I. Heme utilization in the *Caenorhabditis elegans* hypodermal cells is facilitated by heme-responsive gene-2. *J Biol Chem*. 2012;287:9601-9612.
77. Yuan X, Nuno Da Silva, A., Hanna, D., Reddi, A., Hamza, I. Regulation of intracellular and interorgan heme trafficking revealed by subcellular reporters. Manuscript Submitted. 2016.
78. Samuel TK, Sinclair JW, Pinter KL, Hamza I. Culturing *Caenorhabditis elegans* in axenic liquid media and creation of transgenic worms by microparticle bombardment. *J Vis Exp*. 2014:e51796.
79. Jorgensen EM, Mango SE. The art and design of genetic screens: *caenorhabditis elegans*. *Nat Rev Genet*. 2002;3:356-369.
80. Minevich G, Park DS, Blankenberg D, Poole RJ, Hobert O. CloudMap: a cloud-based pipeline for analysis of mutant genome sequences. *Genetics*. 2012;192:1249-1269.
81. Davis MW, Hammarlund M, Harrach T, Hullett P, Olsen S, Jorgensen EM. Rapid single nucleotide polymorphism mapping in *C. elegans*. *BMC Genomics*. 2005;6:118.
82. Zuryn S, Jarriault S. Deep sequencing strategies for mapping and identifying mutations from genetic screens. *Worm*. 2013;2:e25081.
83. Sega GA. A review of the genetic effects of ethyl methanesulfonate. *Mutat Res*. 1984;134:113-142.

84. Hawley RS, Gilliland WD. Sometimes the result is not the answer: the truths and the lies that come from using the complementation test. *Genetics*. 2006;174:5-15.
85. Sherlekar AL, Lints R. Nematode Tango Milonguero - the *C. elegans* male's search for the hermaphrodite vulva. *Semin Cell Dev Biol*. 2014;33:34-41.
86. Worthington MT, Cohn SM, Miller SK, Luo RQ, Berg CL. Characterization of a human plasma membrane heme transporter in intestinal and hepatocyte cell lines. *Am J Physiol Gastrointest Liver Physiol*. 2001;280:G1172-1177.
87. Huynh C, Yuan X, Miguel DC, et al. Heme uptake by *Leishmania amazonensis* is mediated by the transmembrane protein LHR1. *PLoS Pathog*. 2012;8:e1002795.
88. Seidel HS, Rockman MV, Kruglyak L. Widespread genetic incompatibility in *C. elegans* maintained by balancing selection. *Science*. 2008;319:589-594.
89. Hillier LW, Marth GT, Quinlan AR, et al. Whole-genome sequencing and variant discovery in *C. elegans*. *Nat Methods*. 2008;5:183-188.
90. Doitsidou M, Poole RJ, Sarin S, Bigelow H, Hobert O. *C. elegans* mutant identification with a one-step whole-genome-sequencing and SNP mapping strategy. *PLoS One*. 2010;5:e15435.
91. Oka T, Toyomura T, Honjo K, Wada Y, Futai M. Four subunit isoforms of *Caenorhabditis elegans* vacuolar H⁺-ATPase. Cell-specific expression during development. *J Biol Chem*. 2001;276:33079-33085.
92. Rolls MM, Hall DH, Victor M, Stelzer EH, Rapoport TA. Targeting of rough endoplasmic reticulum membrane proteins and ribosomes in invertebrate neurons. *Molecular Biology of the Cell*. 2002;13:1778-1791.
93. Shim J, Lee J. The AP-3 clathrin-associated complex is essential for embryonic and larval development in *Caenorhabditis elegans*. *Molecules and Cells*. 2005;19:452-457.
94. Wakabayashi T, Nakamura N, Sambongi Y, Wada Y, Oka T, Futai M. Identification of the copper chaperone, CUC-1, in *Caenorhabditis elegans*: tissue specific co-expression with the copper transporting ATPase, CUA-1. *Febs Letters*. 1998;440:141-146.
95. Chun H, Kim, B.E. Cua-1 acts as an intestinal copper exporter in *C. elegans*. Manuscript in Preparation. 2016.
96. Klass MR. Aging in the nematode *Caenorhabditis elegans*: major biological and environmental factors influencing life span. *Mech Ageing Dev*. 1977;6:413-429.
97. Schroeder LK, Kremer S, Kramer MJ, et al. Function of the *Caenorhabditis elegans* ABC transporter PGP-2 in the biogenesis of a lysosome-related fat storage organelle. *Molecular Biology of the Cell*. 2007;18:995-1008.
98. Salazar G, Craige B, Styers ML, et al. BLOC-1 complex deficiency alters the targeting of adaptor protein complex-3 cargoes. *Molecular Biology of the Cell*. 2006;17:4014-4026.
99. Di Pietro SM, Falcon-Perez JM, Tenza D, et al. BLOC-1 interacts with BLOC-2 and the AP-3 complex to facilitate protein trafficking on endosomes. *Molecular Biology of the Cell*. 2006;17:4027-4038.
100. Setty SR, Tenza D, Truschel ST, et al. BLOC-1 is required for cargo-specific sorting from vacuolar early endosomes toward lysosome-related organelles. *Molecular Biology of the Cell*. 2007;18:768-780.
101. Zhang H, Kim A, Abraham N, et al. Clathrin and AP-1 regulate apical polarity and lumen formation during *C. elegans* tubulogenesis. *Development*. 2012;139:2071-2083.
102. Hannon GJ. RNA interference. *Nature*. 2002;418:244-251.
103. Krogh A, Larsson B, von Heijne G, Sonnhammer EL. Predicting transmembrane protein topology with a hidden Markov model: application to complete genomes. *Journal of Molecular Biology*. 2001;305:567-580.

104. Mullins C, Bonifacino JS. The molecular machinery for lysosome biogenesis. *Bioessays*. 2001;23:333-343.
105. Nunes F, Wolf M, Hartmann J, Paul RJ. The ABC transporter PGP-2 from *Caenorhabditis elegans* is expressed in the sensory neuron pair AWA and contributes to lysosome formation and lipid storage within the intestine. *Biochem Biophys Res Commun*. 2005;338:862-871.
106. Dell'Angelica EC, Shotelersuk V, Aguilar RC, Gahl WA, Bonifacino JS. Altered trafficking of lysosomal proteins in Hermansky-Pudlak syndrome due to mutations in the beta 3A subunit of the AP-3 adaptor. *Molecular Cell*. 1999;3:11-21.
107. Gu M, Liu Q, Watanabe S, et al. AP2 hemicomplexes contribute independently to synaptic vesicle endocytosis. *Elife*. 2013;2:e00190.
108. Peden AA, Rudge RE, Lui WWY, Robinson MS. Assembly and function of AP-3 complexes in cells expressing mutant subunits. *Journal of Cell Biology*. 2002;156:327-336.
109. de Voer G, Peters D, Taschner PE. *Caenorhabditis elegans* as a model for lysosomal storage disorders. *Biochim Biophys Acta*. 2008;1782:433-446.
110. Delahaye JL, Foster OK, Vine A, et al. *Caenorhabditis elegans* HOPS and CCZ-1 mediate trafficking to lysosome-related organelles independently of RAB-7 and SAND-1. *Molecular Biology of the Cell*. 2014;25:1073-1096.
111. Woodman PG. Biogenesis of the sorting endosome: the role of Rab5. *Traffic*. 2000;1:695-701.
112. Hermann GJ, Schroeder LK, Hieb CA, et al. Genetic analysis of lysosomal trafficking in *Caenorhabditis elegans*. *Mol Biol Cell*. 2005;16:3273-3288.
113. Schroeder LK, Kremer S, Kramer MJ, et al. Function of the *Caenorhabditis elegans* ABC transporter PGP-2 in the biogenesis of a lysosome-related fat storage organelle. *Mol Biol Cell*. 2007;18:995-1008.